BIOMECHANICAL MODELING OF HUMAN HAND

A THESIS SUBMITTED TO
THE GRADUATE SCHOOL OF NATURAL AND APPLIED SCIENCES
OF
MIDDLE EAST TECHNICAL UNIVERSITY

BY

OSMAN KILIÇ

IN PARTIAL FULFILLMENT OF THE REQUIREMENTS
FOR
THE DEGREE OF MASTER OF SCIENCE
IN
MECHANICAL ENGINEERING

SEPTEMBER 2007

BIOMECHANICAL MODELING OF HUMAN HAND

submitted by **OSMAN KILIÇ** in partial fulfillment of the requirements for the degree of **Master of Science in Mechanical Engineering Department, Middle East Technical University** by,

Prof. Dr. Canan Özgen ______________________
Dean, Graduate School of **Natural and Applied Sciences**

Prof. Dr. Kemal İder ______________________
Head of Department, **Mechanical Engineering**

Asst. Prof. Dr. Ergin Tönük ______________________
Supervisor, **Mechanical Engineering Dept., METU**

Prof. Dr. S. Turgut Tümer ______________________
Co-Supervisor, **METU Northern Cyprus Campus President**

Examining Committee Members:

Prof. Dr. Eres Söylemez ______________________
Mechanical Engineering Dept., METU

Asst. Prof. Dr. Ergin Tönük ______________________
Mechanical Engineering Dept., METU

Prof. Dr. Bilgin Kaftanoğlu ______________________
Mechanical Engineering Dept., METU

Prof. Dr. Kemal Özgören ______________________
Mechanical Engineering Dept., METU

Prof. Dr. Gürsel Leblebicioğlu ______________________
Orthopaedics Dept., Hacettepe University, Ankara/Turkey

Date: 13.09.2007

I hereby declare that all information in this document has been obtained and presented in accordance with academic rules and ethical conduct. I also declare that, as required by these rules and conduct, I have fully cited and referenced all material and results that are not original to this work.

Name, Last name: Osman KILIÇ

Signature :

ABSTRACT

BIOMECHANICAL MODELING OF HUMAN HAND

Kılıç, Osman
M.S., Department of Mechanical Engineering
Supervisor : Asst. Prof. Dr. Ergin Tönük
Co-Supervisor: Prof. Dr. S. Turgut Tümer

September 2007, 91 pages

This thesis analyzes the wrist joint of the human hand by using a realistic three-dimensional wrist model. Load distributions among carpal bones, forces on ligaments and joints were examined by using three-dimensional model. Wrist injuries and required surgical operations were examined with the model. The most crucial point of the study was that, using three-dimensional model of the wrist, hand surgeons would be able to predict results of surgical operation. Surgery planning may be done and mechanical results may be evaluated on the wrist model.

Keywords: Biomechanics, Human hand, Wrist

ÖZ

İNSAN ELİNİN BİYOMEKANİK OLARAK MODELLENMESİ

Kılıç, Osman
Yüksek Lisans, Makina Mühendisliği Bölümü
Tez Yöneticisi : Yrd. Doç. Dr. Ergin Tönük
Ortak Tez Yöneticisi: Prof. Dr. S. Turgut Tümer

Eylül 2007, 91 sayfa

Bu çalışma insan eli bileğinin gerçekçi bir yaklaşımla üç boyutlu modelinin oluşturulması ve incelenmesi konularını içermektedir. Üç boyutlu model yardımıyla karpal kemikleri, ligamanlar ve eklem bölgelerindeki yük dağılımları incelenmiştir. Bilek incinmeleri ve gerekli olacak cerrahi operasyonlar model aracılığıyla incelenmiştir. Çalışmanın en önemli noktası, el cerrahlarının üç boyutlu model yardımıyla cerrahi operasyonlar öncesinde sonuçlar hakkında kestirimde bulunmasında yardımcı olmasıdır. Bilek modeli kullanılarak cerrahi planlaması ve değişik cerrahi operasyonların mekanik sonuçları ayrıntılı olarak gözlenebilir.

Anahtar kelimeler: Biyomekanik, İnsan Eli, El Bileği

This thesis is dedicated to my parents, my sister and Meltem who offered me unconditional love and support all the way since the beginning of my studies.

ACKNOWLEDGMENTS

The author wishes to express his deep and sincere gratitude to his supervisor Asst. Prof. Ergin Tönük and co-supervisor Prof. Dr. Turgut Tümer for their excellent supervision, advice and encouragements.

Author is grateful to Prof. Dr. Gürsel Leblebicioğlu for his detailed and constructive criticism and excellent advice through this work.

Support of Dr. Kemal Arda for computed tomography imaging of the wrist is gratefully acknowledged.

The author wishes to give many thanks to Atilla Uz and Tolga Akın for their guidance for understanding of mechanics.

Many thanks to Sevgi Saraç and Metehan Erdoğan from undergraduate years in Middle East Technical University, for everything we shared.

Author owes his loving thanks to Meltem, without her encouragement and patience this thesis might not be written. Her love and persistent confidence in author is considerable for the success of this thesis.

Finally, author is grateful to his parents and sister for their endless patience and support throughout his life.

TABLE OF CONTENTS

LIST OF TABLES

TABLE OF FIGURES

LIST OF ABBREVIATIONS

In this study, abbreviations were used for defining the plots in figures. Used abbreviations are:

DoLig	Force on dorsal ligament.
PaLig	Force on palmar ligament.
Con	Contact force.
Bus	Force on the joint.

These abbreviations were followed by the name of corresponding ligaments or wrist bones. Some abbreviation examples are given below:

DoLig_Scapholunate	Force on the dorsal ligament of scapholunate.
PaLig_Lunotriquetral	Force on the palmar ligament of lunotriquetral.
Con_Capitatum_Scaphoid	Contact force between capitatum and scaphoid bones.
Bus_Lunate_Radius	Joint force between lunatum and radius bones.

CHAPTER 1

INTRODUCTION

This study is focused on building a realistic biomechanical model of the wrist joint for human hand. A three-dimensional wrist model was prepared by using three-dimensional geometry of the bones (obtained from the real computed tomography (CT) data of the author), ligaments and joints. Three-dimensional dynamic model has the ability of analyzing the load distributions among wrist structure elements.

The most important point of the study is that the three-dimensional wrist model can be used to analyze the real life injuries for the wrist. With this method orthopaedics or hand surgeons can compare the injured wrists with healthy wrists; changes in load distributions for components of the wrist can be analyzed. Also, treatment methods for injuries can be modeled on the wrist. Thus, the mechanical results of a surgery can be analyzed on the three-dimensional model proposed before a surgery. With this model, hand surgeons have the chance of trying new surgical methods without risking the patients' health and predicting results of treatment methods, which is commonly referred as surgery planning.

Human hand is one of the most complex structures on the human body having various types of functions. The perfect sensitivity and mechanical strength exist together in the hand by being one of the most essential organs of our movements. Even the tip of a needle can be hold with high sensitivity or a wooden plate can be broken by punch with a high strength.

When the hand's wide range of functional abilities are examined, wrist seems to be the most important part. As compared to the other parts of the human body, wrist has a very large number of bones, ligaments, tendons and muscles in a small area as a joint. So, the wrist is a very complex joint with the combination of many elements.

In literature there is a need for a complete dynamic wrist model (dynamic term is used in medical literature but for engineering applications model can be defined as quasi-static); including the whole bone, ligament, joint and contact structures. Analyzing the healthy and the injured wrists needs a complete three-dimensional study. So, the crucial point of this study is to develop a dynamic three-dimensional wrist model for examining real life cases with the comparison of normal (healthy) wrists with the pathologic wrists.

In Chapter 2, anatomy of the wrist and studies in literature are explained first. In Chapter 3, the methodology for building three-dimensional model is described. Finally in Chapter 4, normal (healthy) and pathologic wrists are analyzed. Kienböck's disease and scapholunate ligament tear were analyzed and the mechanical results of the treatment methods were investigated as pathological cases.

CHAPTER 2

REVIEW OF LITERATURE

2.1. Anatomy of the Wrist

2.1.1. Wrist Bones

Bones are the main base for the wrist where all other parts (ligaments, muscles etc.) are attached. Bones of the wrist are shown in Figure 1 [1]:

Figure 1 Radiograph of the wrist (Dorsal side).

Wrist bones are composed of five metacarpal bones (first, second, …, fifth metacarpal), eight carpal bones (trapezium, trapezoid, capitatum, hamatum, psiforme, scaphoid, lunatum, triquetrum), radius and ulna (totally 15 bones).
Radius and ulna are the bones of the forearm where the wrist acts as a joint between the hand and the forearm.

2.1.2. Joints of the Wrist Bones

Bones of the wrist are surrounded with a synovial membrane and synovial fluid in this membrane acts as a joint between wrist bones. Kuczynski et al. [2] states synovial fluid prevents the friction and wear on the surfaces of bones providing lubrication. Movement of a bone on another may cause serious damage if synovial fluid does not prevent friction forces. This fluid fills all the space between wrist bones. In Figure 2 joints of the wrist are presented as passing through the bones [3].

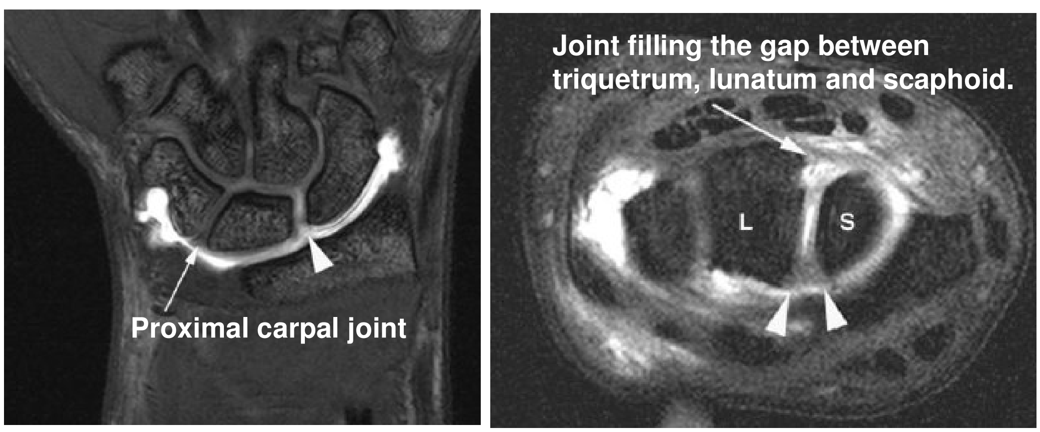

Figure 2 Joints of the wrist bones.

2.1.3. Ligaments of the Wrist

Ligaments are the connectors between wrist bones and provide support for the bone joints. Ligaments are generally confused with tendons which connect muscles to the bones. A ligament connects two bones to each other and has no connection with muscles.

The mechanical function for a ligament is to support the bones and to limit the joint motion range when they are in tension. Ligaments are mechanically active only under the effect of tensile forces and become inactive under the effect of compressive forces. Ligaments can be imagined as packet rubber bands which do not have a function unless a tensile force is applied.

Özçelik et al. [4] states the significance of the ligaments as "understanding the exact contribution of the supporting ligaments to the functional integrity of the wrist is crucial for the diagnosis and treatment of carpal instabilities".

Ligaments of the wrist can be divided into two main groups: Palmar ligaments and dorsal ligaments. Palmar ligaments are on the palmar side of the hand and dorsal ligaments are on the dorsal side. Ligaments of the hand are shown in Figure 3 and Figure 4 and where from left to right ligaments get more superficial [5].

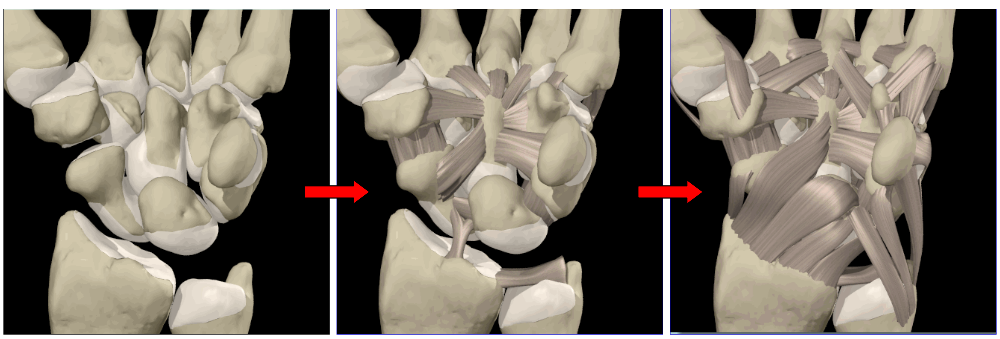

Figure 3 Palmar (Volar) ligaments of the hand.

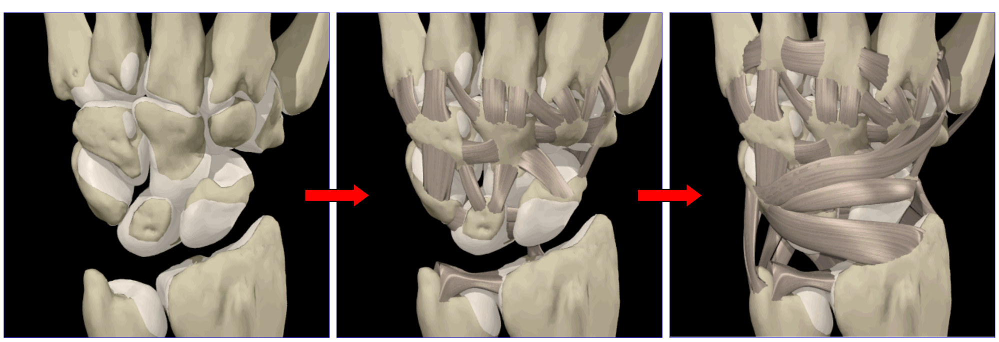

Figure 4 Dorsal ligaments of the hand.

2.1.4. Muscles of the Wrist

Muscles are the actuators for the hand movements. Starting from the forearm to the fingers, muscles control the hand actions. In Figure 5 muscles of the wrist are shown, tendons of the front arm extend from forearm to the fingers on both dorsal and palmar sides.

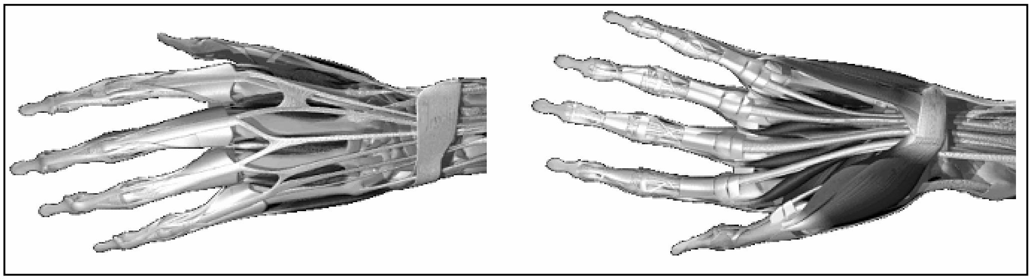

Figure 5 Muscles of the wrist (dorsal side on the left, palmar side on the right).

In the three-dimensional model muscles were not used, instead defined external forces were used as actuators. For analyzing wrist motions, special external forces were used and defined in section 3.1.5. Each of the recommended wrist motions were obtained by applying single component forces.

2.2. Functions of the Wrist

Wrist is one of the most complex joints on the human body. Complexity of the wrist joint supplies the sensitivity and strength for hand together. Hand's wide ranges of functional abilities are supported by the wrist joint. As an example, tip of a needle can be hold with high sensitivity or a powerful punch can be applied on a surface by hand. Wrist has an important role on both of these applications by being a multifunctional joint. Crisco et al. [6] states the importance of the wrist as "the eight bones of the wrist represent a highly complex mechanical structure that has long fascinated clinicians and researchers. Describing carpal bone kinematics remains challenging because of the small size and complicated motion".

Movements of the wrist are defined as flexion, extension, radial deviation, ulnar deviation and combinations of these movements. Definitions of the wrist movements are given in the following figures. Radial deviation and ulnar deviation motions are presented in Figure 6 [7]:

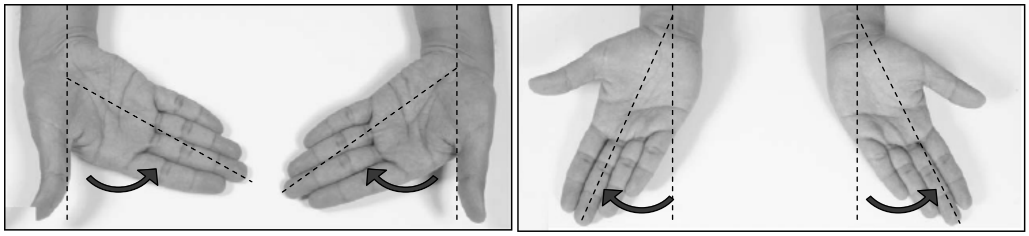

Figure 6 Ulnar deviation of the wrist (on the left) and radial deviation of the wrist (on the right).

Flexion and extension motions are presented in Figure 7 [7]:

Figure 7 Flexion (on the left) and extension (on the right) motions.

Combinations of the wrist movements:

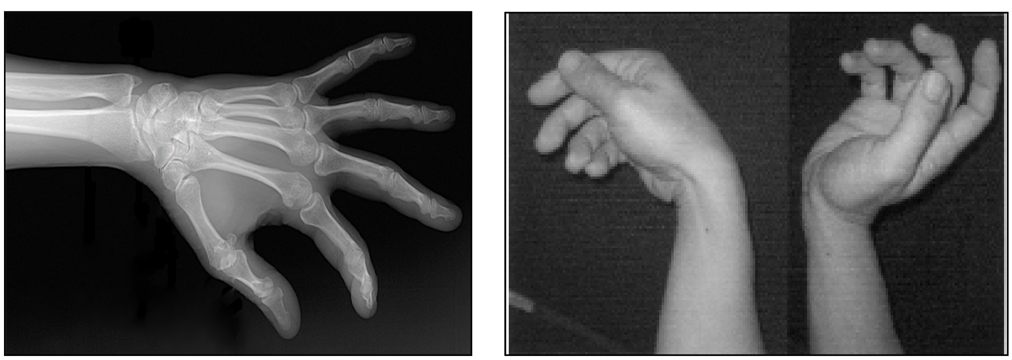

Figure 8 Combinations of wrist movements, radiodorsal and ulnopalmar rotations [1], [8].

2.3. Modeling of Wrist in Literature

Three-dimensional models for the wrist become more accurate with development of new medical imaging technologies and advances in mechanical modeling and simulation. Computed tomography (CT) is one of the most popular and reliable method of imaging bones, ligaments and even nerves.

Recent studies about modeling of human wrist are generally concentrated on finite element modeling. Especially load distributions among proximal row of carpal bones (scaphoid, lunatum, and triquetrum) and radius-ulna are studied. These bones are preferred because most of the load is transmitted from proximal row to radius and ulna.

Scapholunate ligament tear is one of the most common wrist injuries. Johnston et al. [9] states "it is likely that wrist ligaments play a major stabilizing role during these motions and under load. In particular, the scapholunate ligament is believed to be especially critical to normal wrist function". Moeini et al. [10] states the significance of scapholunate ligament as "among the carpal ligaments, the scapholunate is one of the most important, since the stability of the wrist mostly depends this ligament's strength". In section 4.2.2. scapholunate ligament tear and resulting load distributions on the wrist was studied; surgical treatment methods were also examined.

Green et al. [11] studied three-dimensional modeling and animation of two carpal bones. From computed tomography (CT scan) a model is obtained and using an animation software, motions of the bones are observed. Inter bone distances are evaluated with the help of animation software for flexion, extension, radial and ulnar deviation. In Figure 9 a sample picture from the study is given where inter carpal distance between scaphoid and lunatum is obtained.

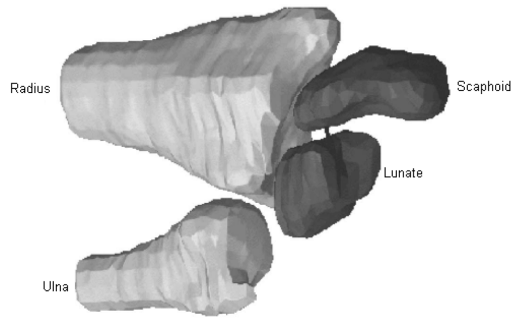

Figure 9 Finite element modeling of two carpal bones.

Another study about carpal load distribution in a static neutral posture is published by Carrigan et al. [12]. CT data of the bones are used in a finite element analysis software and static load distribution under axial loading is examined.

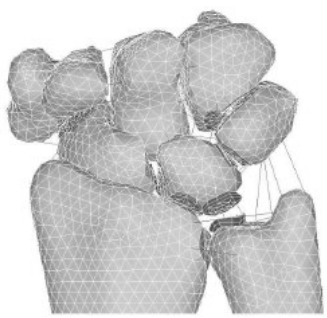

Figure 10 Dorsal view of carpal structure with bones and ligaments [12].

Carpal kinematics of the wrist is examined in a study of in vitro kinematics, published by Crisco et al. [6]. Scapholunate interosseous ligament tear is observed for flexion and extension motion. The difference between injured and healthy patients is compared. Figure 11 simply gives the results of the study, first principal inertial axis of capitate, scaphoid and lunate for normal (N), injured (I) and uninjured (U) wrists are given for comparison (uninjured wrists are the healthy wrists of the patients with injured wrists) [6].

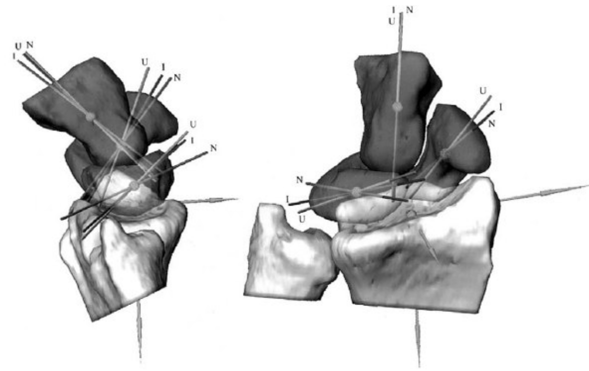

Figure 11 First principal inertial axis of capitate, scaphoid and lunate for normal (N), injured (I, Scapholunate interosseous ligament tear) and uninjured (U) wrists.

In literature, generally in vivo and in vitro kinematics is studied by using finite element method. Using medical imaging data, a three-dimensional model is built up and load distributions are observed. Such models are used for local studies with two or three bones.

In finite element analysis method, wrist is modeled as deformable flexible bodies and the resulting forces on the flexible bodies are evaluated, but in this study wrist bones were modeled as rigid elements and using a multi-body dynamics code MSC. ADAMS 2003 (MSC. Software Corporation, United States of America) wrist was analyzed with rigid multi-body dynamics. All of the wrist bones were modeled as rigid bodies that the deformation was not a parameter for contact forces. Ligaments and joints were modeled as deformable structures for connecting rigid bones.
In literature, there is a need for a wrist model containing whole wrist structure and load distributions among all carpal bones and ligaments. Not only static loading, but also quasi-static loading for flexion, extension, radial and ulnar deviation motions is required for a complete study of the wrist.

This study satisfies the need for a complete wrist model analyzing the quasi-static load distributions for the wrist.

In chapter 3, the detailed methodology for building up the three-dimensional model of the wrist is explained.

CHAPTER 3

METHODOLOGY

This study is focused on building a realistic biomechanical wrist model, which can be used to examine both static and quasi-static loading of the wrist. A three-dimensional model was used for investigation of mechanics of the wrist. Healthy and injured wrists were analyzed and differences for load distributions were compared. For treatment methods of injured wrists, effects of surgical operations were studied.

For modeling and analyzing the wrist MSC. ADAMS 2003 software was used. All ligaments, joints and contact structures were manually located on the three-dimensional bone models.

Three-dimensional model was built up step by step and mainly four structures were developed: Firstly, geometry of the bone structures were obtained by CT scan data; then contacts and joints between wrist bones were modeled. Finally, ligaments were placed between wrist bones according to the anatomic locations [5], [13]. Muscles were not used in the model; instead external forces were used as actuators.

Detailed explanations about three-dimensional wrist modeling and analysis are presented in the following sections.

3.1. Three-Dimensional Modeling of the Wrist

Three-dimensional model of the wrist includes bones, ligaments, joints and external forces (actuators as muscles). Effects of all these components are different for the wrist mechanism.

A simple joint model is defined for explaining how three-dimensional model was built. Bones were connected to each other with ligaments and joints. Bones could be in contact with each other or come into contact with each other under the effect of muscle contractions and external forces. So, a contact was defined between the wrist bones which is shown in Figure 12.

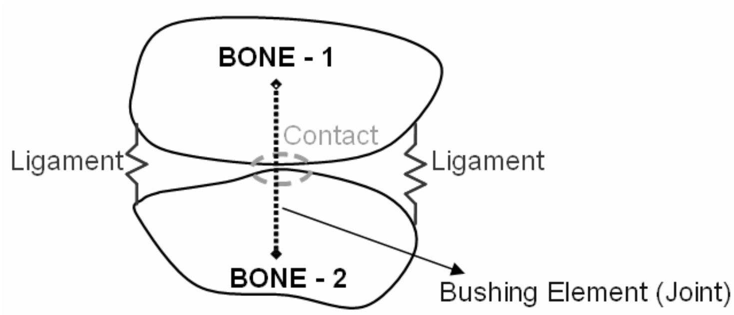

Figure 12 Bone, ligament, joint and contact structure of the three-dimensional model.

3.1.1. Modeling of Wrist Bones

Computed tomography (CT) scan was used for building three-dimensional bone structures that the real sizes and shapes of the bones were kept as original. CT data (Dicom images) of author's right wrist was taken as CAD data where the wrist was scanned slice by slice. CT scan device of GE Medical Systems was used for imaging the wrist where the thickness of each slice was 1.25 mm. Figure 13 shows the palmar and dorsal view of the three-dimensional bone models. On the wrist six bones were shown in different color, the purpose was to show the fixed and mobile bones of the wrist. Tubiana [14] indicates distal row of carpal bones, second and third metacarpals act as if they are fixed (i.e. relative motions of these bones with respect to each other are negligible).

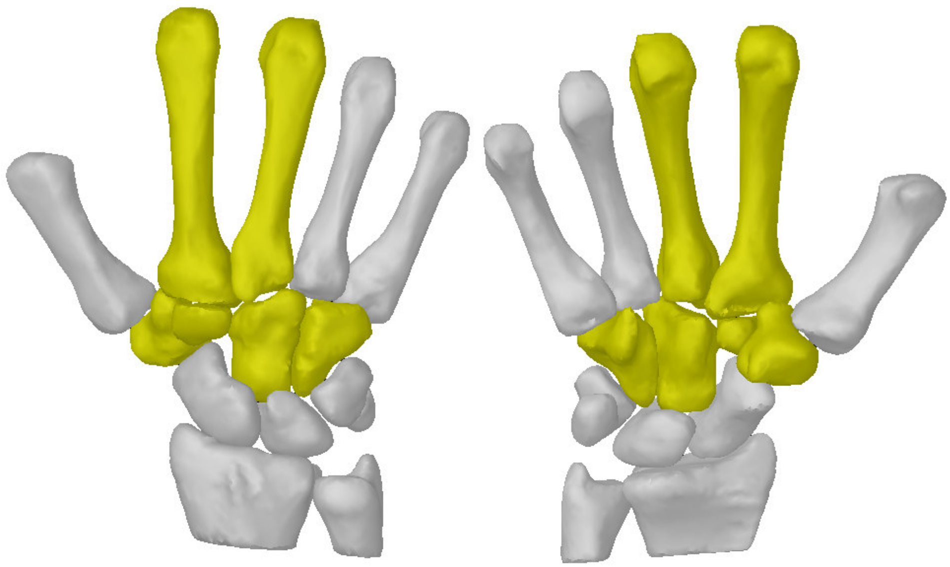

Figure 13 Bones of the wrist: dorsal view on the left, palmar view on the right. Bone models are the author's own CT scan of the right hand.

In three-dimensional model these bones were fixed to each other, so that model was simplified since there was no need for a joint or a ligament for these bones. Only joints and ligaments surrounding these bones were used. This simplification also made analysis faster and easier.

Bones can be assumed as the main structure of the whole system. Wrist contains large number of small bones and these bones have three main motion types. An and Chao [15] define three motion types as: spinning, rolling and sliding. Although for mechanical engineering spinning can be obtained by combining rolling (without slipping) and sliding.

Joints, ligaments and contact between wrist bones were modeled in order to provide all three motion types.

In Figure 14, 2D definitions of spinning, sliding and rolling motions for two bones are given [15].

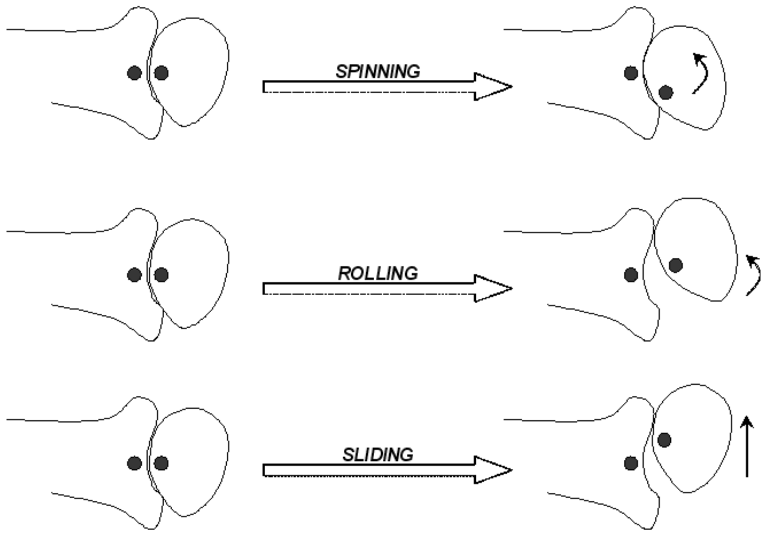

Figure 14 Three types of motions for the bones: spinning, rolling and sliding.

3.1.2. Modeling of Contact Between Wrist Bones

For the unloaded free position of the hand some wrist bones are initially in contact with each other, but some bones are not. In Figure 15 a contact can be observed between capitatum and lunatum. But, between radius / scaphoid and radius / lunatum a contact can not be observed.

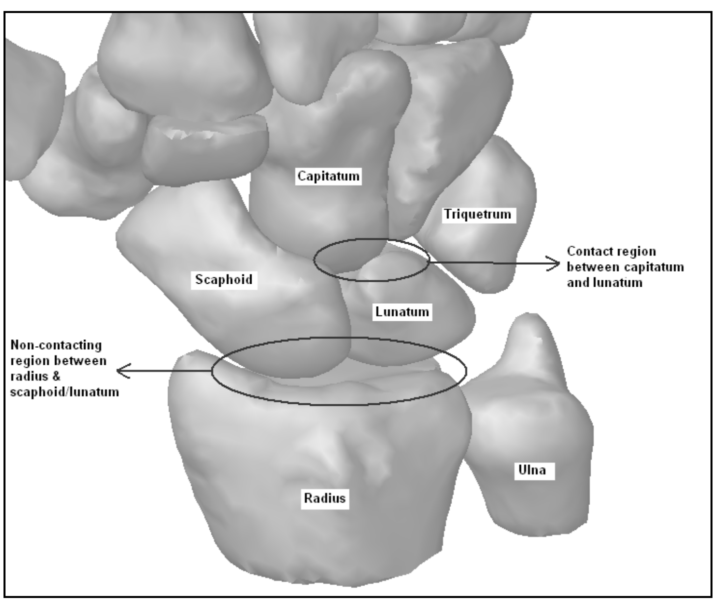

Figure 15 Contacting and non-contacting bones of the wrist.

Under axial loading (compressive), scaphoid and lunatum move towards radius where a contact starts. When the axial load is removed scaphoid and lunatum get back to the initial position preserving the initial gap.

Frictional force between wrist bones was assumed to be zero. An and Chao [15] states synovial fluid provides perfect lubrication between the bones that the frictional force can assumed to be zero. The assumption of zero frictional force between bones (under contact) was a very important simplification for the three-dimensional model. Assumption of zero friction force reduced the number of calculations and analysis time.

For defining a contact between wrist bones; a penetration depth was defined for deformation but taken as a small value for the assumption of rigid bodies (bones).
MSC. ADAMS needs an impact force exponent (e) for contact elements. Force exponent (e) defines the stiffening characteristics of the contact. If “e > 1” contact has stiffening characteristics, if “e < 1” contact has softening characteristics. For modeling contact of bones in MSC. ADAMS value of “e” is generally taken as ~1.1.

Simply below formula defines the contact force:

$$F = \left[(k \cdot d) + (C \cdot v)\right] \cdot e \qquad \text{(Equation 1)}$$

Definitions of the variables are:

$F =$ Contact force	$C =$ Contact damping
$k =$ Contact stiffness	$v =$ Penetration velocity
$d =$ Penetration depth	$e =$ Impact force exponent

Penetration depth (d) for contact algorithm was taken as 0.01 mm; a small value was used for the assumption of rigid bodies. Damping (C) and stiffness (k) values for contact are given in Appendix A. Damping and stiffness values were defined for general applications of bone like biomaterials in MSC. ADAMS. Also, many trials were done in order to tune the model for the analyzing the wrist (with the supervision of hand surgeons).

In the wrist model, radius and ulna were fixed in space and six wrist bones were attached to each other (trapezoid, trapezium, capitatum, hamatum, second and third metacarpal bones). In the wrist model there were eight movable parts therefore degrees of freedom of the model was 48.

3.1.3. Modeling of Wrist Joints

Joints between the wrist bones were modeled as bushing elements in MSC. ADAMS. Bushing elements are three-dimensional joints which have translational and rotational spring/damper components. So, joints of the wrist or synovial fluid were modeled as bushing elements.

Wrist joint is actually enclosed by the synovial membrane which is filled with synovial fluid. As the synovial fluid provides zero friction force for the contact, the stiffness and damping coefficients for the joints were taken as small values in the direction of bone movements (both for rotational and translational). Bushing elements' stiffness and damping coefficients are presnted in Appendix B.

Bushing elements were attached to the centroid of wrist bones. In Figure 16 two-dimensional illustration of a bushing element is given. Bones were connected from center of mass points.

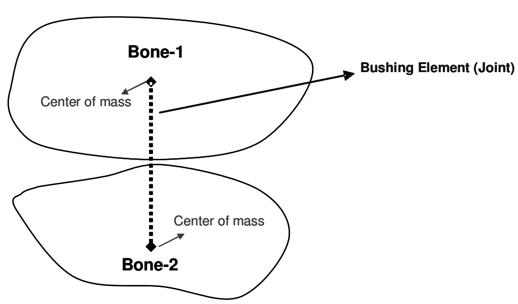

Figure 16 Modeling of bushing elements.

Bushing elements were also helpful in modeling soft tissues of the hand. Soft tissues were not modeled as the components of the wrist but stiffness and damping characteristics were simulated by bushing elements (joints).

3.1.4. Modeling of Wrist Ligaments

Ligaments are spring like structures between bones for supporting and limiting the motion range of the movements. Ligaments are active only in tension and inactive in compression that is why ligaments are mechanically similar to the packet rubber bands.

In Figure 17, a ligament example is shown which exerts 100 N force under elongation of 2 mm. Ligaments do not have a linear stiffness value, a parabolic curve is drawn for reaching 2 mm of elongation under the force of 100N.

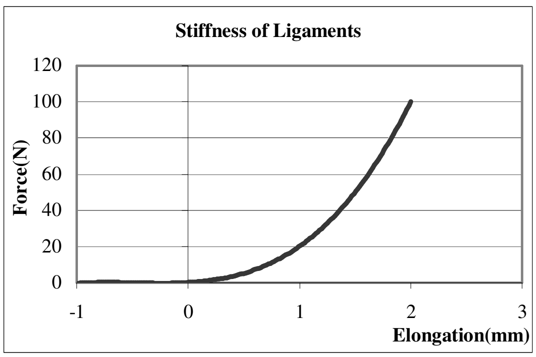

Figure 17 Stiffening properties of ligaments.

Damping values for the ligaments are also nonlinear as shown in Figure 18.

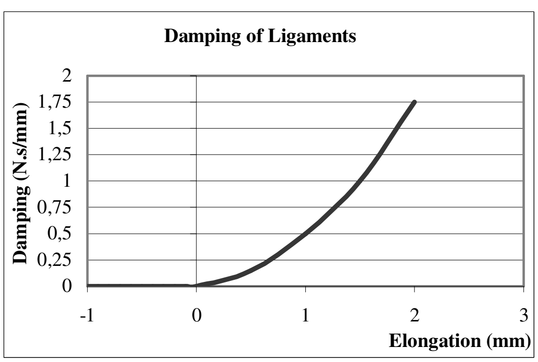

Figure 18 Damping properties of ligaments.

In order to reach the defined stiffness and damping values (from literature) different cubic splines were used in the model. Carrigan et al. [12] defines the stiffness of the scapholunate ligament as 230 N/mm and in the model a cubic spline was used to define the stiffness of scapholunate ligament as shown in Figure 19. Another important point about stiffness values of the ligaments was slope of the cubic splines at zero elongation was also zero.

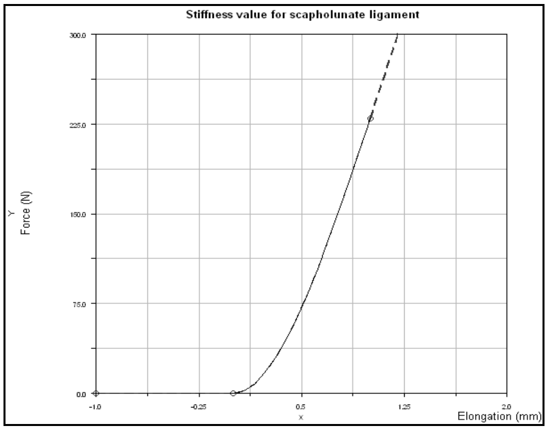

Figure 19 Cubic spline defining the stiffness value of scapholunate ligament.

Totally 52 ligaments were used in the model. Palmar and dorsal views of the ligaments are shown in Figure 20:

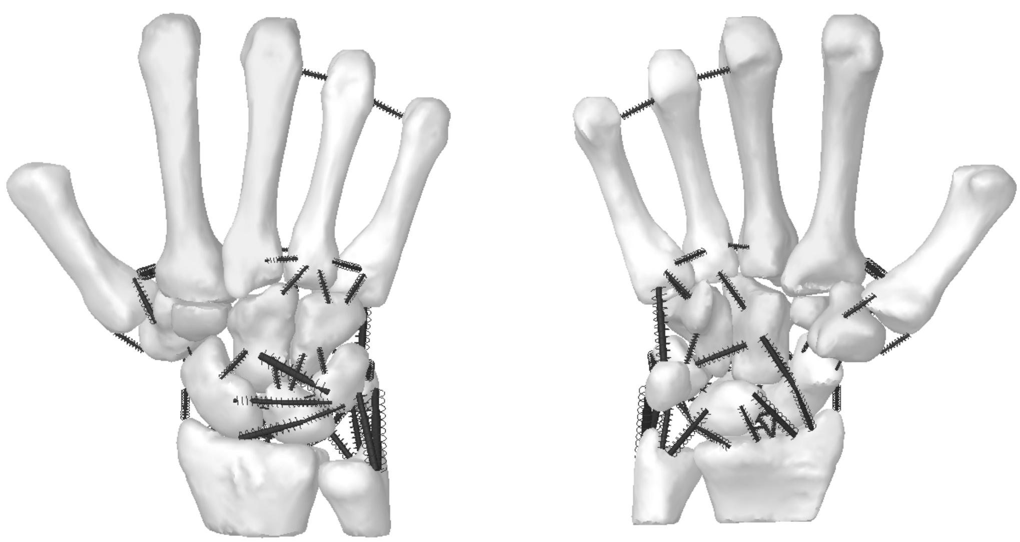

Figure 20 Ligaments of the wrist located on the three-dimensional model (dorsal side on the left, palmar side on the right).

Some of the ligaments were modeled as more than one spring damper pairs. In Figure 21 examples for ligaments having more than one part were given. In three-dimensional model scaholunotriquetral, radiolunotriquetral and radioscaphocapitate ligaments were modeled by two spring-damper pairs where scapholunate, lunotriquetral and scaphotrapezial ligaments were modeled by three spring-damper pairs.

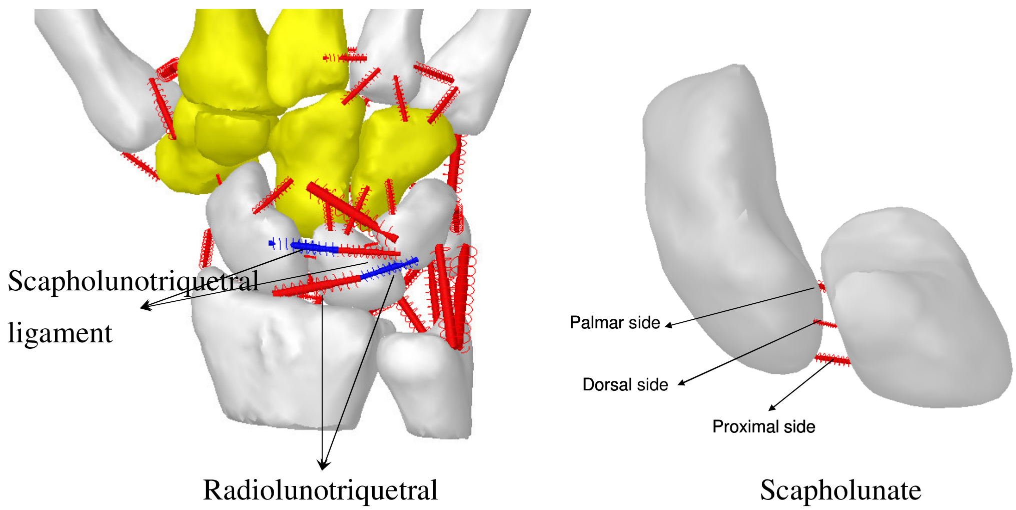

Figure 21 Ligaments modeled by more than a single spring-damper pair.

Scaholunotriquetral and radiolunotriquetral ligaments have three attachment points; therefore ligaments were divided into two parts having the same mechanical properties. Only the length of the second part is different from the first part due to the location of insertion points. Number of fibres in each ligament part does not change significantly so that two parts have same mechanical properties. In Interactive Hand Anatomy [5] dorsal radiolunotriquetral (radiocarpal) ligament is defined as "The dorsal radiocarpal ligament courses from the postero-distal radius to the ulnar side of the carpus. It attaches principally to the triquetral but also to the lunate". This means that radiolunotriquetral ligament has two insertions connected to three different bones with the same mechanical properties.

Scapholunate is a special ligament having a “U” shaped structure; starts from palmar side, continues to proximal side and ends at the dorsal side. In Interactive Hand Anatomy [5] scapholunate ligament is shown as three parts (Figure 22):

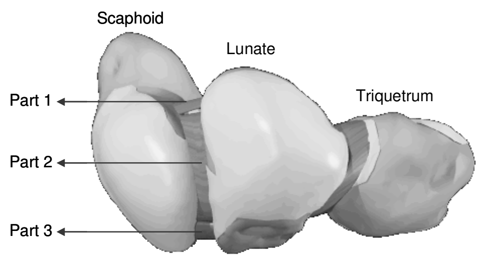

Figure 22 Proximal view of scapholunate ligament [5]; part 1 is on the palmar side, part 2 is on the proximal side, part 3 is on the dorsal side of the wrist.

Carrigan et al. [12] and Nowak et al. [16] have in vivo studies for calculating stiffness values of ligaments. Experimental tensile tests are completed to find mechanical properties of wrist ligaments. Fresh frozen cadavers are used for tensile tests. In three-dimensional model results of these studies were used for ligaments' stiffness values. Wrist ligaments' names, locations (insertions to the wrist bones), stiffness and damping values (used in three-dimensional model) are presented in Appendix C.

3.1.5. Modeling of External Forces for Wrist Motions

Muscles of the wrist were not used in three-dimensional model. External forces were used to simulate the movements of hand which are controlled by muscle contraction forces. For analyzing the wrist four main motion types were examined: flexion, extension, radial deviation and ulnar deviation. Therefore, to simulate the muscle contraction forces on the bones external forces were defined.

External forces were applied to the third metacarpal bone (Figure 23). As explained before third metacarpal bone is one of the bones of rigidly modeled bone group. Application of external forces on one of these bones had the advantage of controlling whole wrist rotation from a single bone. Also a single component force was enough to rotate whole model from just one location.

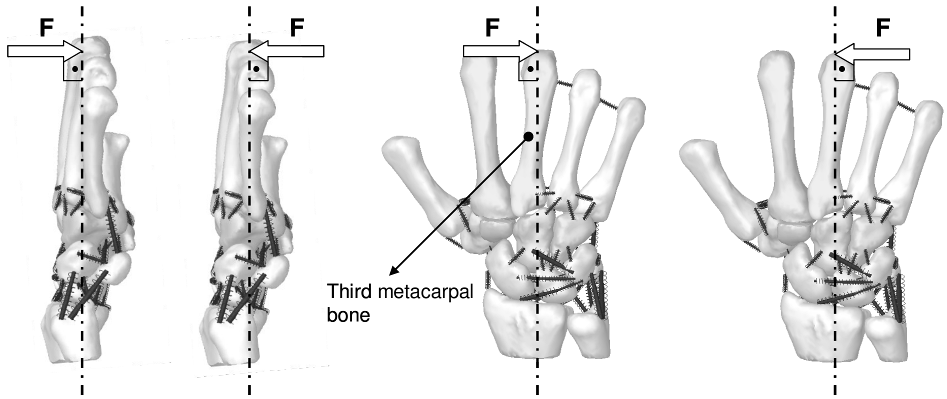

Figure 23 Definition of forces for hand movements. From left to the right forces for flexion, extension, ulnar deviation and radial deviation are defined.

Forces were applied to the distal pole of the third metacarpal bone. For flexion and extension motions forces were perpendicular to the palmar or dorsal plane. For radial and ulnar deviation motions forces were on the palmar or dorsal plane, perpendicular to the central axis of the third metacarpal bone. Forces were moving with third metacarpal bone; always being perpendicular to the third metacarpal bone. Also, magnitudes of forces were constant at any instant time for the analysis. Figure 24 represents an example for application of external forces for flexion motion, magnitude of the force was constant and the force was always perpendicular to the third metacarpal bone.

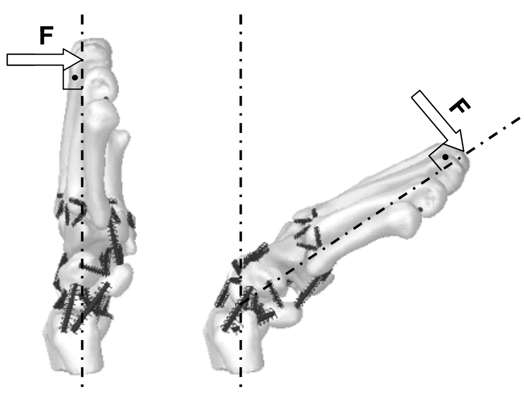

Figure 24 External forces with constant magnitude, perpendicular to the third metacarpal bone.

The same method was used for extension, radial and ulnar deviation motions. But for each different case directions of forces were changed.

In Chapter 4 applications of external forces and resulting wrist motions are studied in detail.

CHAPTER 4

RESULTS

Three-dimensional model of the wrist was studied for both healthy (uninjured) and injured wrists. Four main motions of the wrist (flexion, extension, radial deviation and ulnar deviation) and axial loading were examined for healthy and injured wrists.

For healthy wrist model, results of the analysis were compared with the real life orthopaedics and data from literature.

For injured wrist models, pathological or surgical treatment methods were similarly applied to the three-dimensional model. The injured wrists and the treated wrists were analyzed and the mechanical results of the surgical operations were compared.

4.1. Analysis of Healthy Wrists

4.1.1. Flexion Motion of the Wrist Joint

Flexion motion of the wrist was simulated with a single force applied to the upper pole of third metacarpal bone. Force was constant with magnitude of 20 N and modeled as moving with third metacarpal bone. During motion of the wrist, the angle between the force and the third metacarpal bone was always 90 degrees.

20 N force is a general magnitude force for the hand to rotate for flexion to reach the motion limit. Beyazova et al. states motion limit of the wrist for flexion is around 80 degrees [17].

20 N force was applied for analyzing the flexion motion as defined in Figure 25:

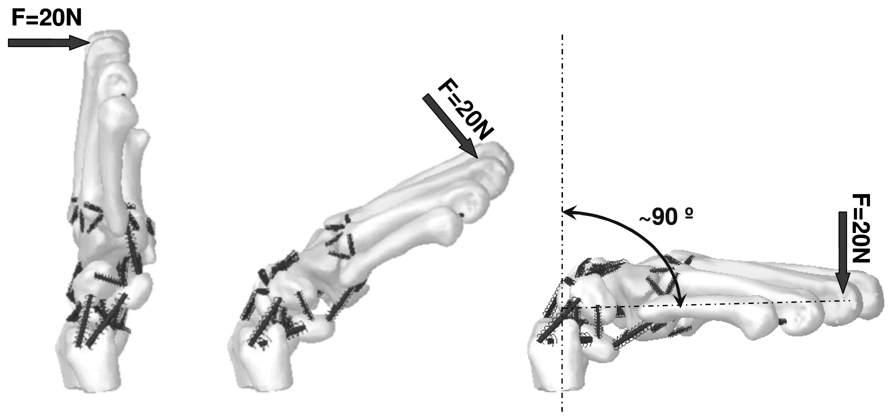

Figure 25 Flexion motion of a healthy wrist in three-dimensional model.

The results of the analysis (three-dimensional model) for 20 N force revealed that flexion motion made approximately 90 degrees of rotation with respect to the initial situation. Maximum flexion angle was also measured from the author’ s hand (since the bone models belong to the author) that maximum 90 degrees of flexion was found as in three-dimensional model. Therefore, 90 degrees of flexion was an appropriate result comparing the real life.

Load distributions on bones, ligaments, joints and contact forces for flexion motion are presented below:

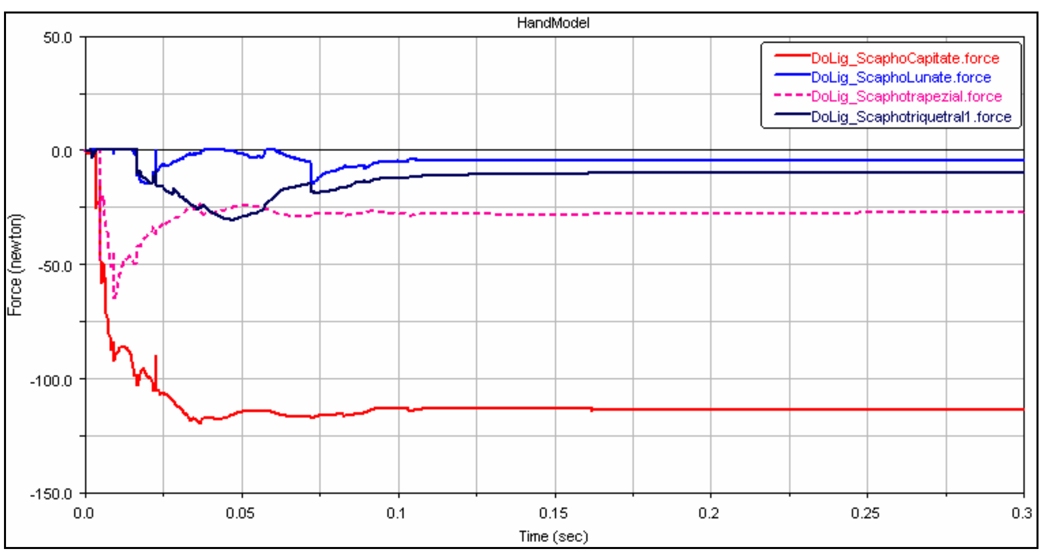

Figure 26 Load distributions of dorsal scaphoid ligaments for flexion motion.

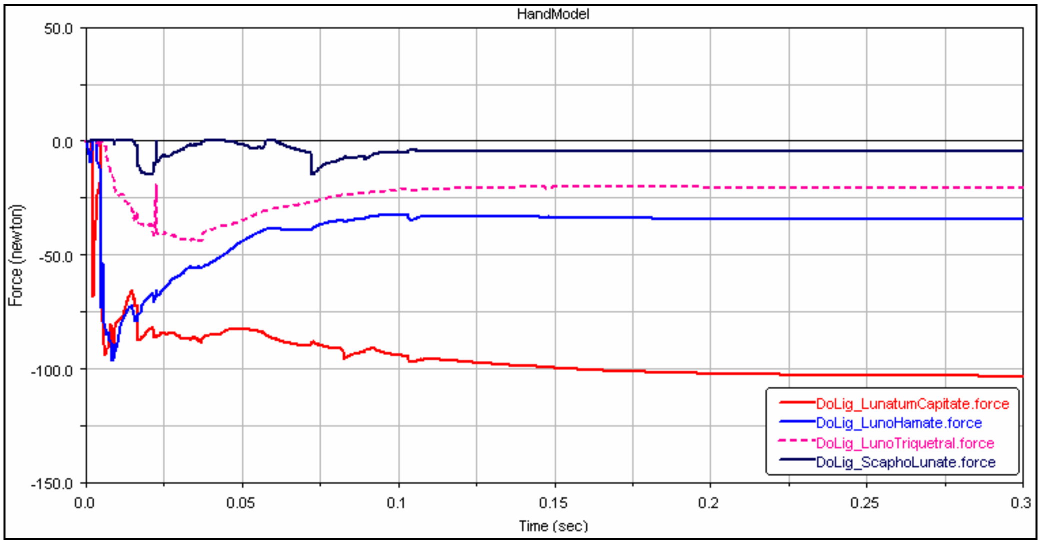

Figure 27 Load distributions of dorsal lunatum ligaments for flexion motion.

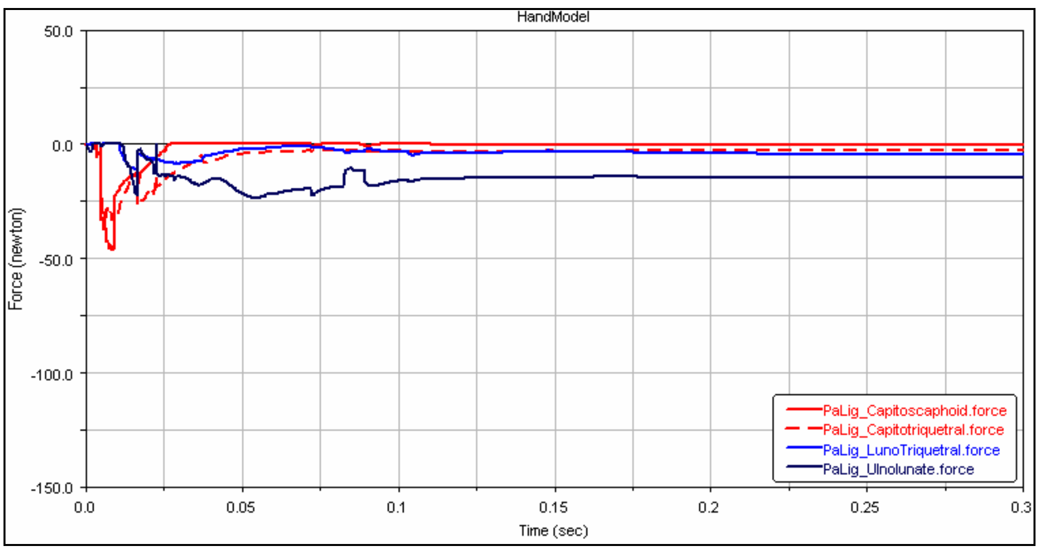

Figure 28 Load distributions of palmar ligaments for flexion motion.

For flexion motion, dorsal ligaments were expected to be in tension and palmar ligaments were expected to be in compression. Since ligaments are active only under tensile forces, maximum loads were expected to be on the dorsal side of the wrist for flexion motion. Load distributions in Figure 26, Figure 27 and Figure 28 indicated that the loads carried by dorsal ligaments were much higher than the loads on palmar ligaments for flexion motion. Palmar ligaments had relatively small force values caused by rotations of the wrist bones. Among dorsal ligaments scaphocapitate and lunocapitate ligaments carried higher loads.

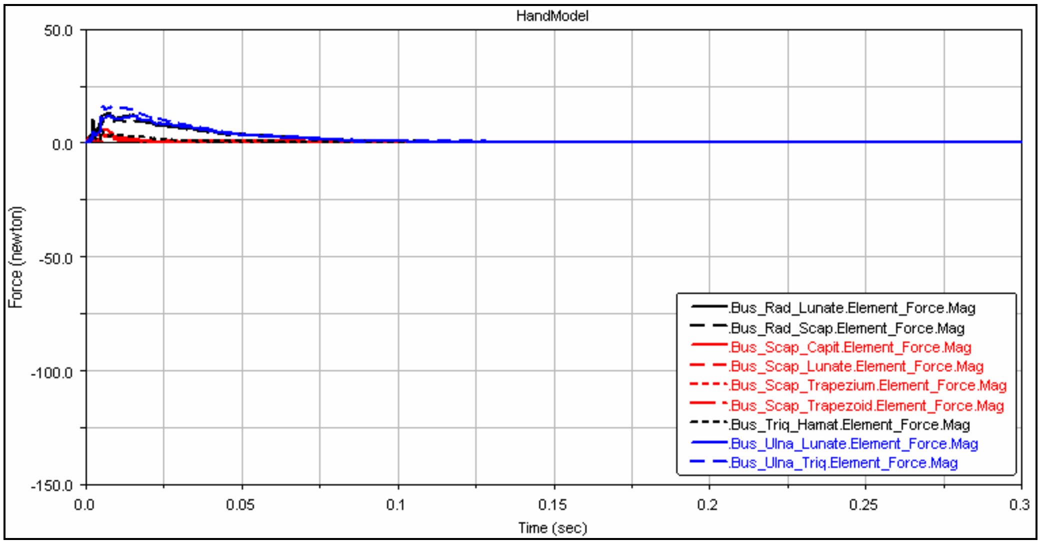

Figure 29 Load distributions of joints (bushing elements) for flexion motion.

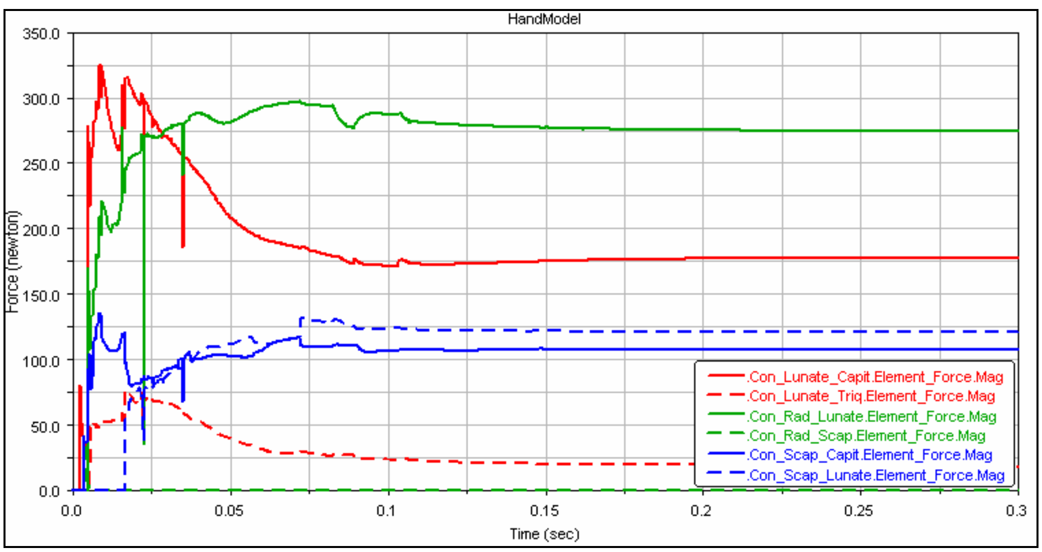

Figure 30 Load distributions of contact forces for flexion motion.

Bushing elements (joints) had lower force values compared to the ligaments and contact forces (Figure 29). This kind of loading was expected that the stiffness and damping values of joints were taken as very small in three-dimensional model.

Especially for contact forces between mid-carpal bones, large amount of the load was transferred from capitatum to scaphoid and lunatum for flexion motion (Figure 30). Load transferred from capitatum to the lunatum was about 175 N and the load transferred from capitatum to the scaphoid was about 110 N. So, maximum load was carried by lunatum and capitatum bones in mid-carpal region.

Mid-carpal contact loads were transferred to the forearm from lunatum to the radius. Due to the rotation of the wrist bones scaphoid did not have a contact with radius. Thus, carrying most of the load in mid-carpal region and transferring to the forearm, lunatum bone was the main pivot point for flexion motion.

4.1.2. Extension Motion of the Wrist Joint

Extension motion of the wrist was simulated with a single force applied to the upper pole of third metacarpal bone. Force was constant with magnitude of 20 N and modeled as a moving load with third metacarpal bone. During motion of the wrist, the angle between the force and the third metacarpal bone was always 90 degrees.

20 N force is a general magnitude force for the hand to rotate for extension to reach the motion limit. Beyazova et al. states motion limit of the wrist for extension is around 70 degrees [17].

The results of the analysis (three-dimensional model) for 20 N force showed that extension motion made approximately 90 degrees of rotation with respect to the initial situation. Maximum extension angle was measured from the author's hand (since the bone models belong to the author) that maximum 90 degrees of flexion was found as in three-dimensional model. So, 90 degrees of flexion was an appropriate result comparing real life.

20 N force was applied for analyzing the flexion and extension motion as defined in Figure 31:

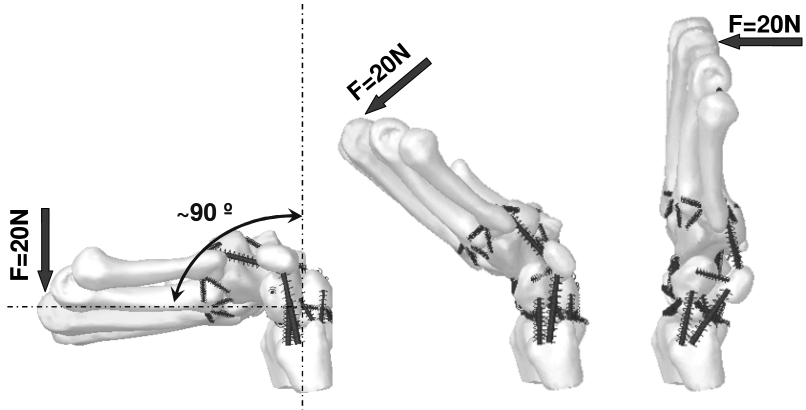

Figure 31 Extension motion of a healthy wrist in three-dimensional model.

Load distributions on bones, ligaments, joints and contact forces for extension motion are given below:

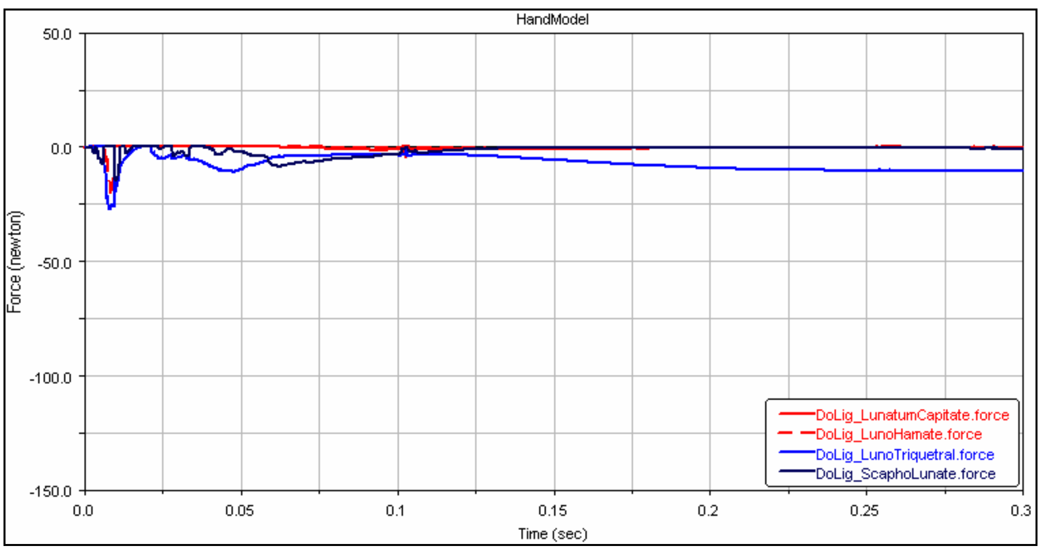

Figure 32 Load distributions of dorsal ligaments of lunatum for extension.

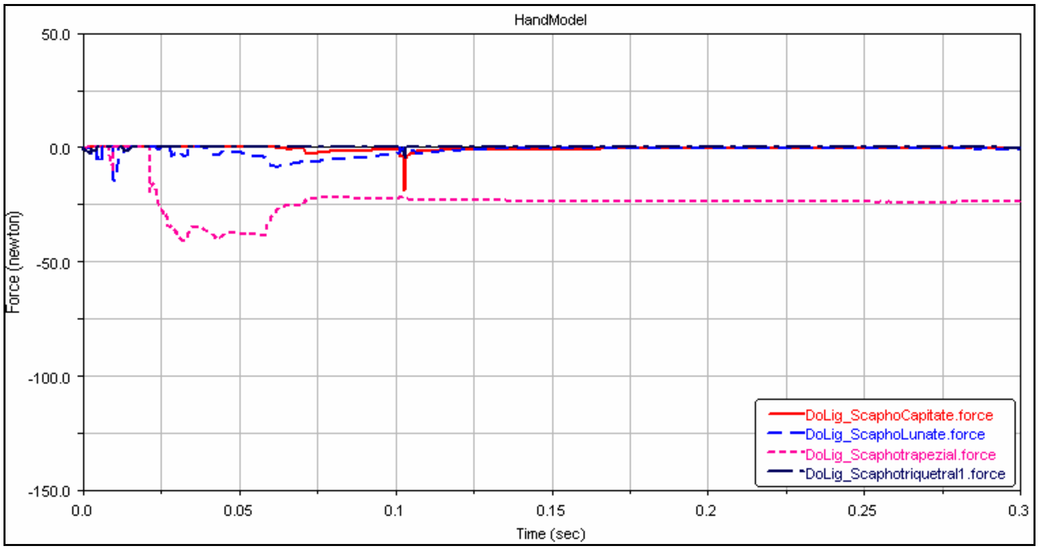

Figure 33 Load distributions of dorsal ligaments of scaphoid for extension.

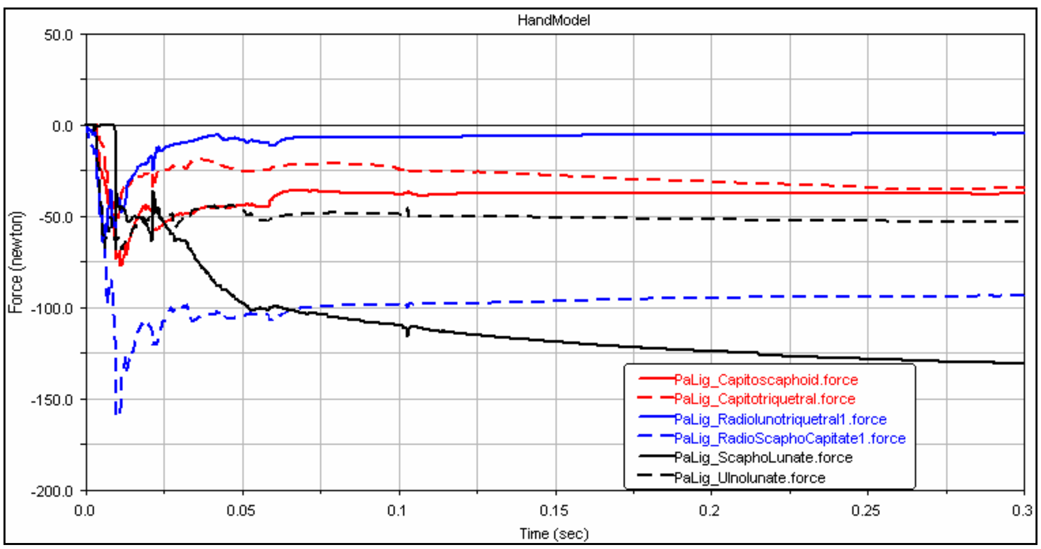

Figure 34 Load distributions of palmar ligaments for extension.

For extension motion, dorsal ligaments were expected to be in compression and palmar ligaments were expected to be in tension, thus palmar ligaments were expected to carry maximum loads. Load distributions in Figure 32, Figure 33 and Figure 34 indicated that the loads carried by palmar ligaments were much higher than the loads on dorsal ligaments for extension motion.

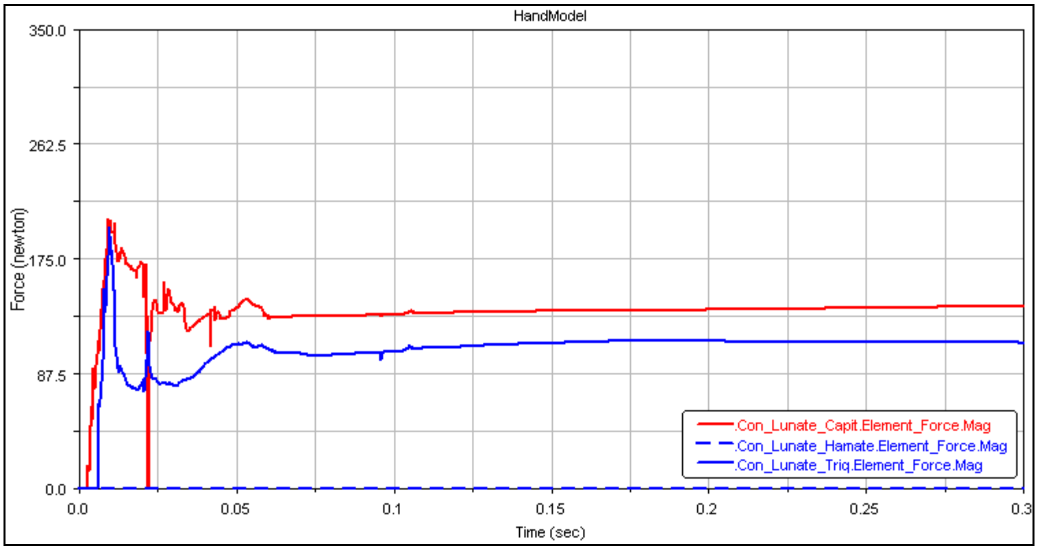

Figure 35 Contact force distributions of lunatum for extension.

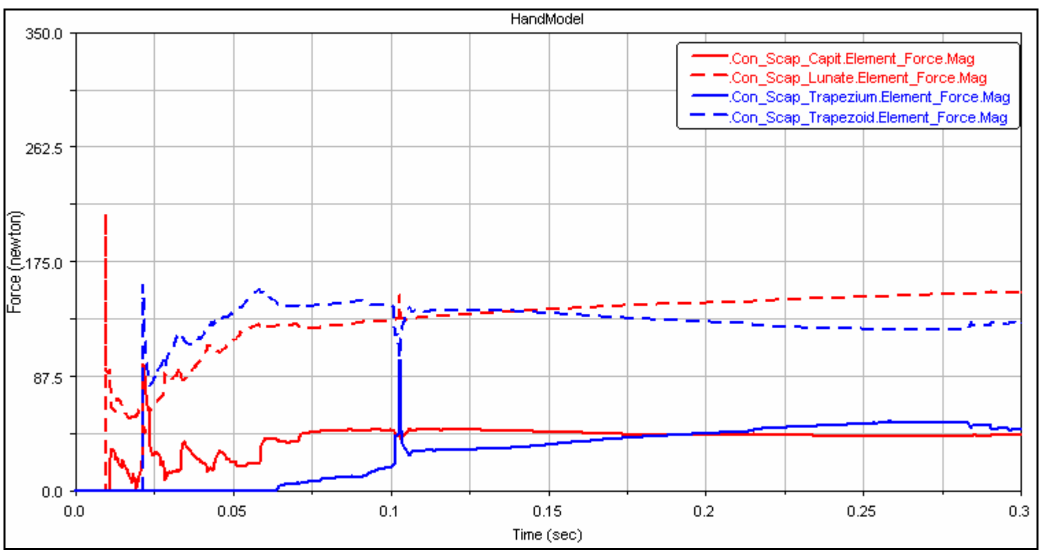

Figure 36 Contact force distributions of scaphoid for extension.

For mid-carpal contact forces, large amount of the load was transferred from capitatum to scaphoid and lunatum for extension motion (Figure 35 and Figure 36). Analysis for extension motion showed that most of the load was carried by scaphoid. As the results in Figure 37 were evaluated, the contact force between scaphoid and radius was larger than the contact force between lunatum and radius. This means that scaphoid was the critical bone carrying most of the load for extension motion.

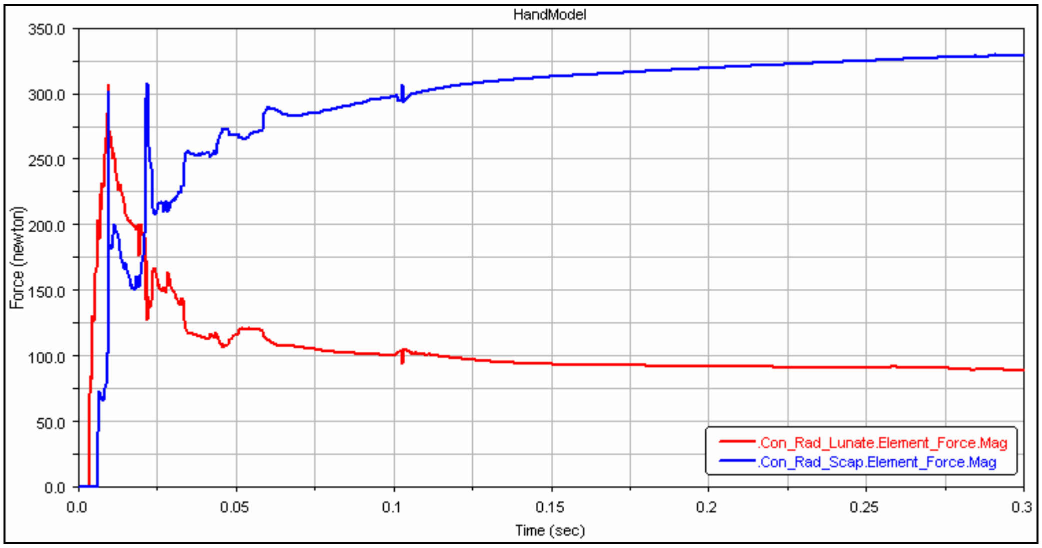

Figure 37 Contact force distributions of radius for extension.

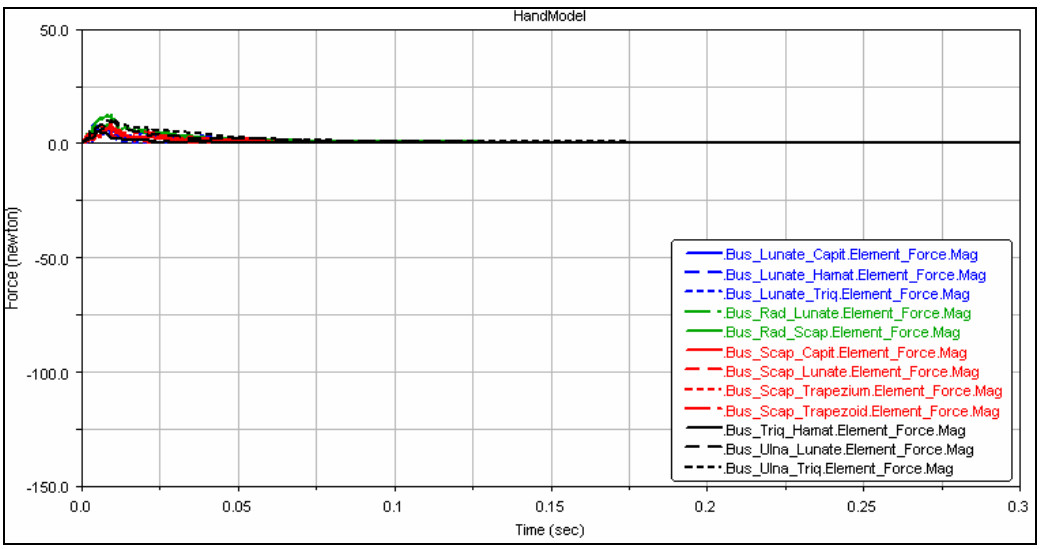

Figure 38 Joint load distributions for extension.

Forces on joints (bushing elements) were very small as shown in Figure 38. That was an expected result since the joints were not modeled as stiff components.

4.1.3. Ulnar and Radial Deviation Motions of the Wrist Joint

Like flexion and extension motions, 20 N constant force was applied to the upper pole of the third metacarpal bone. During motion of the wrist, the angle between the force and the third metacarpal bone was always 90 degrees (on palmar plane).

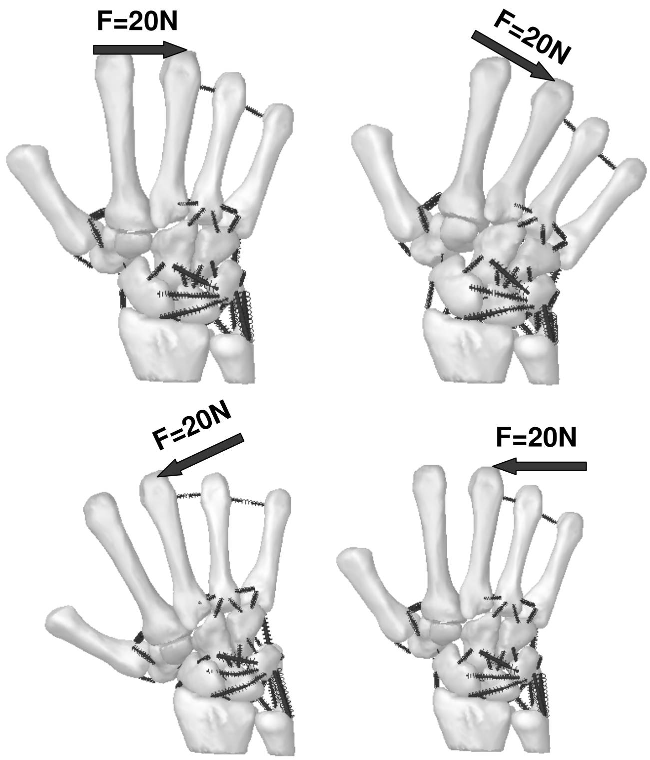

Figure 39 Ulnar deviation (on the top) and radial deviation (on the bottom) of healthy wrist.

Moritomo et al. [8] defines the motion of the scaphoid and lunatum as “During wrist radial deviation the proximal portion of the scaphoid, the lunate, and the triquetrum moved radiodorsally and the distal portion of the scaphoid moved ulnopalmarly relative to the capitate”. Figure 40 shows the sliding motion of scaphoid and lunatum bones for radial and ulnar deviation [8].

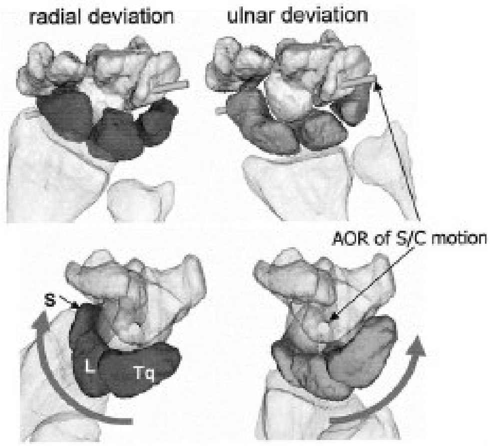

Figure 40 Sliding motions of scaphoid and lunatum for ulnar and radial deviation [8].

Moojen et al. [18] defines the radial and ulnar deviation motion as “At 20º radial deviation of the wrist, the scaphoid flexes an average of 15º (range 5-27º). At 20º ulnar deviation of the wrist, the mean extension of the scaphoid was 20º (range 0–36º) with an average of 10º of ulnar deviation, relative to the radius”.

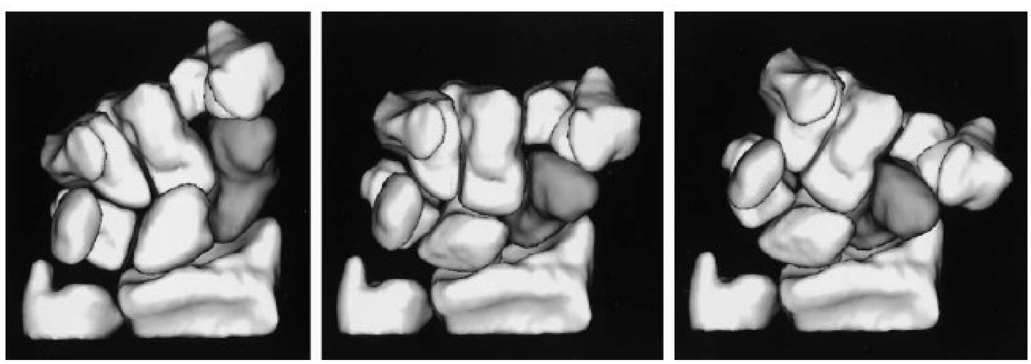

Figure 41 Radial and ulnar deviation of the wrist; first picture is ulnar deviation motion, second and third pictures are redial deviation motion [18].

Nuttall et al. [19] states “... the scaphoid can either flex, translate or supinate on the radius, or more commonly move by combination of two or three of these during radial and ulnar deviation”. Analysis results of ulnar and radial deviation motions are presented in detail on the following pages.

4.1.3.A. Ulnar Deviation Motion of the Wrist Joint

Beyazova et al. [17] states motion limits of the wrist for ulnar deviation is approximately 30 degrees. The results of the analysis (three-dimensional model) for 20 N force showed that ulnar deviation motion made approximately 30 degrees of rotation, which is consistent with the studies of Beyazova et al [17].

From Figure 42 to Figure 45 loads on palmar and dorsal ligaments are presented. Analysis of ulnar deviation motion showed that dorsal ligaments of lonucapitate, scaphocapitate, scaphotrapezial and palmar ligament radialcollateral were the main supporting elements of the wrist. Palmar radial collateral ligament was expected to carry a higher load due to the location of being on the upper most pole of the radius. Radial collateral ligament was the most distant ligament to the center of rotation for ulnar deviation. Lunocapitate, scaphocapitate and scaphotrapezial ligaments had high tensile forces because these ligaments supported the mid-carpal region during ulnar deviation motion.

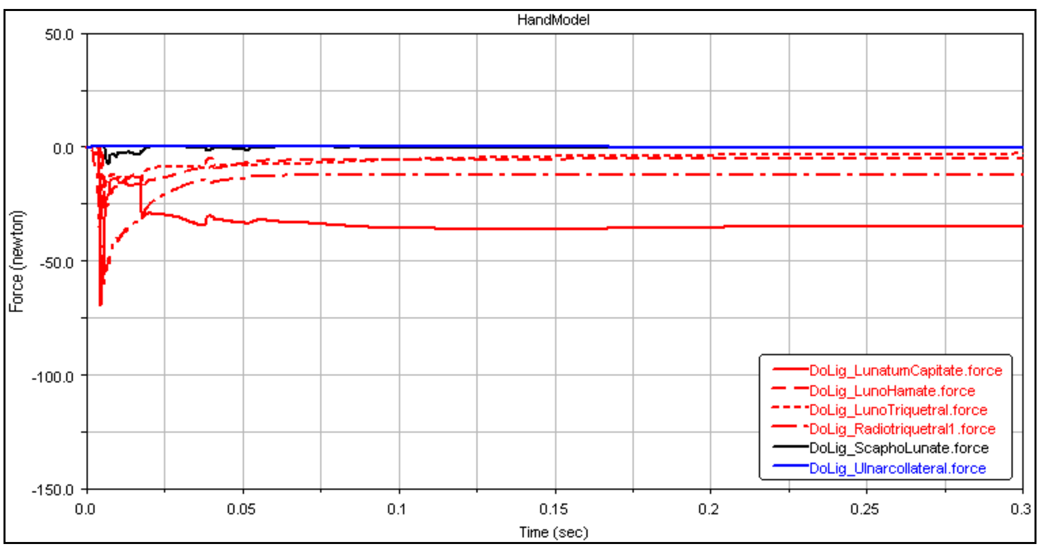

Figure 42 Load distributions of dorsal ligaments of lunatum and radius for ulnar deviation.

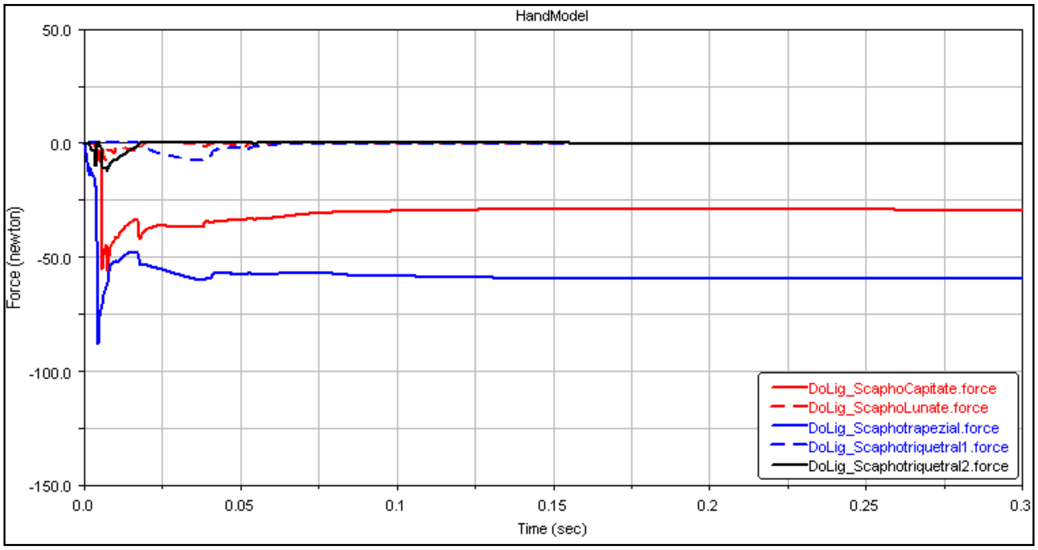

Figure 43 Load distributions of dorsal ligaments of scaphoid for ulnar deviation.

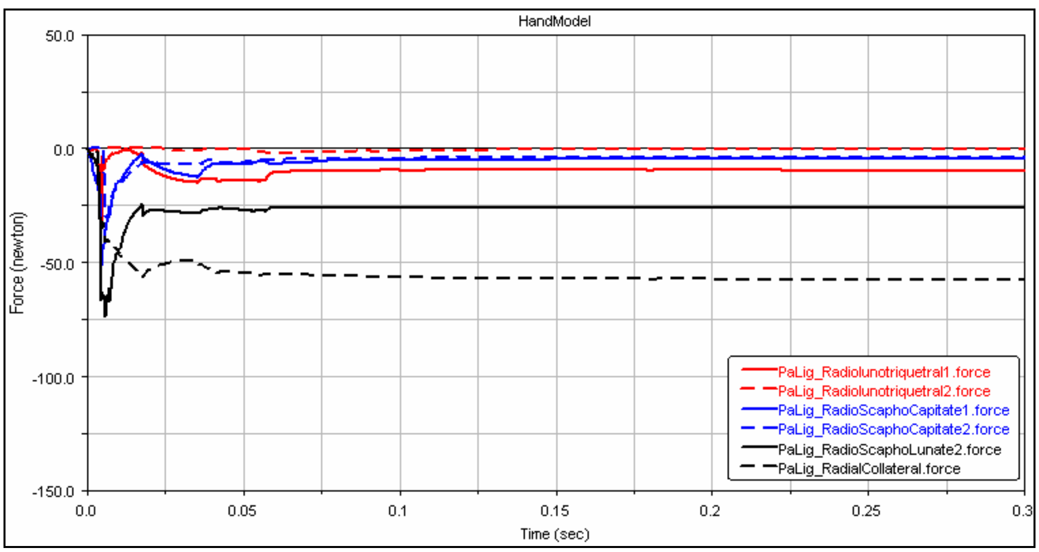

Figure 44 Load distributions of palmar ligaments of radius for ulnar deviation.

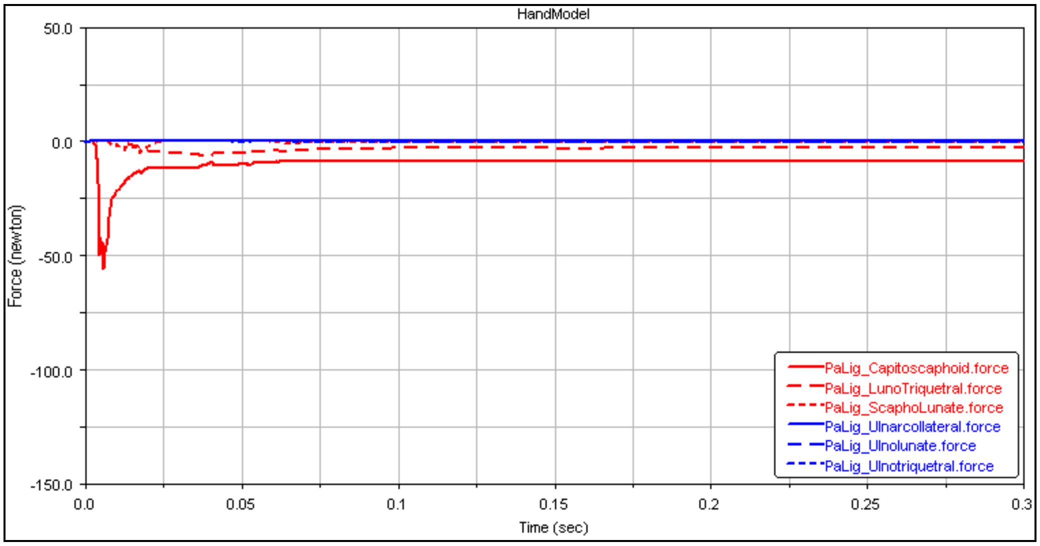

Figure 45 Load distributions of palmar ligaments for ulnar deviation.

In Figure 46 contact forces on wrist bones are presented for ulnar deviation. Like flexion motion most of the load was transferred from capitatum bone to lunatum and scaphoid, then load was transferred from lunatum to the radius. Also the contact forces between scaphoid / capitatum and scaphoid / lunatum were significant for ulnar deviation motion.

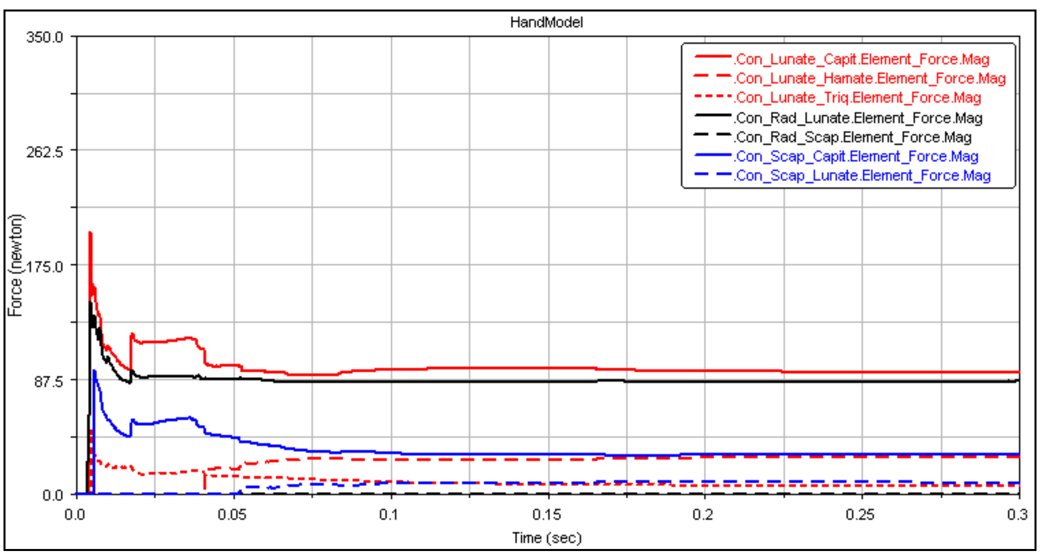

Figure 46 Contact force distributions of the wrist bones for ulnar deviation.

Joint forces were small as expected:

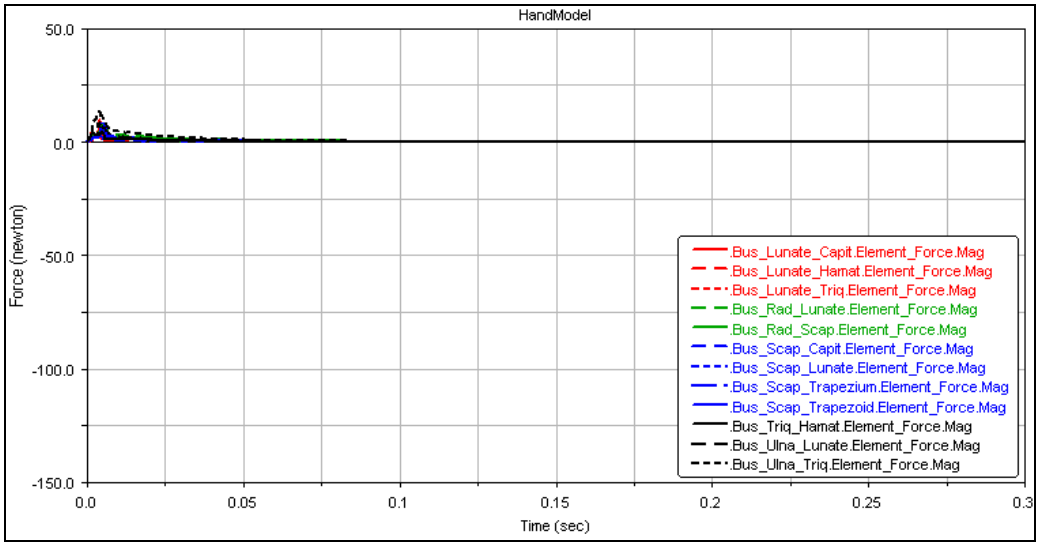

Figure 47 Joint load distributions of wrist bones for ulnar deviation.

4.1.3.B. Radial Deviation Motion of the Wrist Joint

Beyazova et al. [17] states motion limits of the wrist for radial deviation is approximately 20 degrees. The results of the analysis (three-dimensional model) for 20 N force showed that radial deviation motion made approximately 20 degrees of rotation, which is similar to the studies of Beyazova et al.

From Figure 48 to Figure 50 loads on palmar and dorsal ligaments are presented. Analysis of radial deviation motion indicated that dorsal ulnarcollateral, dorsal ligament between triquetrum and hamatum, palmar ulnarcollateral and palmar radiolunotriquetral were the main supporting elements of the wrist. Palmar and dorsal ulnar collateral ligaments were expected to carry higher loads due to the location of being on the upper most pole of ulna. Being at the most distant to the center of rotation, ulnar collateral ligaments provided support between wrist and the forearm. As compared to the ulnar deviation, ulnar collateral and radial collateral ligaments had antagonistic (working opposite) tasks. Radiolunotriquetral ligament and the ligament between triquetrum and hamatum are important to support mid-carpal components for radial deviation motion.

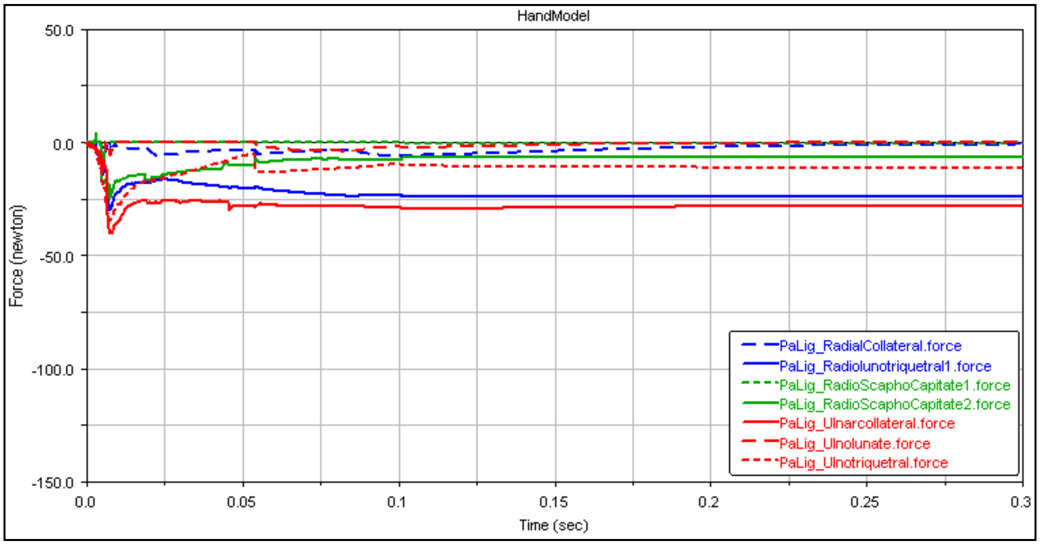

Figure 48 Load distributions of palmar ligaments of radius and ulna for radial deviation.

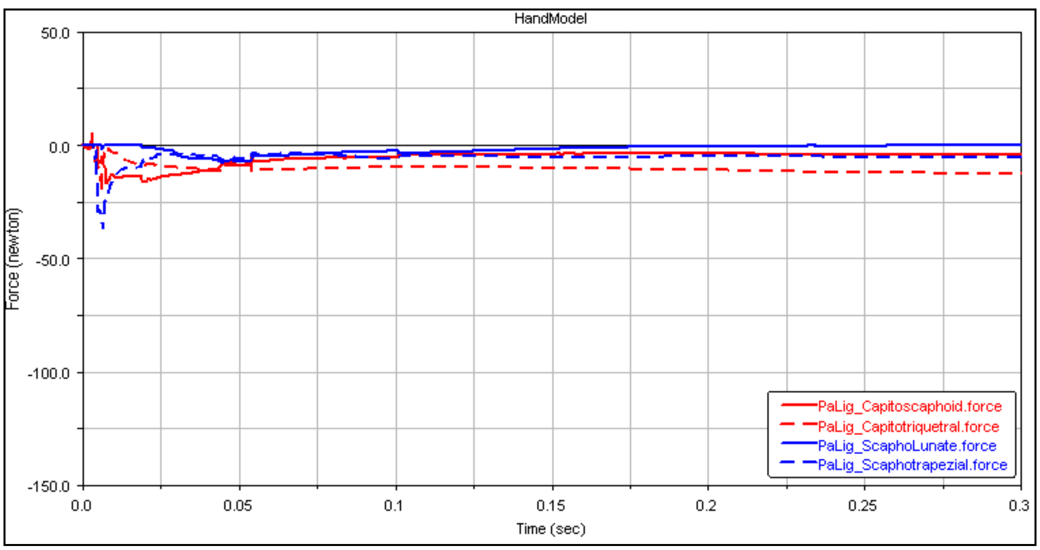

Figure 49 Load distributions of palmar ligaments of capitate and scaphoid for radial deviation.

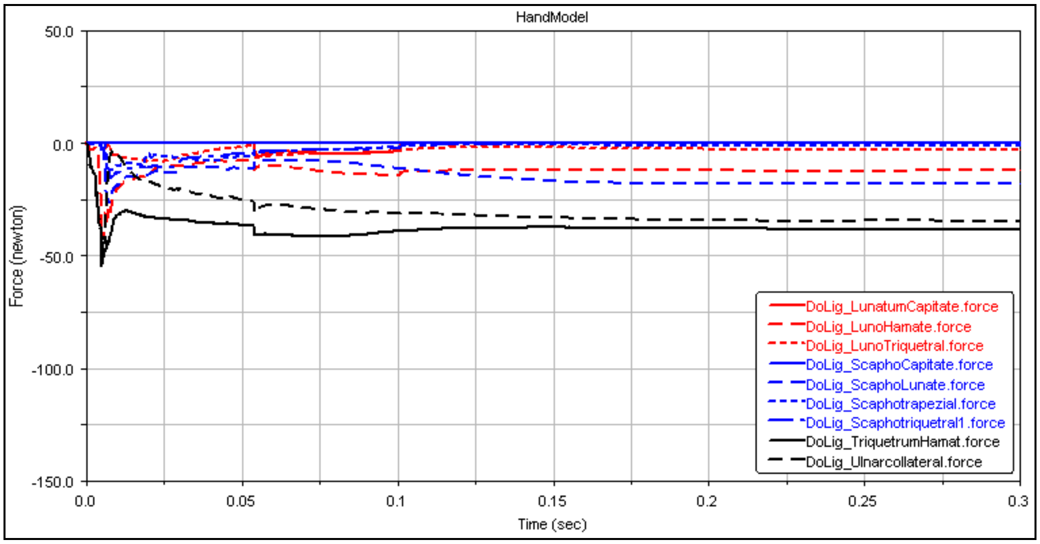

Figure 50 Load distributions of dorsal ligaments for radial deviation.

Similarly to the ulnar deviation motion, contact forces were mainly focused on lunatum bone for mid-carpal region (Figure 51). While the forces were transferred to the forearm (radius) the contact loads were shared between scaphoid and lunatum. At about 0.25 seconds of the analysis, contact forces of both scaphoid and lunatum were the same (approximately 42.9 N, which is the equilibrium value).

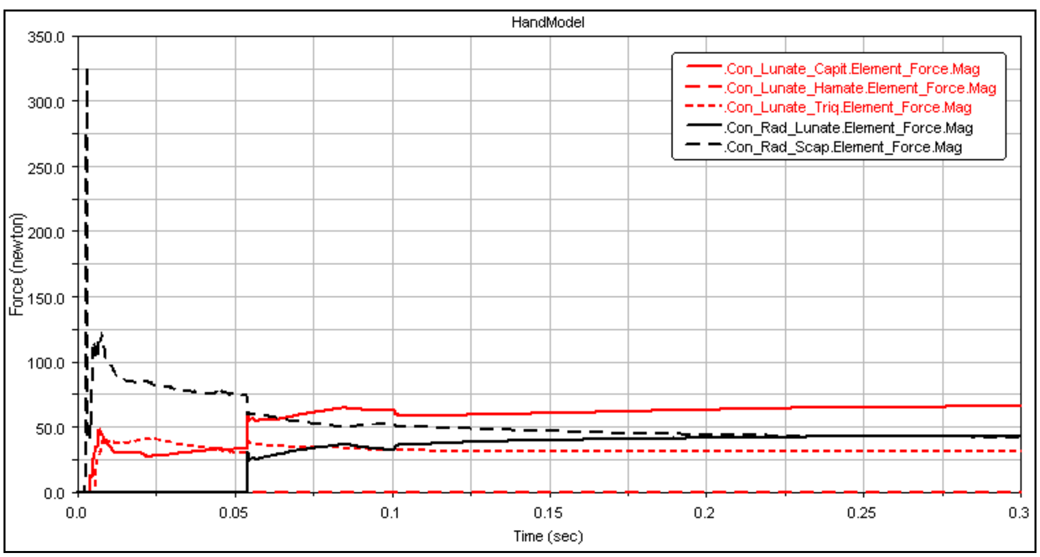

Figure 51 Contact force distributions of lunatum and radius for radial deviation.

During radial deviation motion, contact forces between scaphoid and trapezium/trapezoid were as high as contact forces between scaphoid and lunatum (Figure 52).

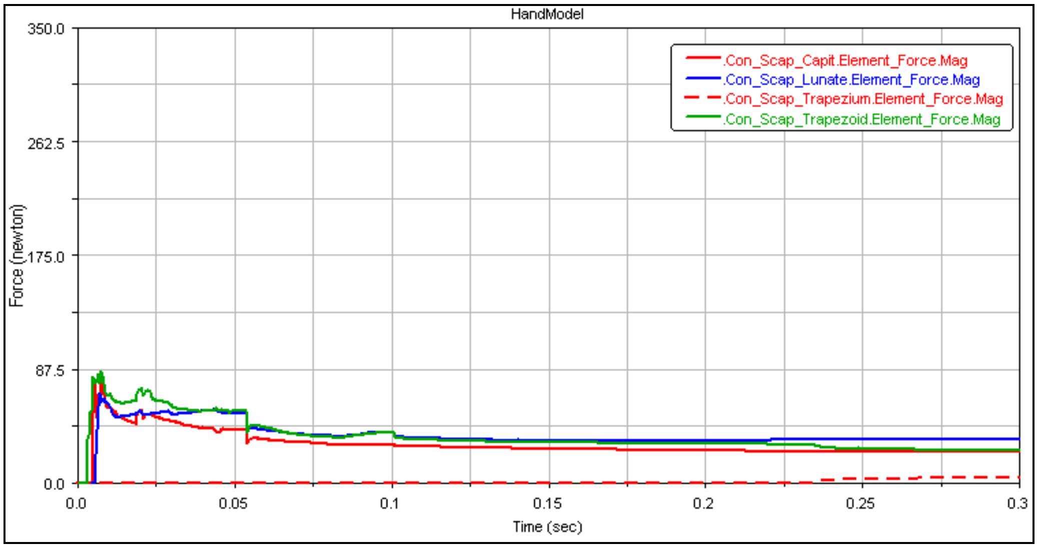

Figure 52 Contact force distributions of scaphoid for radial deviation.

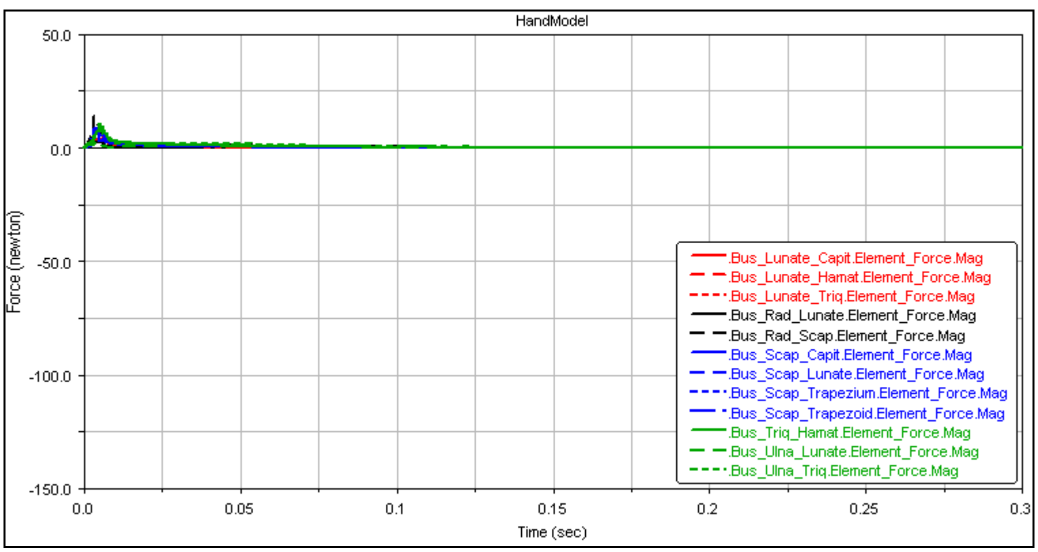

Figure 53 Joint load distributions of wrist bones for radial deviation.

Similar to the previous analysis, load distributions on joints were small as compared to forces on ligaments and contacts.

In the analysis of radial deviation motion 20 degrees of rotation was achieved but, there was an unexpected situation for scaphoid bone.

For radial deviation motion scaphoid bone was expected to make a sliding motion over radius. Sliding motion of scaphoid is shown in Figure 54 for ulnar and radial deviation [8].

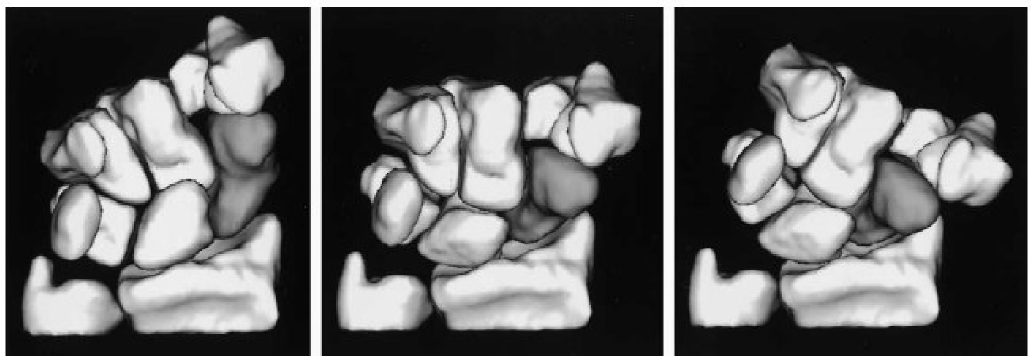

Figure 54 Sliding motion of scaphoid over radius for radial deviation motion.

Instead of sliding motion, scaphoid made a rotation where distal pole of the scaphoid turned to palmar side (Figure 56).

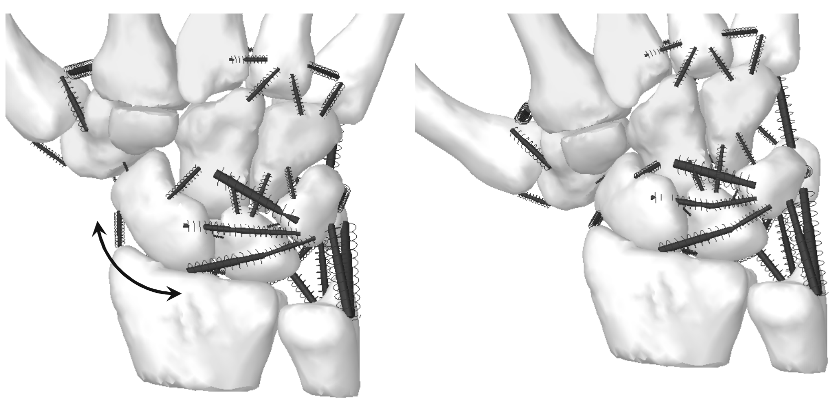

Figure 55 Rotation of scaphoid during radial deviation motion (neutral posiyion on the left, radial deviation on the right).

4.1.4. Axial Loading of the Wrist

Axial loading of the wrist was analyzed as two different types of loading: compressive and tensile.

4.1.4.A. Axial Loading of the Wrist Joint (Tensile)

Axial loading was simulated with a single force applied to the upper pole of third metacarpal bone. Tensile type of axial loading was analyzed with defined constant force (F) as shown in Figure 56.

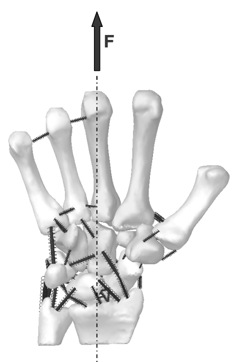

Figure 56 Axial loading of the wrist (tensile).

Force (F) was defined such that force remained constant (500 N) in magnitude and had a fixed direction in space. Direction vector of the applied force did not change with time. Figure 57 compares the normal position with respect to final position of the wrist under the effect of 500 N axial load.

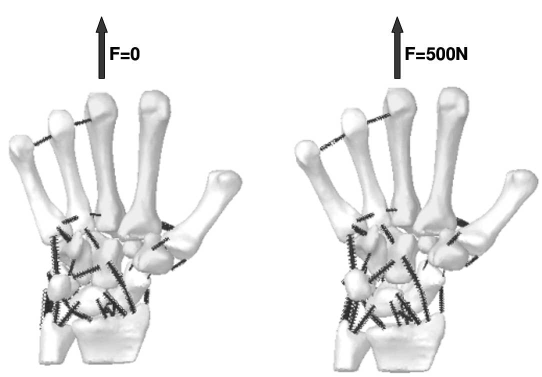

Figure 57 Axial loading (tensile) of unloaded (left hand side) and loaded (right hand side) wrists.

In Figure 58 and Figure 59 load distributions among palmar and dorsal ligaments are shown. If mid-carpal ligaments were considered, palmar ligaments would be the main supporting components. The reason was that the loading on palmar ligaments were higher than dorsal ligaments.

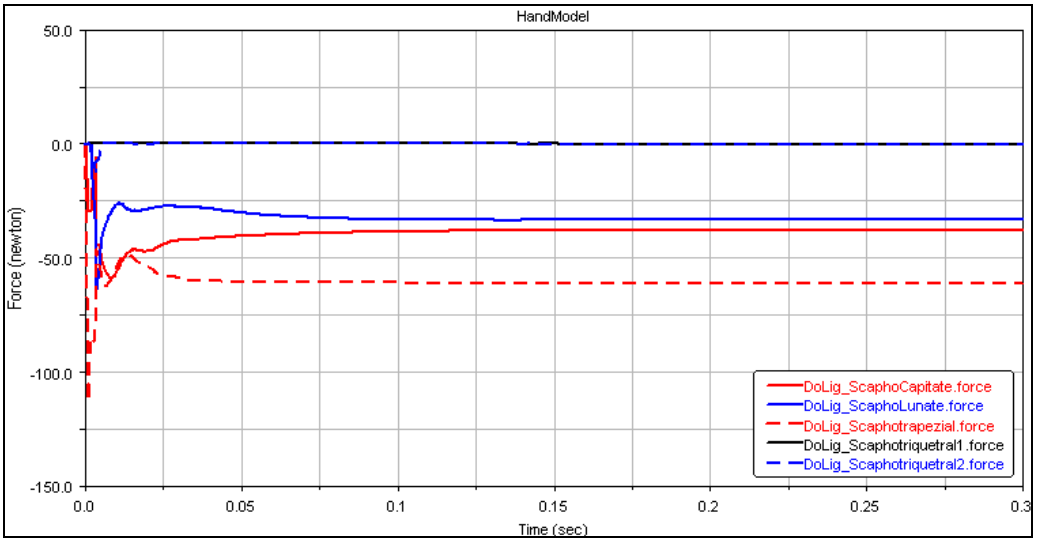

Figure 58 Load distributions of dorsal ligaments for 500 N axial loading (tension).

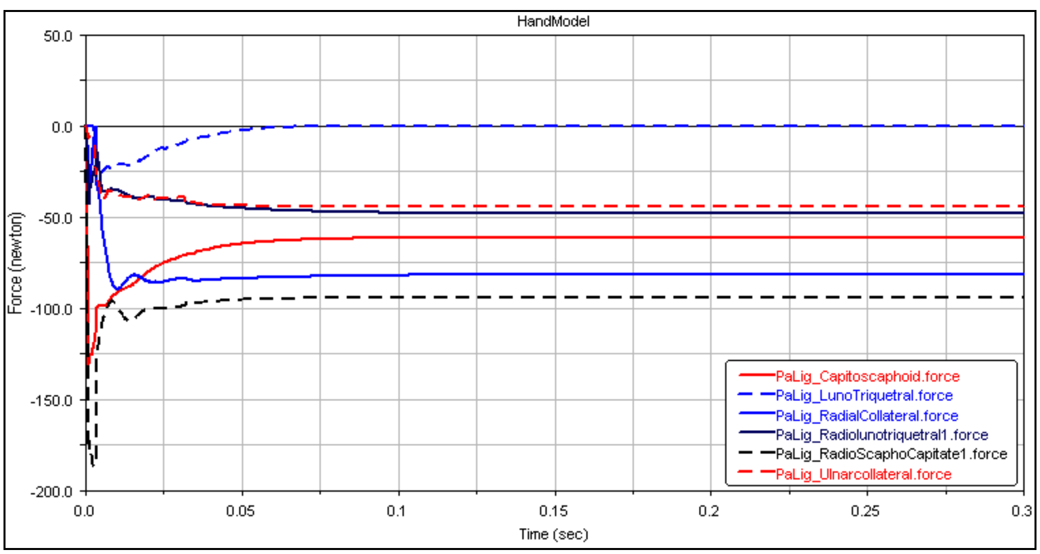

Figure 59 Load distributions of palmar ligaments for 500 N axial loading (tension).

Joints (bushing elements) had smaller force values than the loads of ligaments. Such a result was expected since the stiffness and damping values were taken as small.

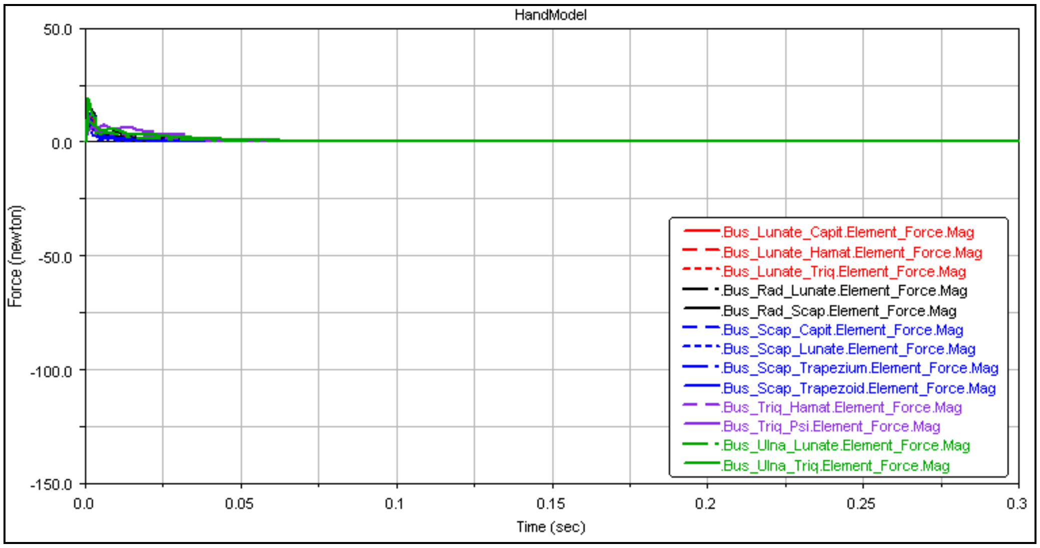

Figure 60 Load distributions of joints (bushing elements) for 500N axial loading (tension).

4.1.4.B. Axial Loading of the Wrist Joint (Compressive)

If an axial force (compressive) is applied to the wrist, wrist rotates to the palmar side. Kobayashi et al. [20] states "The three bones of the proximal carpal row were found to consistently rotate and displace in similar directions: they all translate palmarly and ulnarly". Gupta [21] states "The distal pole of the scaphoid forms the distal most structure of the proximal carpal row to come in contact with the distal carpal row where most of the compressive force gets utilized producing flexion torque to the scaphoid".

In three-dimensional model, a rotation motion (flexion to the palmar side) was observed for 100 N axial loading (compressive) analysis. Figure 61 shows the position of the hand under 100 N axial loading at the analysis time of 0.015 second. Analysis time for axial loading was taken as very short due to the start of flexion motion.

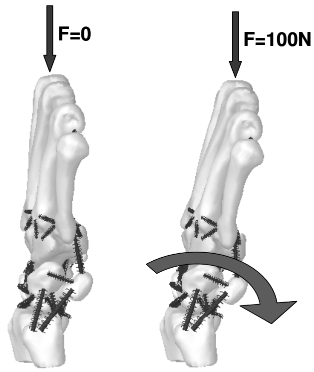

Figure 61 Axial loading (compression) of the healthy wrist causes flexion motion. Positions of the wrist for unloaded (on the left) and 100 N loaded (on the right) cases.

In this part of study, 100 N compressive force caused most of the wrist bones to come into contact with each other. So, the most essential point for compressive type of axial loading was contact forces. In Figure 62 contact forces for axial loading are given:

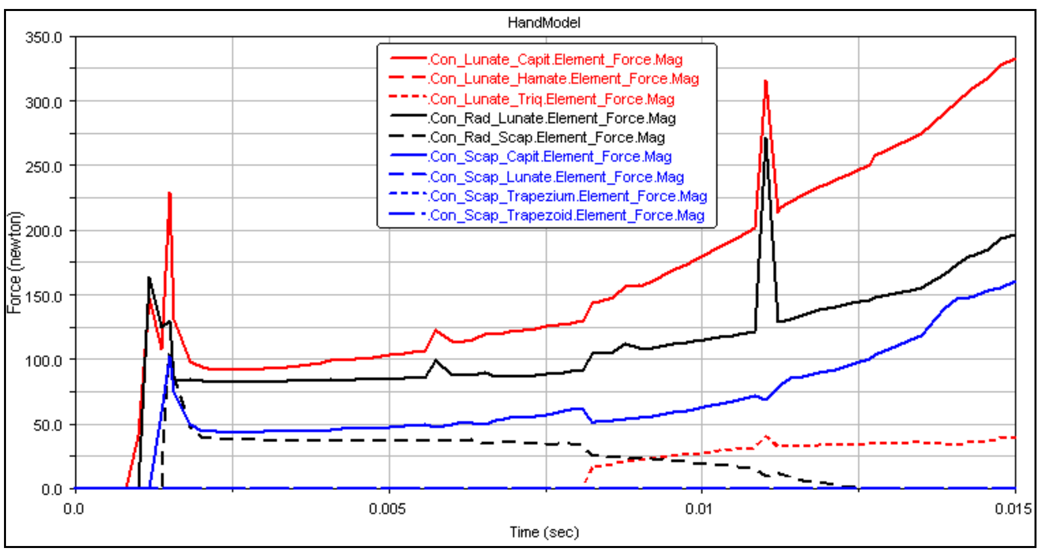

Figure 62 Load distributions of contact elements for 100N axial loading (compression).

Results of 100 N axial loading indicated there was no contact for ulna with any other bone that no contact force was observed. The significant point of the analysis was the difference between contact loads on scaphoid and lunatum. Analysis of the three-dimensional model showed that lunatum carried more load than scaphoid did.

Lunatum bone had 60% of axial loading where scaphoid shared 40% of the load. Contact load distributions on wrist bones are shown in Figure 63 for axial loading:

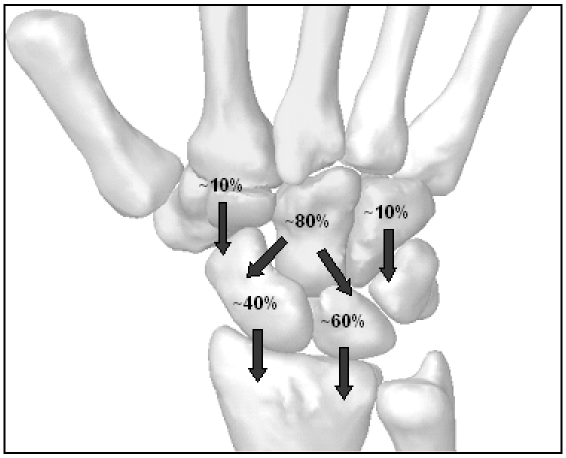

Figure 63 Load distribution analysis of the three-dimensional model for axial loading.

Previous studies about axial loading of the wrist have different results for the loads on scaphoid and lunatum. Patterson et al. [22] described the axial load distribution among carpal bones as shown in Figure 64. The loading between mid-carpal joints are very close but, for the radiocarpal side most of the load is carried by scaphoid bone (contact load between scaphoid and radius is 60%). Patterson et al. states contact forces between scaphoid, lunatum and radius are proportional to the contact areas.

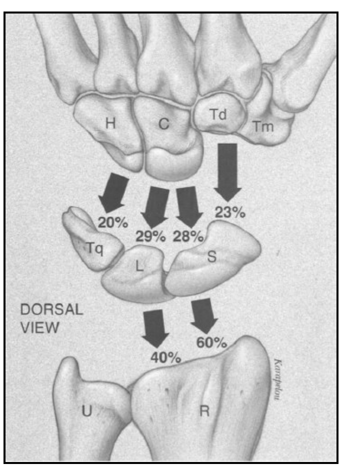

Figure 64 Load distributions on radiocarpal and midcarpal joints [22].

In another study about load distributions between carpal bones under the action of axial loading is done by Güdemez [23]. Güdemez [23] defines contact load distributions as shown in Figure 65.

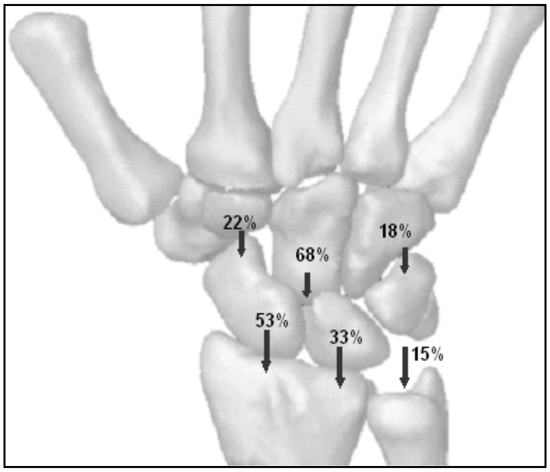

Figure 65 Load transfer between wrist bones to the proximal side (bone picture was taken from the three-dimensional model of the author).

Analysis results of three-dimensional model showed that there was no relation between contact forces and contact areas for wrist bones. Lunatum bone had smaller contact area with radius than scaphoid had (with radius). But, lunatum bone had larger contact forces compared to scaphoid.

Mid-carpal region had a force concentration on capitatum bone (80%). Force concentration was shared between scaphoid and lunatum bones. Finally, contact forces were transferred to the radius (forearm) again by lunatum and scaphoid.

4.2. Analysis of the Injured Wrists (Pathological Cases)

In this section pathological cases for the wrist injuries were analyzed. Two different kinds of wrist problems were studied: Kienböck's disease and scapholunate ligament tear. Healthy and injured wrists were compared and the results of treatment methods were investigated.

4.2.1. Kienböck's Disease (Lunatomalacia)

Kienböck's disease is the devascularization of the lunatum bone resulting with wrist pain and loss of wrist strength.

Epsten and Dalinka [24] state "Lunate osteonecrosis (Kienböck's disease) is an uncommon cause of wrist pain and loss of grip strength. It is most often seen in men between the ages of 18 and 40, and more than 95% of patients have a history of heavy manual labor. The etiology of Kienböck's disease is unknown. It represents devascularization of the lunate because of chronic repetitive injury or a single traumatic event. The large articular surface of the lunate only permits a precarious blood supply rendering the lunate relatively vulnerable to traumatic disruption of its vascular supply. The proximal pole is relatively avascular and exposed to a large axial load because of its central position in the carpus. The forces on the lunate are accentuated when the ulna is shortened relative to the radius. This provides the biomechanical explanation for the association of Kienböck's disease with negative ulnar variance".

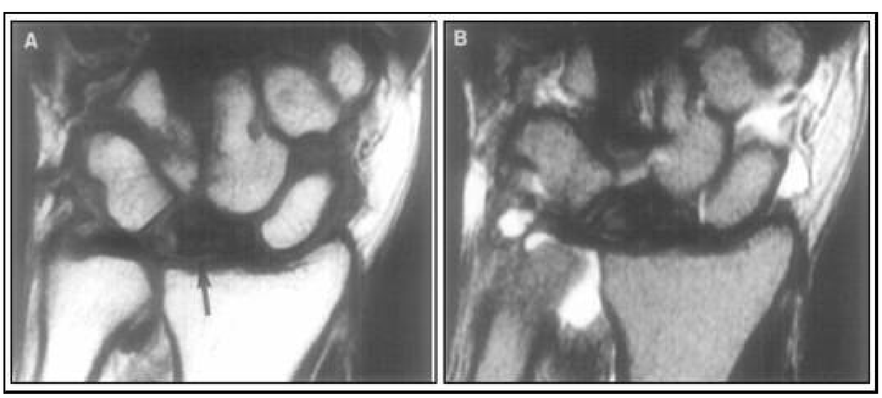

Figure 66 Kienböck's disease: devascularization of Luantum bone [3].

Lamasa et al. define causes of Kienböck's disease as [25]:

1) Short ulna (ulna minus variance)

2) Small lunatum bone

3) Ligament ruptures (like scapholunate ligament rupture)

4) Insufficient blood supply

Kienböck's disease causes lunatum bone to loose the original shape with decreasing bone rigidity. Figure 67 shows the three stages of lunatomalacia resulting with lunatum fracture defined by Stahl-Lichtman [26].

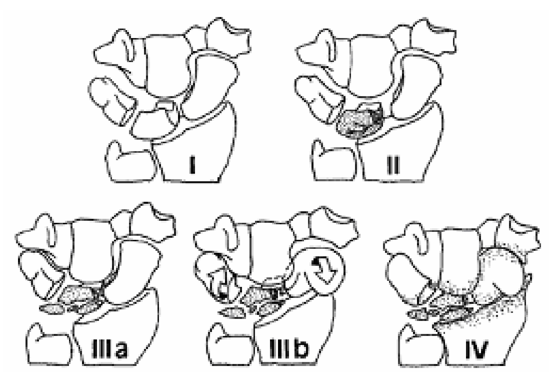

Figure 67 Stahl-Lichtman's staging system for Kienböck's disease.

Elias and Vidal [26] define treatment methods of Kienböck's disease as below operations:

1) Immobilization (only applicable for early stages)

2) Bone revascularization (treatment for insufficient blood supply)

3) Joint leveling procedures (radial shortening / ulnar lengthening)

4) Diminishing the ulnar slope of the distal radius

5) Curettage and cancellous bone grafting (through a small window made in the dorsal aspect of the lunate, a thorough curettage of the avascular lunate is performed until bleeding bone is visualized.)

6) Capitate shortening

In this study, Kienböck's disease was analyzed with extra loading on lunatum bone where most of the contact load was transferred from capitatum bone to lunatum. So, as a treatment method capitate shortening was modeled and results were examined.

Elias and Vidal [27] state “Experimental studies have demonstrated shortening of the capitate to be the most effective lunate decompressive procedure and the early clinical results. However, reduction of lunocapitate forces obtained at the expense of dramatically overloading the adjacent triquetral-hamate and scapho-trapezial joints”. Leblebicioğlu et al. [28] defines capitate shortening as one of the optimal treatment methods for Kienböck’s disease from surgical studies. Figure 68 shows the contact region between capitatum and lunatum bone. As a recovering method proximal pole of the capitatum bone is removed. Therefore, loading on the lunatum bone (due to axial loading) is distributed through other inter-carpal bones.

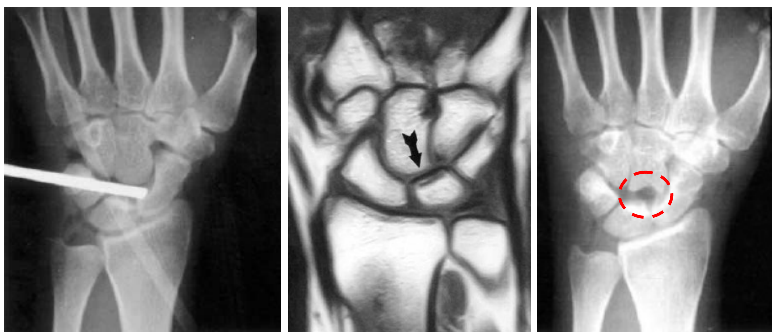

Figure 68 Kienböck’s disease, load transfer between capitatum and lunatum [28].

As explained in section 4.1.4.B. highest contact forces between mid-carpal bones were transferred from capitatum to lunatum. Result of axial loading on a healthy wrist showed that the largest amount of the load was carried by lunatum (Figure 69).

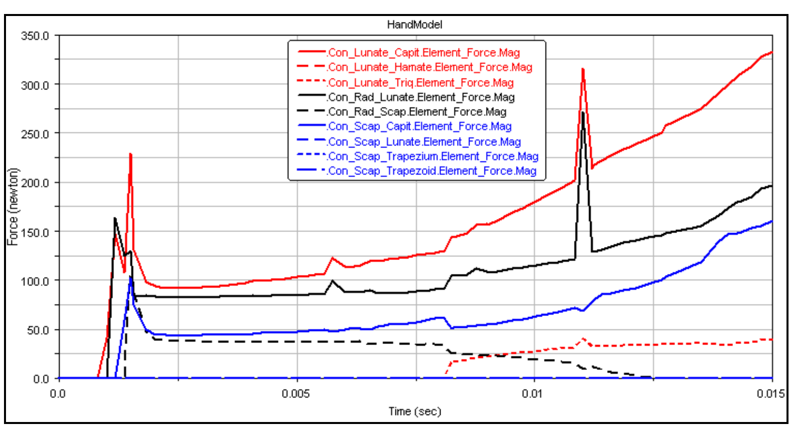

Figure 69 Load distributions of contact elements for 100N axial loading (compression).

As the maximum load for mid-carpal contact forces was observed between capitatum and lunatum, capitate shortening method was examined as the treatment method. Because capitate shortening method reduces the load on lunatum and distributes contact forces to the other wrist bones.

Figure 70 shows the model of the hand used in the three-dimensional model. Actually ulna was shorter than the radius in the model and below figure shows the level difference between radius and ulna. Lamasa et al. [25] defines short ulna (ulna minus variance) as one of the reasons of Kienböck's disease. But short ulna does not cause Kienböck's disease for all wrists, so the three-dimensional model was a good example of a healthy wrist with short ulna.

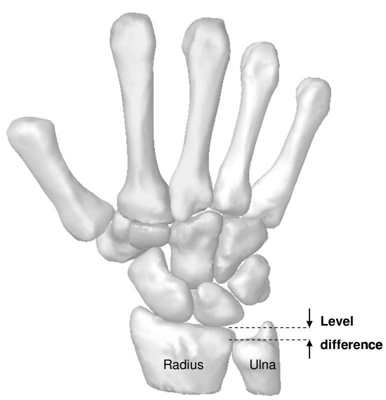

Figure 70 Short ulna (Ulna minus variance).

Capitate shortening is one of the common treatment methods for Kienböck's disease. In three-dimensional model a cup shaped part was removed from lower pole of the capitatum bone (close to the side of lunatum) and the resulting load distributions were observed.

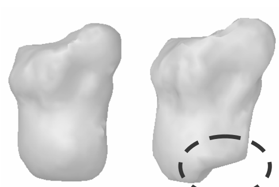

Figure 71 Capitate shortening (on the left before shortening and on the right after capitate shortening).

In order to analyze Kienböck’s disease and capitate shortening operation compressive type axial loading and flexion motion was examined.

Compressive type axial loading was the most crucial analysis to observe contact load distribution on lunatum for Kienböck’s disease. Because, for this kind of loading most of the forces were distributed through contact elements.

Flexion motion was also analyzed to observe the changes in loading as an example for dynamic case having a large range of rotation.

4.2.1.A. Axial Loading of the Wrist for Kienböck’ s Disease

In order to analyze capitate shortening and observe the resulting changes, compressive axial loading was examined. Axial loading is one of the main reasons for Kienböck’s disease causing high contact forces between capitatum and lunatum.

Axial loading was applied as defined in section 4.1.4.B.

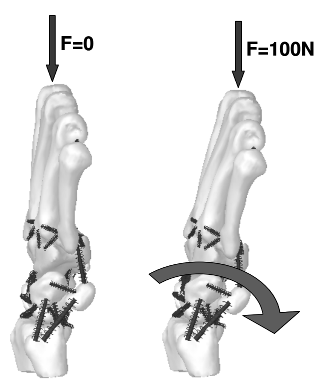

Figure 72 100 N axial loading (compressive) for Kienböck's disease.

Results of the analysis for Kienböck’s disease are given as “before surgery” and “after surgery” (after capitate shortening) in below figures for comparison.

Figure 73 and Figure 74 show the contact forces on lunatum bone before and after capitate shortening operation. Capitate shortening reduced contact load transferred from capitatum to lunatum bone. Since the load on lunatum bone was reduced, treatment of capitate shortening can be defined as a solution for Kienböck's disease. But, on the contrary contact forces between lunatum, hamatum and triquetrum were increased (Figure 74). Result was parallel to the studies of Elias and Vidal [27] where capitate shortening caused extra loading on triquetrum and hamatum.

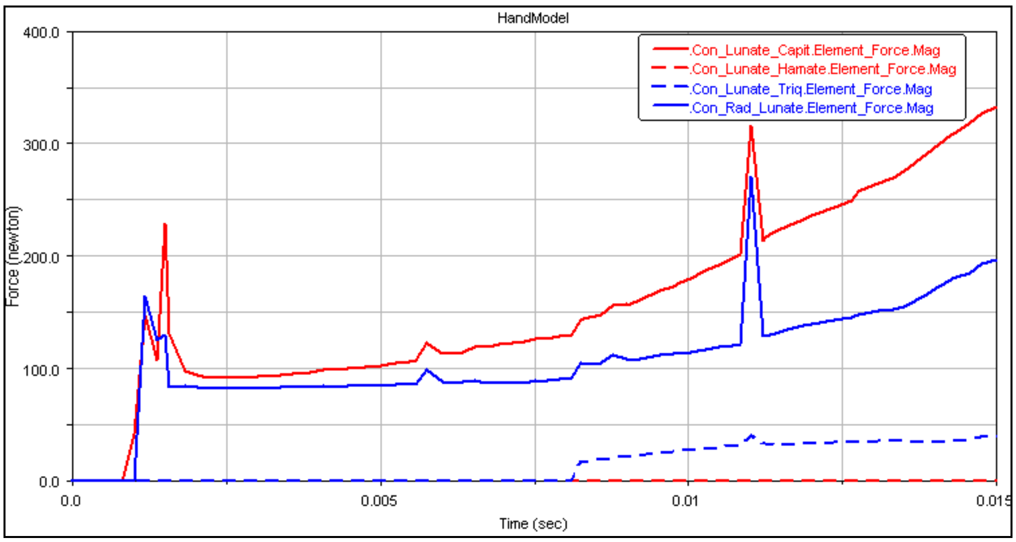

Figure 73 Contact load distribution of lunatum before surgery.

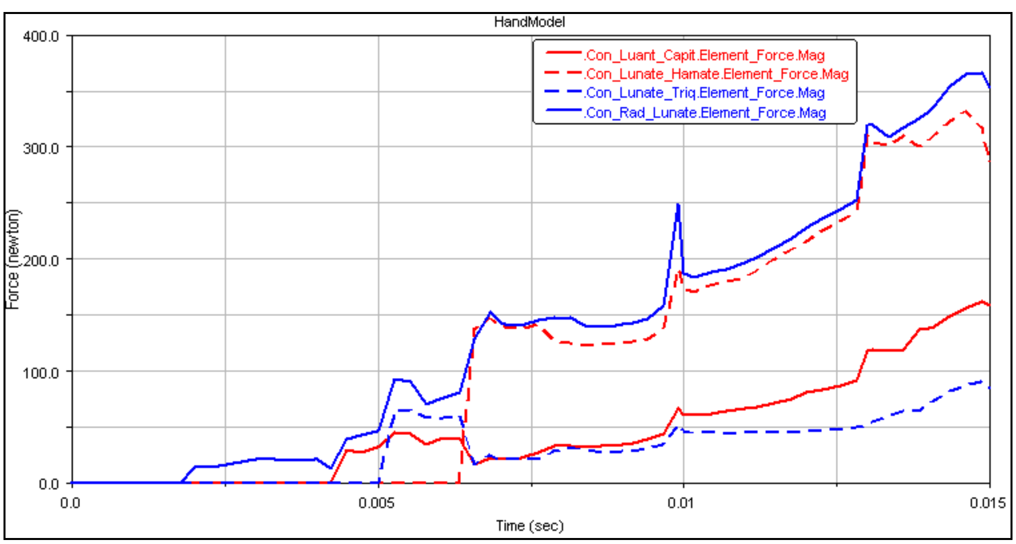

Figure 74 Contact load distribution on lunatum bone after surgery.

Figure 75 and Figure 76 show the changes for contact forces on scaphoid before and after capitate shortening. Scaphoid shared some portion of the loading on lunatum bone; transferring extra load to trapezoid and trapezium. Extra loading on triquetrum and trapezial region made scaphoid and lunatum to contact with higher loads. So, as in Figure 76 contact force between scaphoid and lunatum was increased.

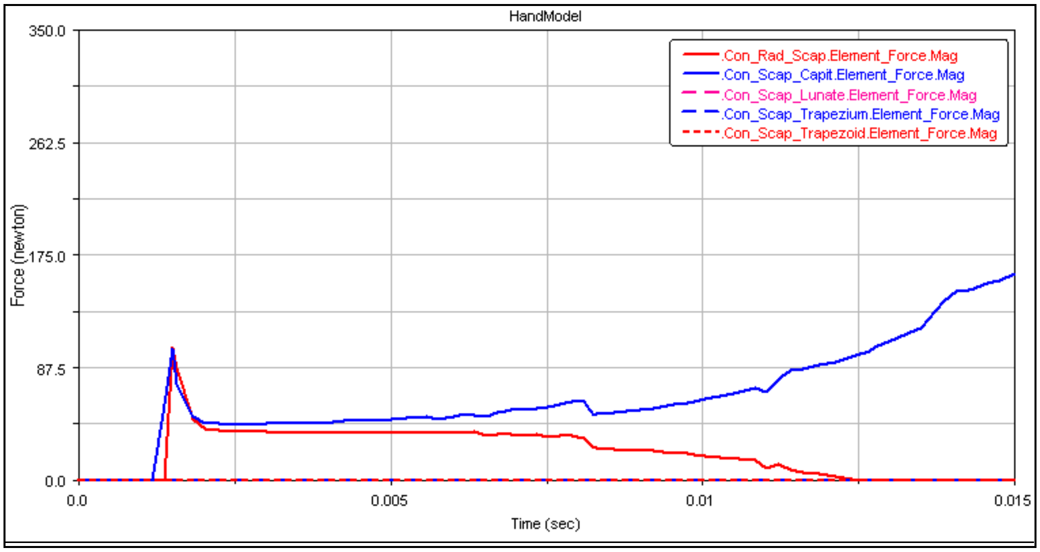

Figure 75 Contact load distribution on scaphoid bone before surgery.

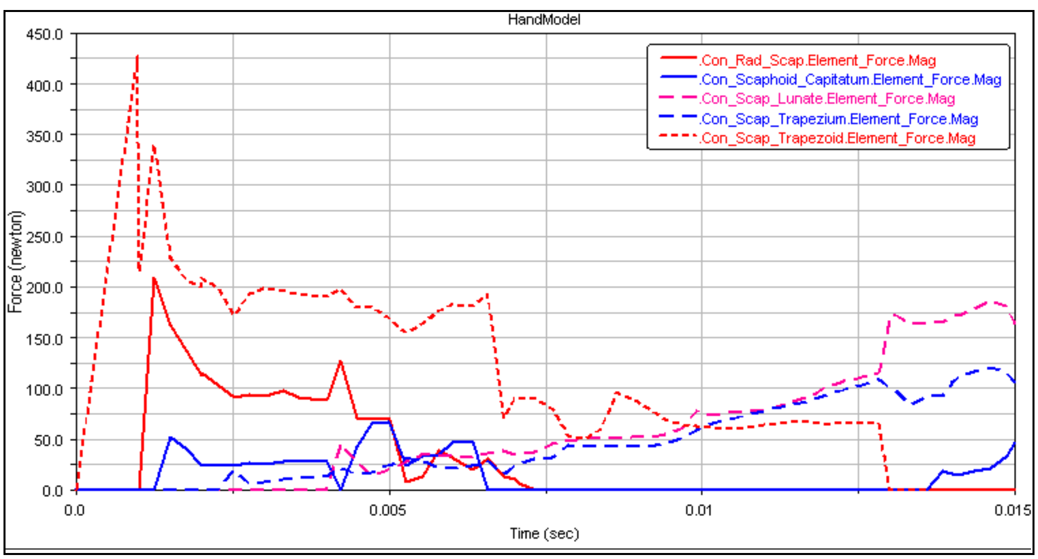

Figure 76 Contact load distribution on scaphoid bone after surgery.

Figure 77 and Figure 78 show that capitate shortening caused unstable loading on palmar ligaments. After surgery (capitate shortening) tensile forces on ligaments were increased.

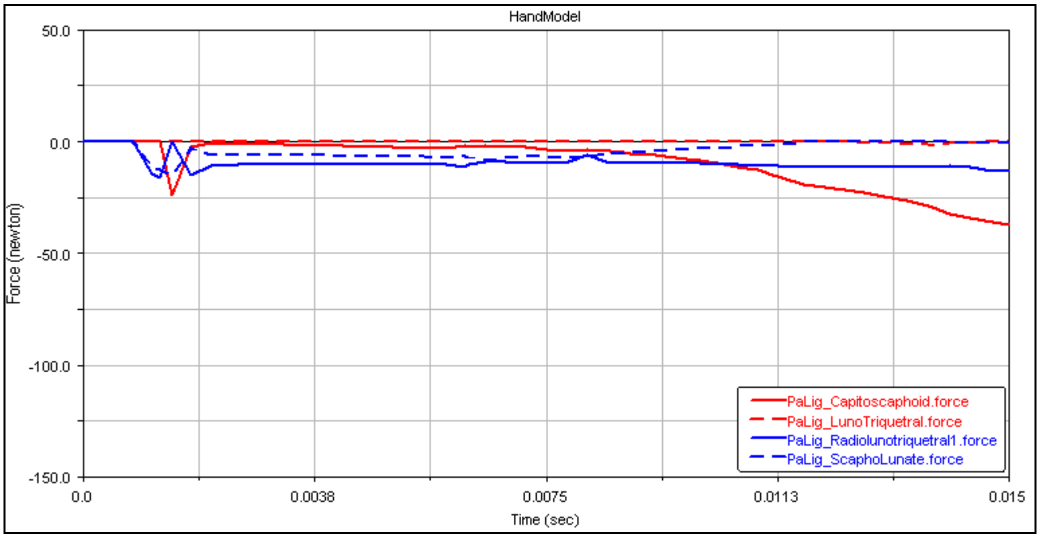

Figure 77 Load distributions of palmar ligaments <u>before surgery</u>.

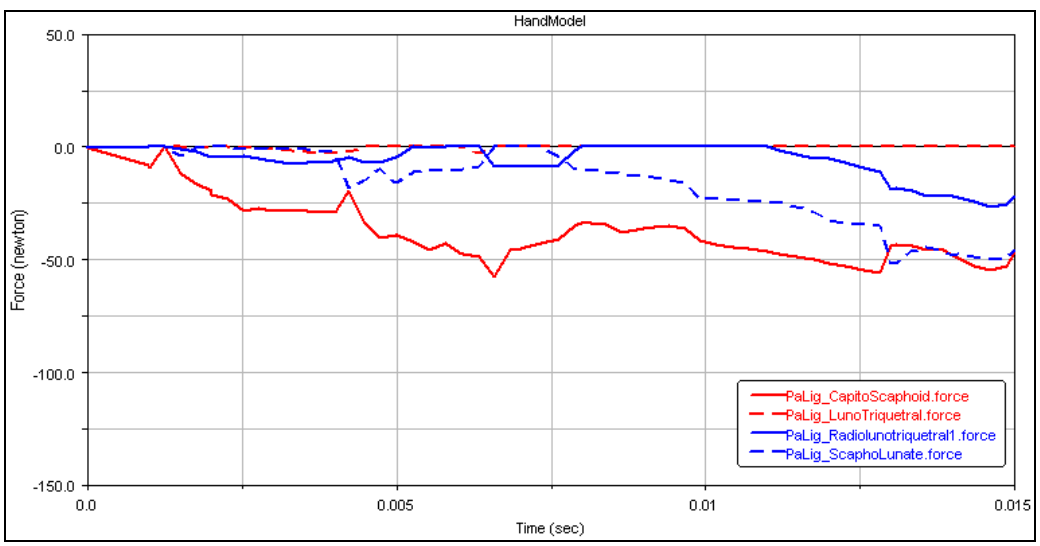

Figure 78 Load distributions of palmar ligaments <u>after surgery</u>.

Capitate shortening causes unstable loading on dorsal ligaments like palmar ligaments. Dorsal ligaments of scaphotrapezial and scaphocapitate ligament had significantly extra loading after surgery (Figure 79 and Figure 80).

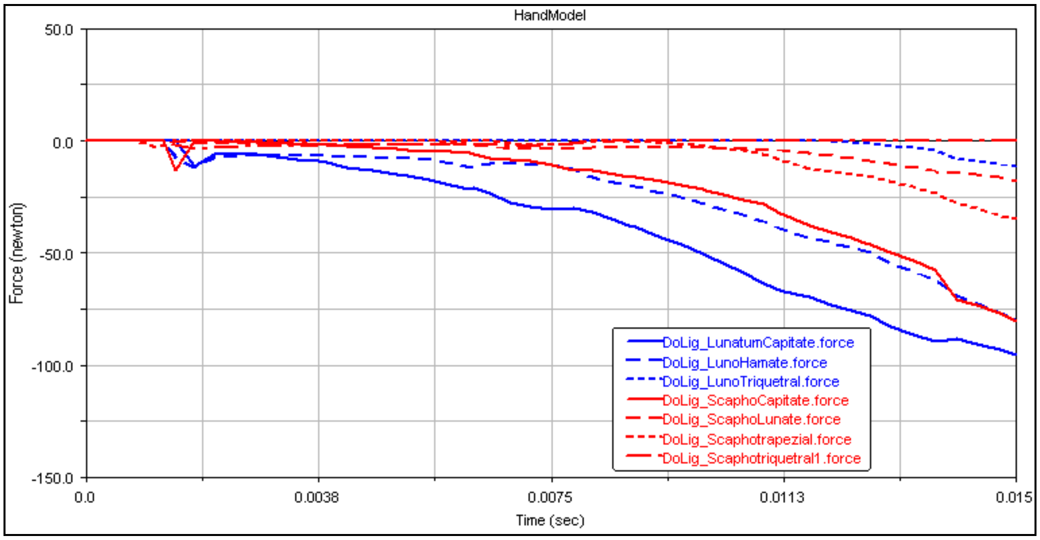

Figure 79 Load distributions of dorsal ligaments before surgery.

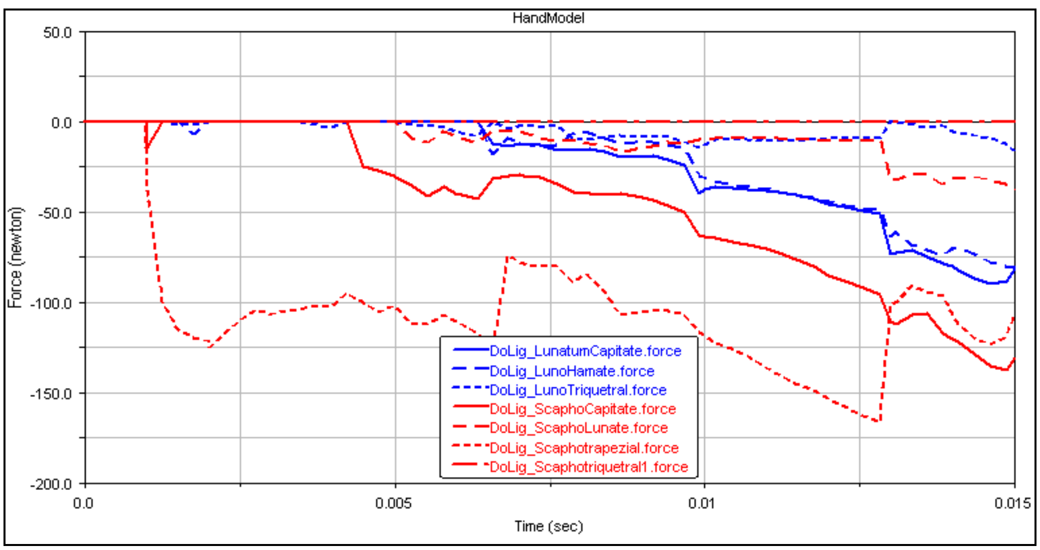

Figure 80 Load distributions of dorsal ligaments after surgery.

Analyzes of Kienböck's disease for 100 N compressive axial loading showed that capitate shortening reduced the loads on lunatum bone; where loads on scaphoid, trapezoid, trapezium and palmar / dorsal ligaments were increased. Also, such a surgery caused unstable and extra loading on palmar and dorsal ligaments.

4.2.1.B. Flexion Motion of the Wrist for Kienböck' s Disease

Axial loading was the most critical analysis for Kienböck's disease (with higher contact forces between lunatum and capitatum) and in this section flexion motion was analyzed to study a dynamic case with larger rage of motion.

After capitate shortening operation wrist was to flex more than the normal (healthy) wrist. Healthy wrist flexed approximately 90 degrees of rotation (from section 4.1.1.), where capitate shortened wrist flexed approximately 100 degrees of rotation (Figure 86).

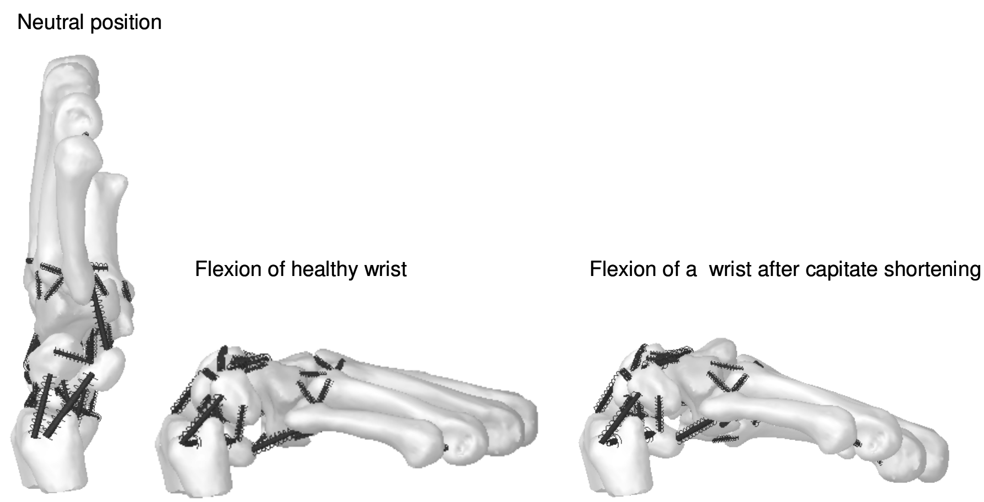

Figure 81 Flexion of the wrist after capitate shortening (1st neutral position, 2nd flexion of a healthy wrist, 3rd flexion of a wrist with capitate shortening).

Flexion motion analysis for capitate shortening showed contact load between lunatum and capitatum was reduced about 30 % (Figure 82 and Figure 83).

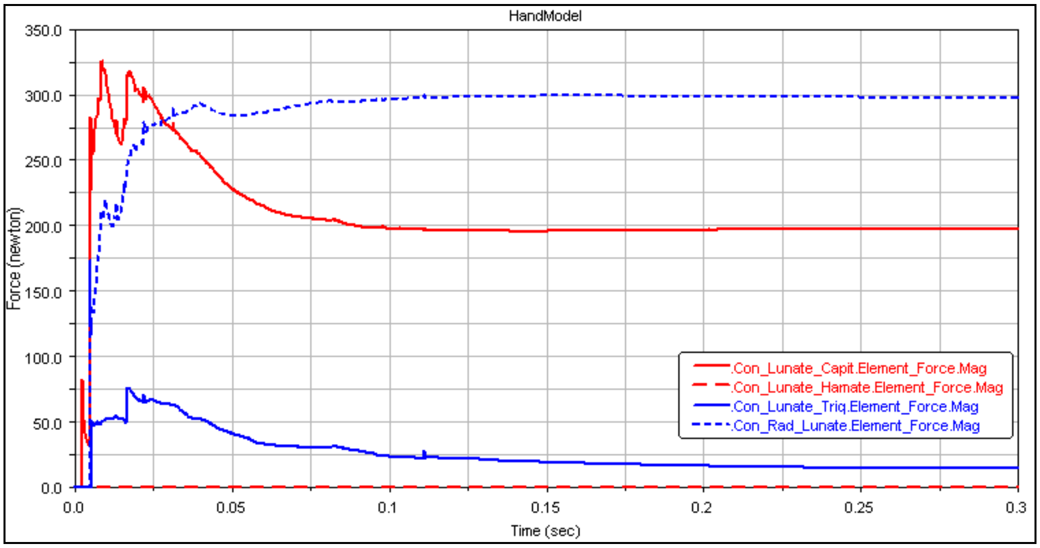

Figure 82 Contact force distribution on lunatum bone <u>before surgery</u>.

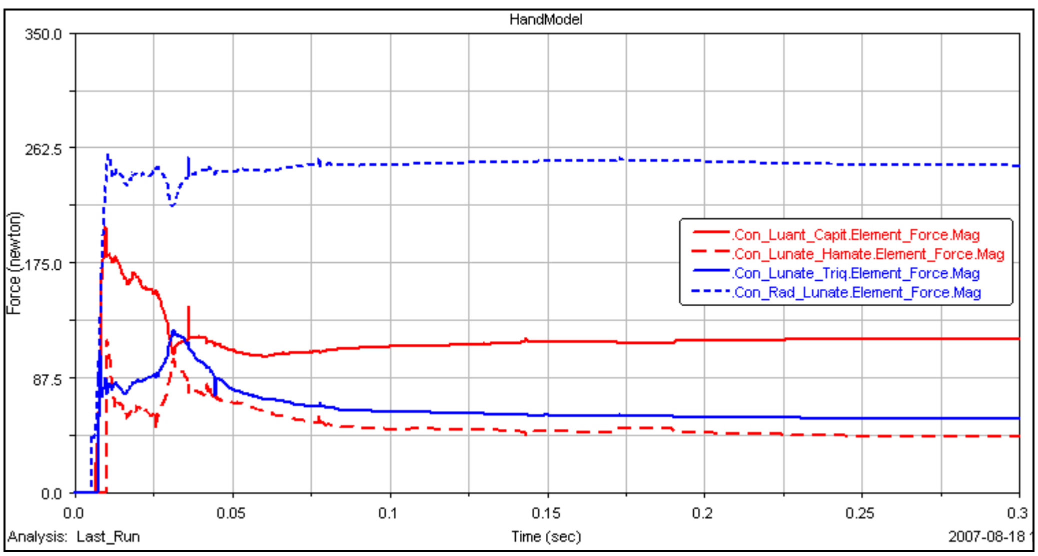

Figure 83 Contact force distribution on lunatum bone <u>after surgery</u>.

Similar to the compressive axial loading results, some of the contact forces on lunatum bone were transferred to scaphoid. Changes on contact forces of capitatum and trapezial region were observed for flexion motion in Figure 85.

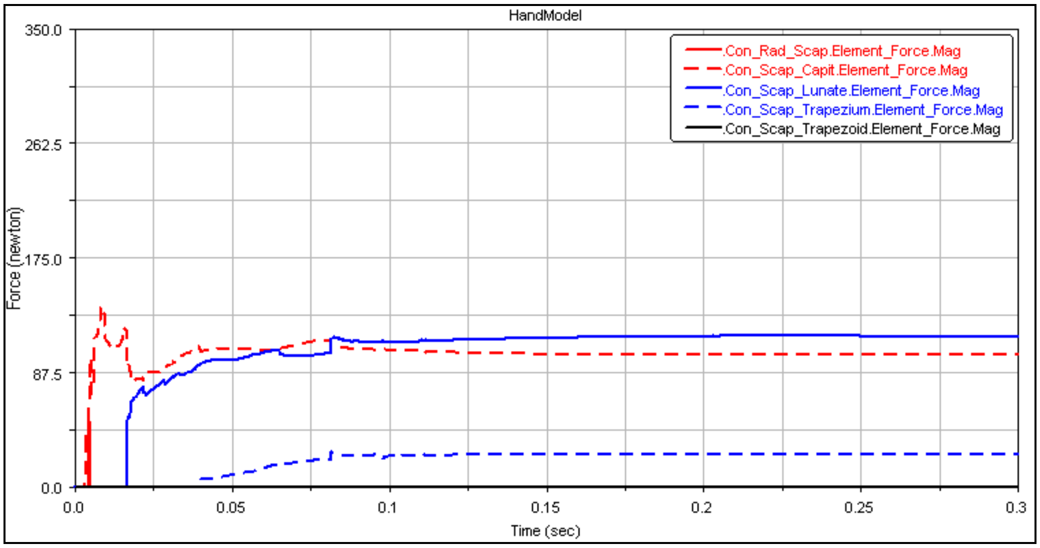

Figure 84 Contact force distribution on scaphoid bone before surgery.

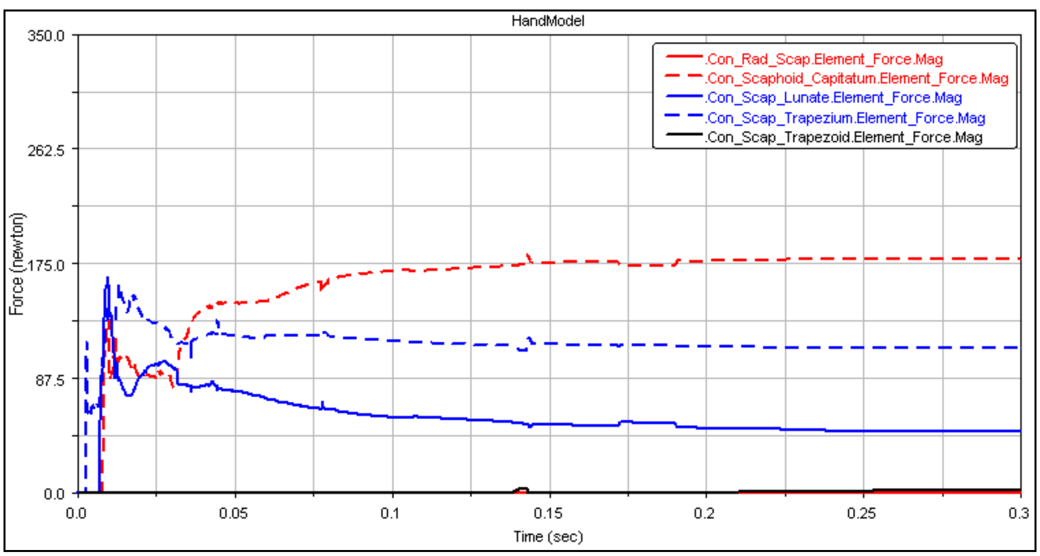

Figure 85 Contact force distribution on scaphoid bone after surgery.

For flexion motion, most of the palmar ligaments had smaller tensile forces after surgery. There was a significant decrease on palmar radioscapholunate ligament force.

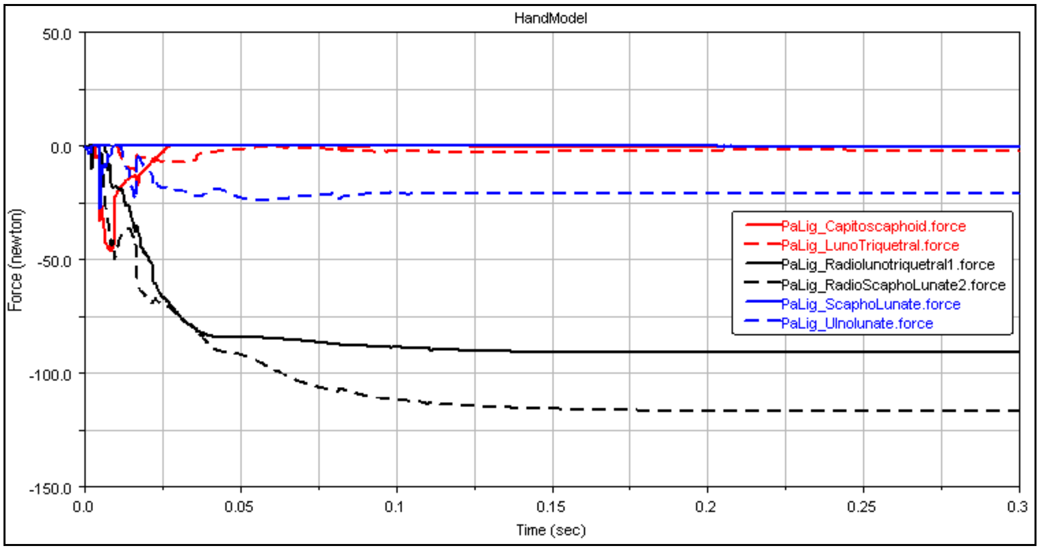

Figure 86 Load distributions of palmar ligaments <u>before surgery</u>.

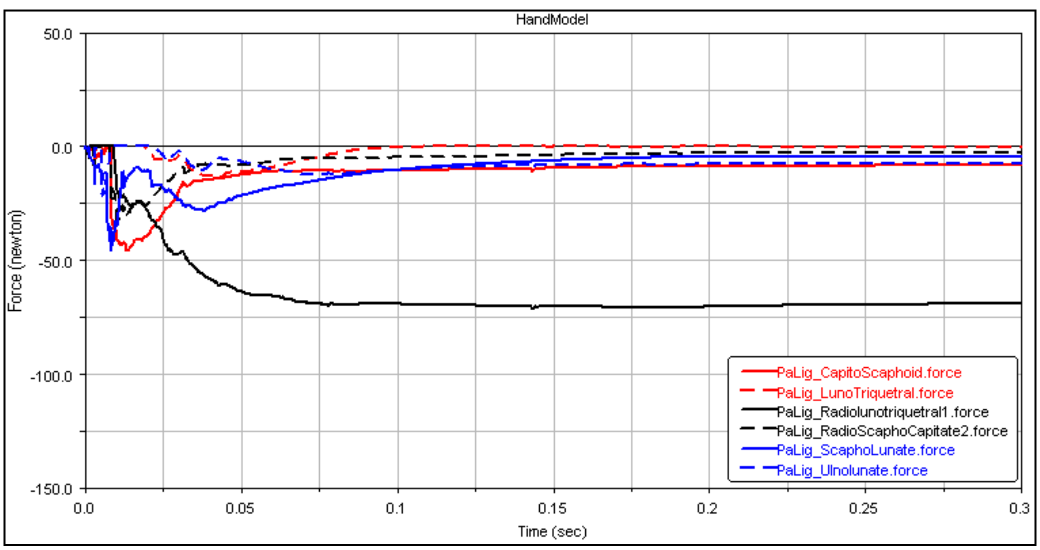

Figure 87 Load distributions of palmar ligaments <u>after surgery</u>.

Since capitate shortened wrist was to flex more than a healthy wrist, loads on dorsal ligaments were increased as shown in Figure 88 and Figure 89.

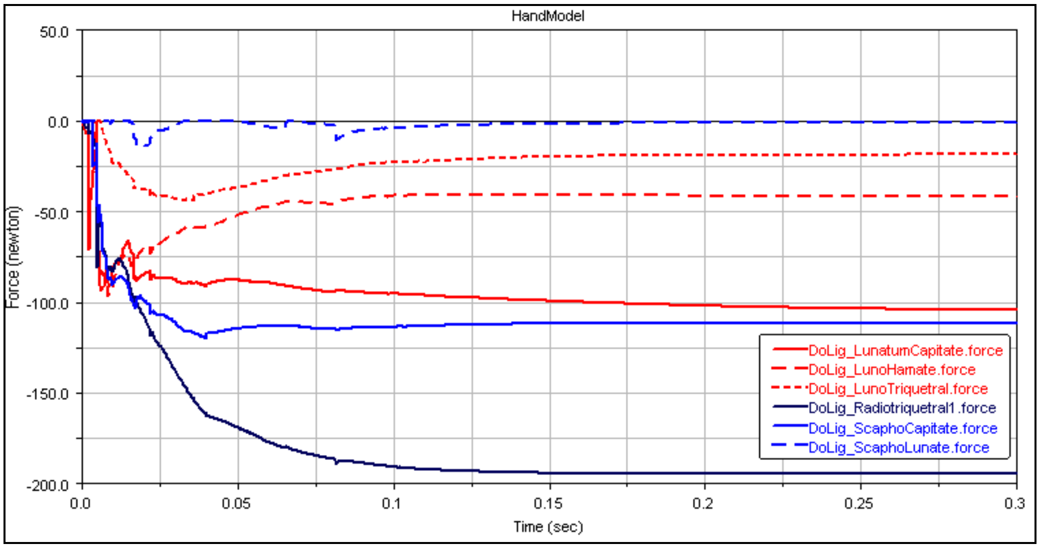

Figure 88 Load distributions of dorsal ligaments before surgery.

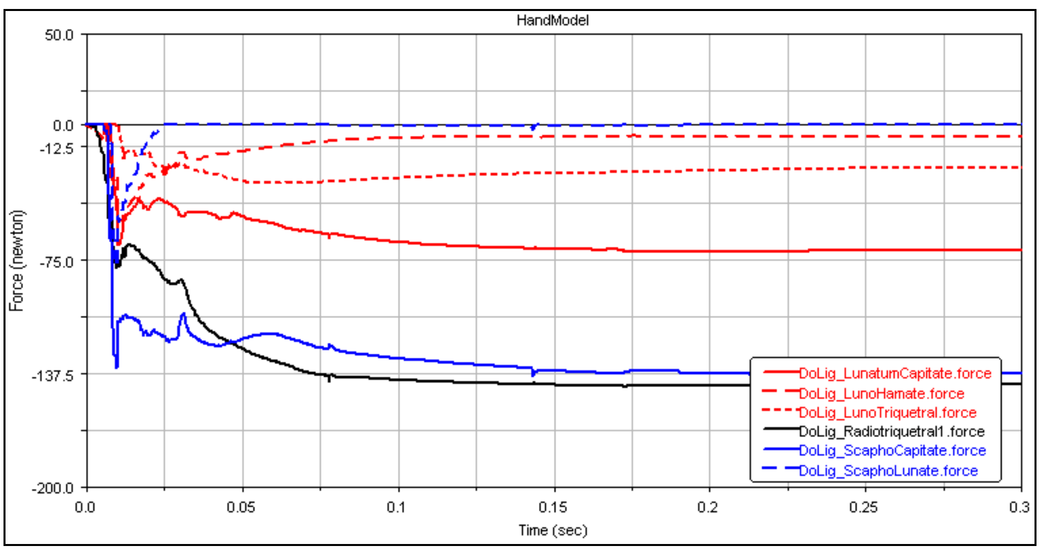

Figure 89 Load distributions of dorsal ligaments after surgery.

Load distribution analysis for flexion motion (for Kienböck's disease) yield approximately the same results with axial loading analysis. The common point for two studies was that the load on lunatum bone was reduced and transferred to the surrounding bones and ligaments.

4.2.2. Scapholunate Ligament Tear

Scapholunate interosseous ligament is a very important ligament which connects scaphoid to lunatum. Being a very active ligament for wrist loading, scapholunate tear is a very common injury. Garcia-Elias [26] states scapholunate ligament injury as the most frequent ligamentous injury of the wrist.

As a result of scapholunate ligament tear, the controlling mechanism for the gap between scaphoid and lunatum becomes functionless. In Figure 90 the gap between scaphoid and lunatum is shown for a scapholunate ligament tear.

Figure 90 Gap between scaphoid and lunatum [29].

Garcia-Elias [26] defines the gap between scaphoid and lunatum for normal wrists with a range from 1.3 mm to 2.6 mm (patients with 25 normal right wrists). The gap for patients with scapholunate ligament tear changes from 2 mm to 3.8 mm (22 patients with injured ligaments). Therefore, scapholunate ligament has an important role for scaphoid-lunate bone system.

In a study of scapholunate ligament tears, Crisco et al. [6] define the results of the injury for flexion and extension motions as:

"The injured and contralateral lunate in the injured patients extended less than half as much as the lunate in the normal wrists. The lunates in the injured and contralateral wrists of patients tended to flex more than the lunates in the normal group.

We found that the neutral posture of the scaphoid and lunate of both wrists of unilaterally injured subjects were more extended and more ulnarly deviated than those of normal subjects, with similar neutral capitate postures.

During motion the lunate extended less in wrist extension and scaphoid flexed more in wrist flexion in both wrists, as compared with normals. These findings may provide information that could help to advance the diagnosis and treatment of patients with this common injury, considering that the scaphoid lunate gaps measured on the posteroanterior radiographs of our patients were nondiagnostic for this injury."

In three-dimensional model scapholunate ligament was modeled as three different parts (which is explained in detail in section 3.1.4.). In real life, scapholunate ligament surrounds the gap between scaphoid and lunatum. So, in the model three different spring-damper pairs were used for one single continuous ligament. The reason for modeling the ligament in three parts was that only point to point spring / damper elements were available for MSC. ADAMS. Figure 91 shows the three parts of scapholunate ligament:

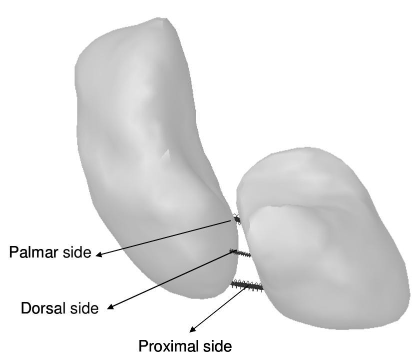

Figure 91 Palmar, dorsal and proximal sides of scapholunate ligament in three-dimensional model.

Henry [30] defines the scapholunate ligament injury and resulting treatment method as “Acute scapholunate and lunotriquetral interosseous ligament injuries must be stabilized for anatomically correct healing to prevent progressive carpal instability. Shortcomings of reconstruction procedures place a priority on achieving a successful initial repair. The traditional repair strategy involves open reduction and internal fixation and results in significant long-term wrist stiffness”.

Parallel to the studies of Crisco et al. [6] and Henry [30], scapholunate ligament tear was analyzed as two different cases: First case was the injured writs with scapholunate ligament tear and the second case was fixation of scaphoid to lunatum as a treatment method. Two cases were studied simultaneously to compare differences of load distributions.

Differences between healthy, injured (scapholunate ligament tear) and treated (fixation of scaphoid and lunatum) was analyzed for flexion, extension, radial and ulnar deviation motions. Analysis for scapholunate ligament tear was done with the same analysis method used in sections 4.1.1, 4.1.2, 4.1.3 and 4.1.4.

For scapholunate ligament tears, distances between scaphoid/lunatum and contact forces between wrist bones were observed comparing with healthy wrists.

4.2.2.A. Flexion of the Wrist with Scapholunate Ligament Tear

Figure 92 presents the distance between scaphoid and lunatum for healthy, injured and treated wrists. Analysis showed that maximum distance between scaphoid and lunatum was 3.9 mm for healthy wrist and 4.1 mm for the wrist with ligament tear.

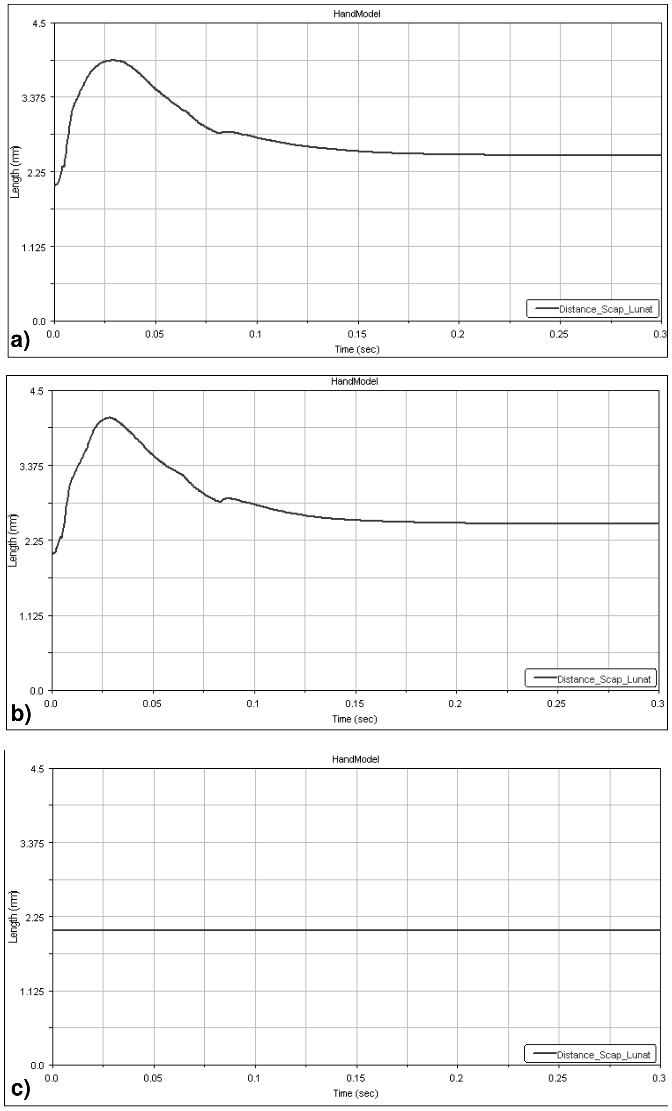

Figure 92 Distance between scaphoid and lunatum (a) healthy wrist, b) wrist with scapholunate ligament tear, c) scaphoid and lunatum fixed wrist).

Figure 93 , Figure 94 and Figure 95 shows the contact forces on scaphoid, lunatum and radius. Actually there was not a considerable difference between the healthy and injured wrists, but contact forces changed for the wrist with fixed bones.

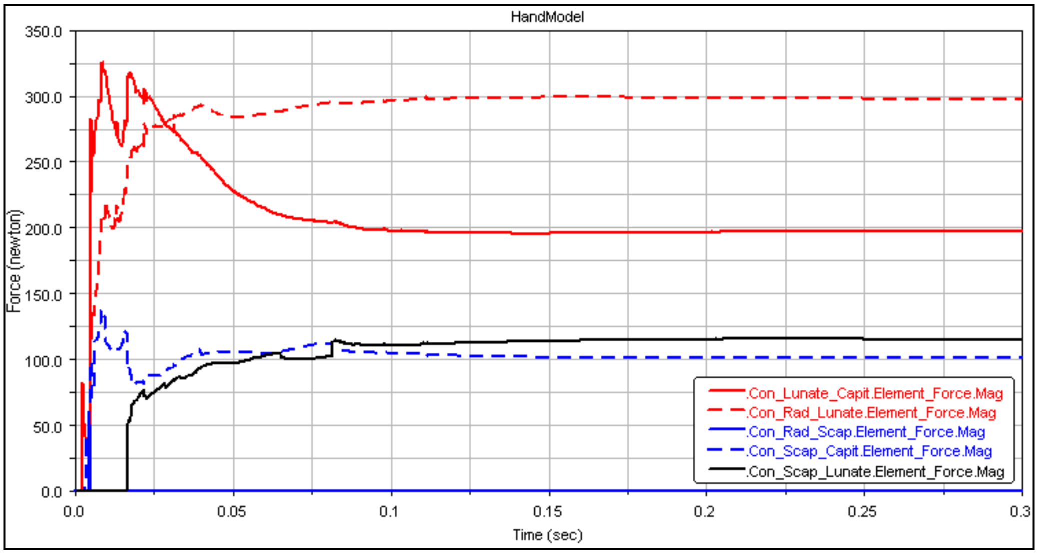

Figure 93 Contact force distribution between capitatum, scaphoid, lunatum and radius (healthy wrist).

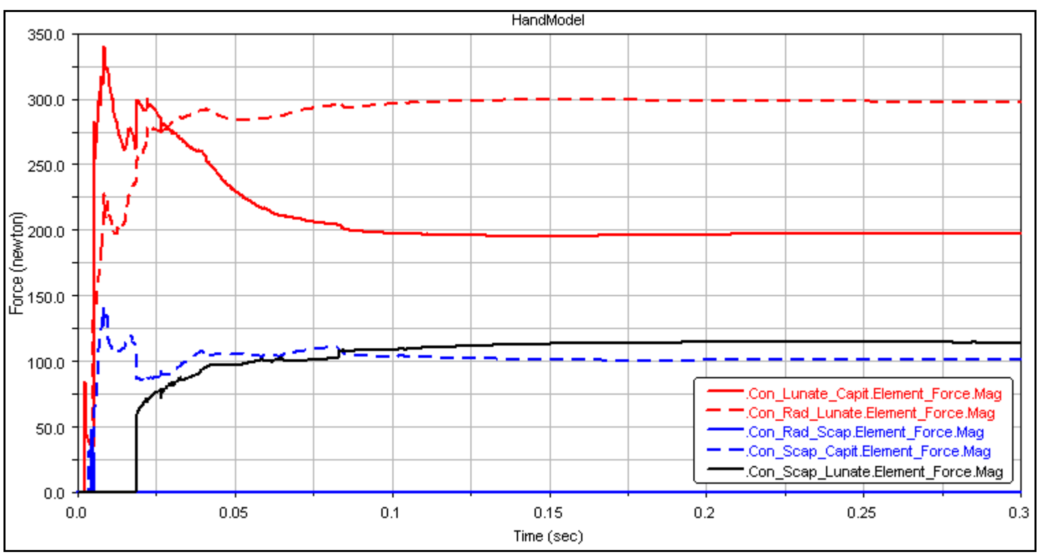

Figure 94 Contact force distribution between capitatum, scaphoid, lunatum and radius (wrist with scapholunate ligament tear).

Due to fixed bones, rotational motion of lunatum was restricted with the movements of scaphoid. Thus, the loading on lunatum bone was increased especially on the contact region of radius.

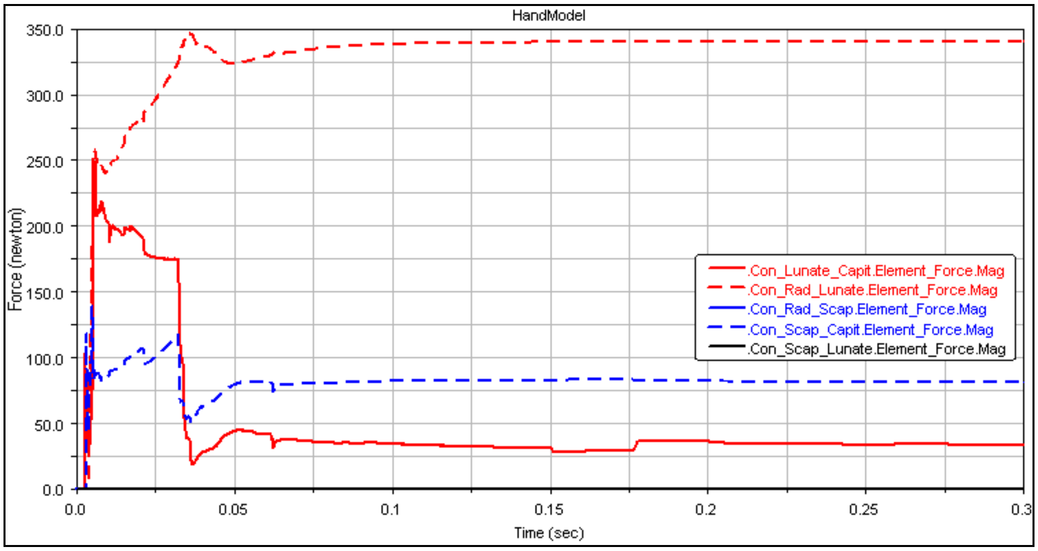

Figure 95 Contact force distribution between capitatum, scaphoid, lunatum and radius (wrist with scaphoid and lunatum fixed).

Another important point was that wrist with scapholunate ligament tear flexed less than healthy wrist. Flexion angle for healthy wrist was 90 degrees and for injured wrist was 70 degrees. Motion range of the wrist with fixed bones (scaphoid and lunatum) were limited and about 60 degrees of rotation.

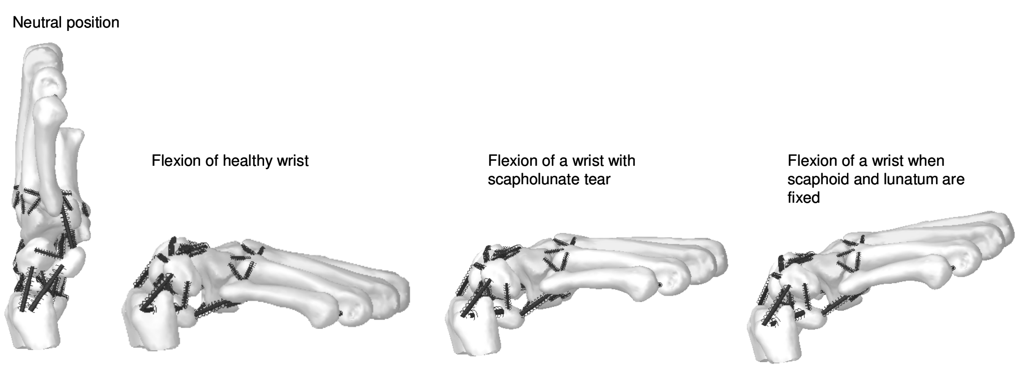

Figure 96 Angle of flexion for healthy, injured and treated wrists.

4.2.2.B. Extension of the Wrist with Scapholunate Ligament Tear

Figure 97 presents the gap between scaphoid and lunatum. Healthy wrist was more stable than the injured wrist if the gap was concerned. Maximum distance between scaphoid and lunatum was 2.9 mm for healthy wrist and 3.2 mm for injured wrist.

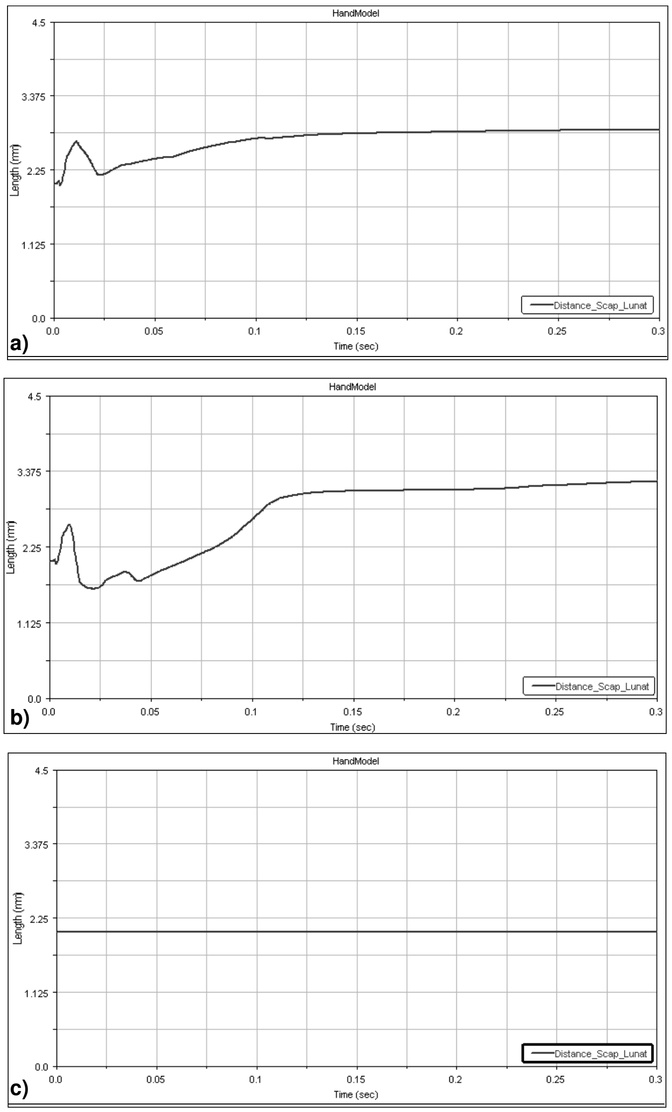

Figure 97 Distance between scaphoid and lunatum (a) healthy wrist, b) wrist with scapholunate ligament tear, c) scaphoid and lunatum fixed wrist).

Contact force differences for healthy and injured wrists are presented in Figure 98 and Figure 99. Contact forces between scaphoid/lunatum and scaphoid/capitatum were increased, but magnitudes of other contact forces remained approximately the same with injury. Fixation of bones increased contact forces between lunatum and capitatum but, contact forces on scaphoid was reduced (Figure 100).

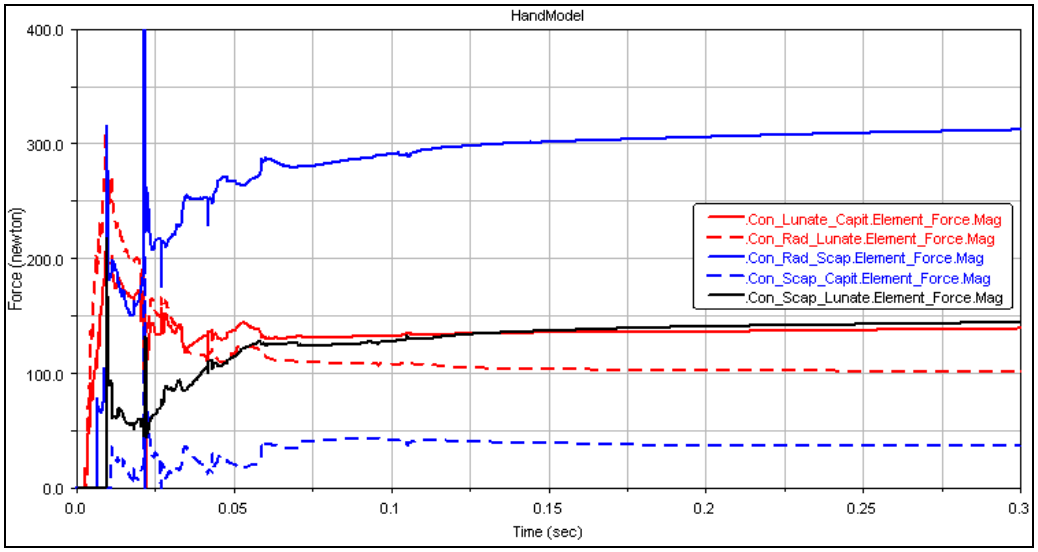

Figure 98 Contact force distribution between capitatum, scaphoid, lunatum and radius (healthy wrist).

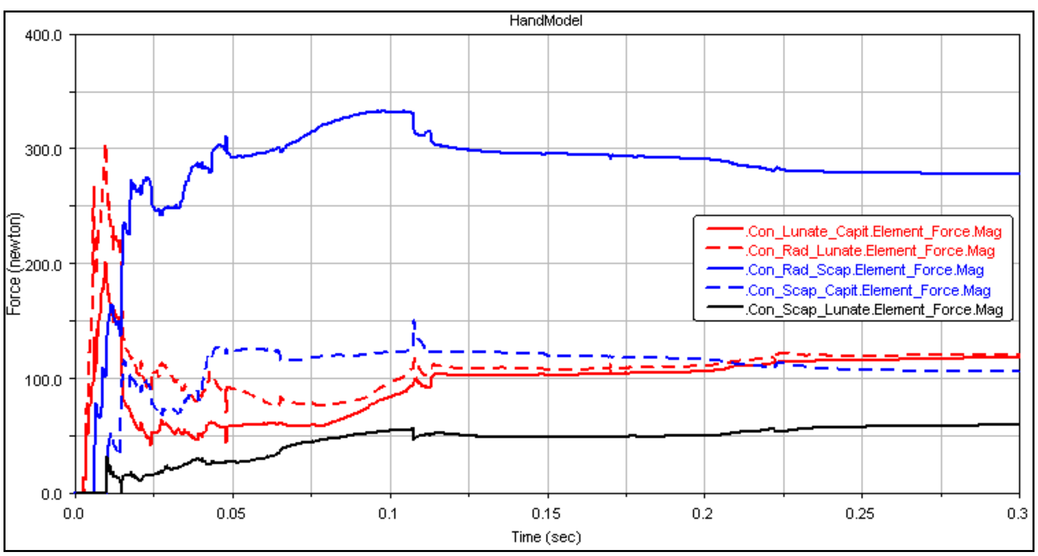

Figure 99 Contact force distribution between capitatum, scaphoid, lunatum and radius (wrist with scapholunate ligament tear).

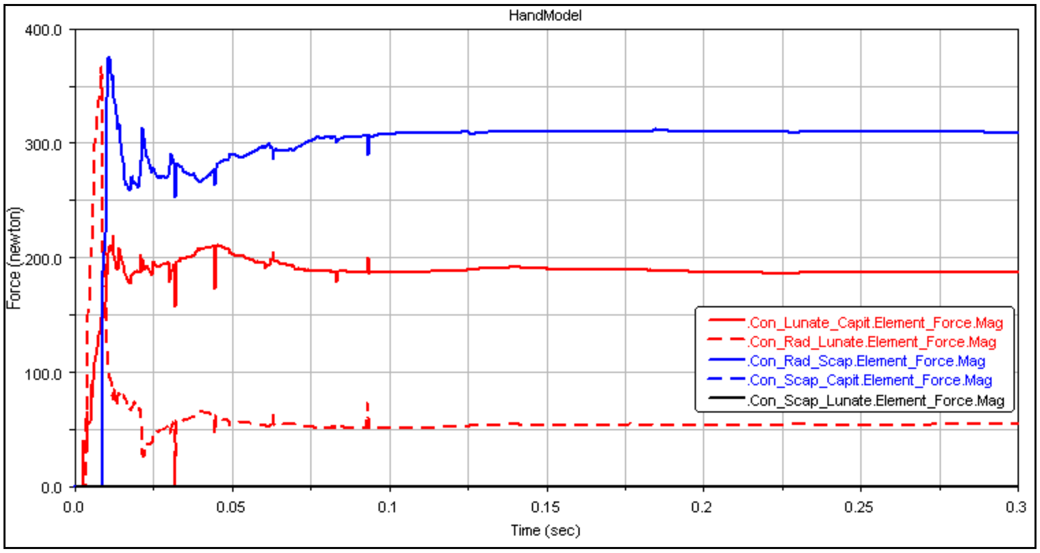

Figure 100 Contact force distribution between capitatum, scaphoid, lunatum and radius (wrist with scaphoid and lunatum fixed).

Extension angle for healthy wrist was 90 degrees and for injured wrist extension angle was measured as 60 degrees (Figure 101). Where, motion range of the wrist with fixed bones was limited with approximately 65 degrees of rotation.

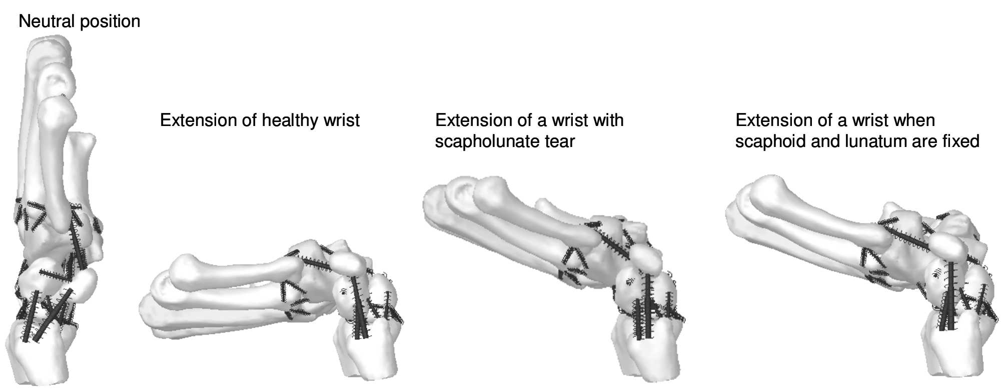

Figure 101 Angle of extension for healthy, injured and treated wrists.

Both for flexion and extension motions, scapholunate ligament tear caused a decrease in motion range. As a treatment method was applied which reduced motion range for flexion motion, even less than the ligament injured case. But fixation of bones increased motion range of extension motion.

4.2.2.C. Ulnar Deviation of the Wrist with Scapholunate Ligament Tear

Figure 102 presents the distance between scaphoid and lunatum for scapholunate ligament injury. Results indicated that the distance between scaphoid and lunatum was not affected for ulnar deviation motion.

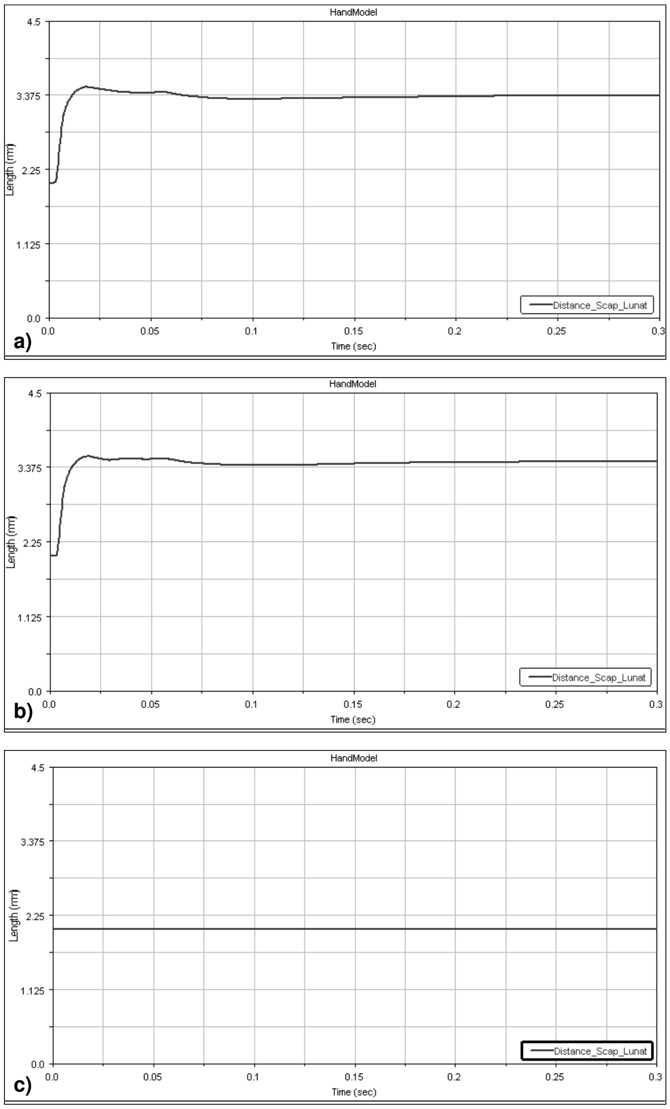

Figure 102 Distance between scaphoid and lunatum (a) healthy wrist, b) wrist with scapholunate ligament tear, c) scaphoid and lunatum fixed wrist).

Contact force distributions of carpal ligaments under the effect of scapholunate ligament injury are given in Figure 103, Figure 104 and Figure 105:

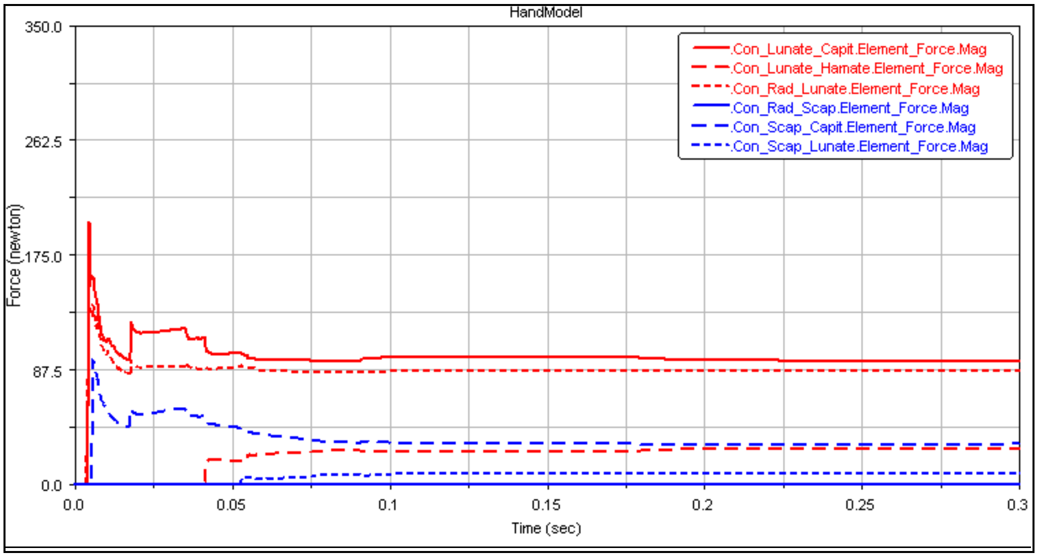

Figure 103 Contact force distribution between capitatum, scaphoid, lunatum and radius (healthy wrist).

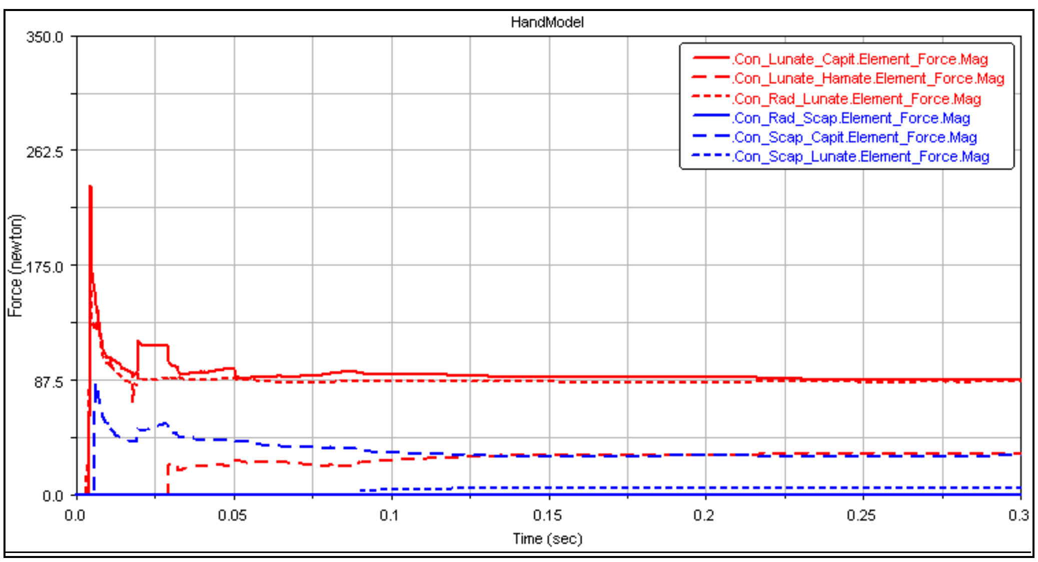

Figure 104 Contact force distribution between capitatum, scaphoid, lunatum and radius (wrist with scapholunate ligament tear).

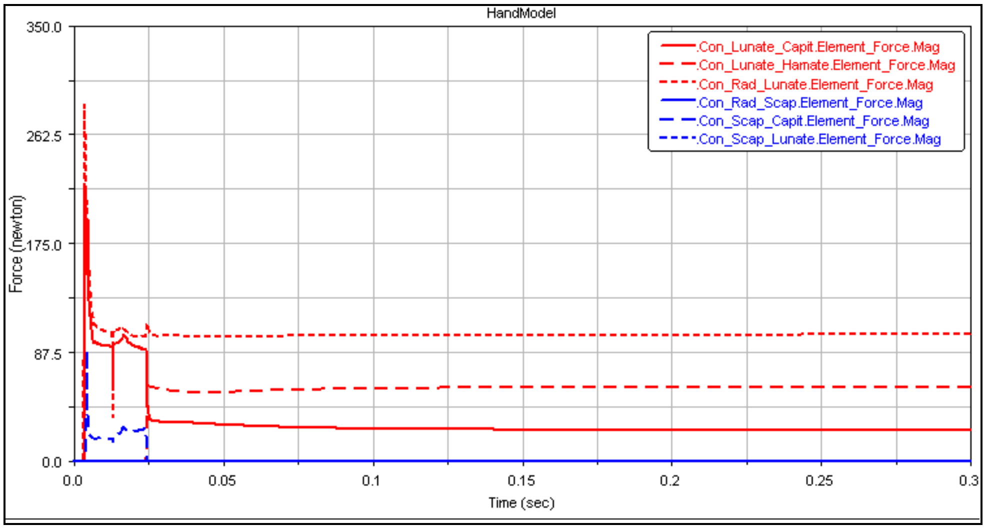

Figure 105 Contact force distribution between capitatum, scaphoid, lunatum and radius (wrist with scaphoid and lunatum fixed).

If the contact forces were compared for healthy and injured wrists, a considerable difference was not observed (Figure 103 and Figure 104). But fixation of scaphoid and lunatum made some changes on load distributions. Contact forces between lunatum/capitatum and scaphoid/capitatum were decreased, where contact force between lunatum and hamatum was increased.

Rotation angle for ulnar deviation did not change for scapholunate tear (Figure 106). Healthy and injured wrists made approximately 30 degrees of rotation. After fixation of scaphoid and lunatum ulnar deviation made approximately 20 degrees of rotation. Thus, fixation of bones reduced the motion range of the wrist for ulnar deviation.

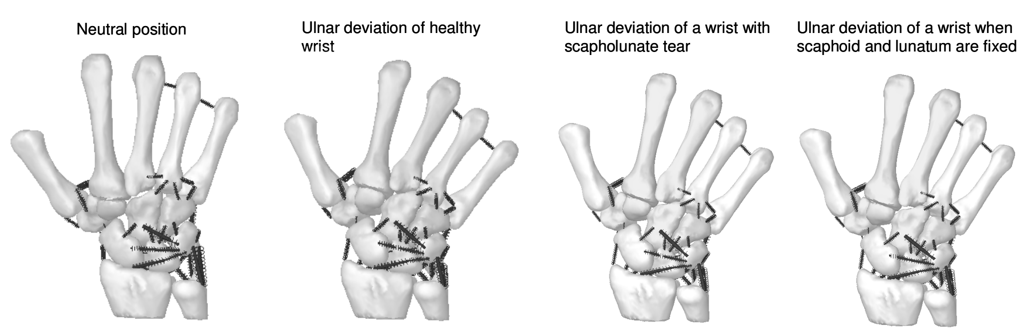

Figure 106 Angle of ulnar deviation for healthy, injured and treated wrists.

4.2.2.D. Radial Deviation of Wrist with Scapholunate Ligament Tear

Distance between scaphoid and lunatum was affected by scapholunate ligament tear (Figure 107). During radial deviation motion distance between scaphoid and lunatum was 1.6 mm for healthy wrist and 1.9 mm for the injured wrist.

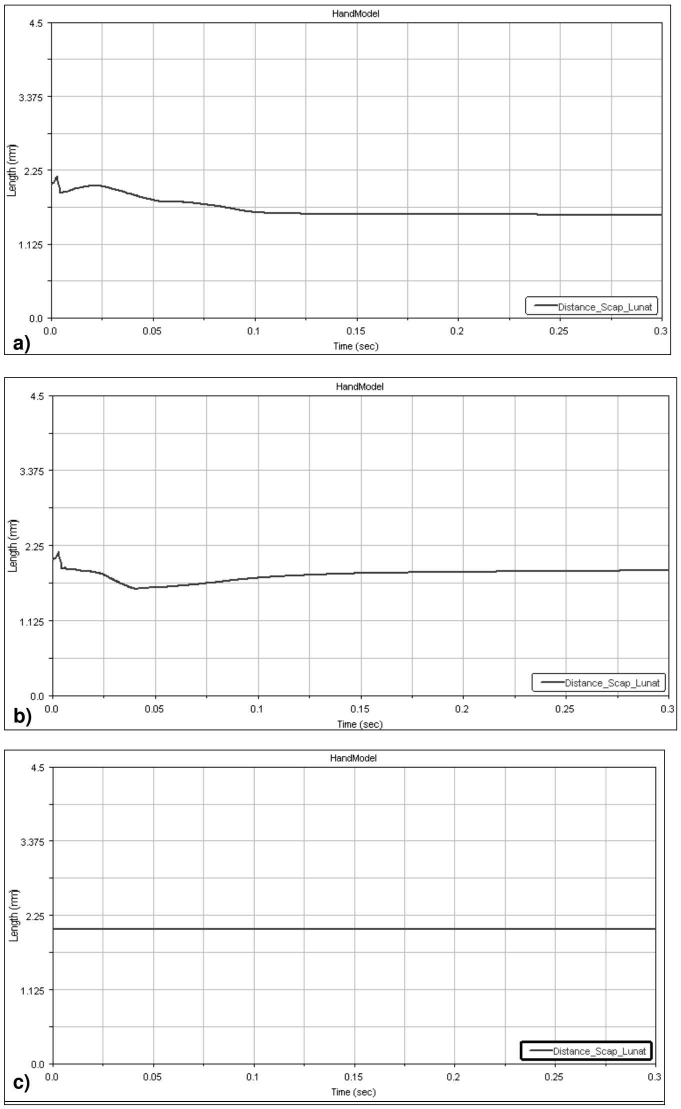

Figure 107 Distance between scaphoid and lunatum (a) healthy wrist, b) wrist with scapholunate ligament tear, c) scaphoid and lunatum fixed wrist).

After scapholunate ligament injury contact force between scaphoid and radius was decreased. Also, contact force between scaphoid and lunatum was nearly diminished with ligament tear (Figure 108 and Figure 109). After fixation of scaphoid and lunatum bones contact forces between scaphoid and trapezial region was increased. Results in Figure 110 indicated that bone fixation increased the contact force between scaphoid and radius, which was nearly diminished after ligament tear. Thus, bone fixation corrected load distribution between scaphoid and radius.

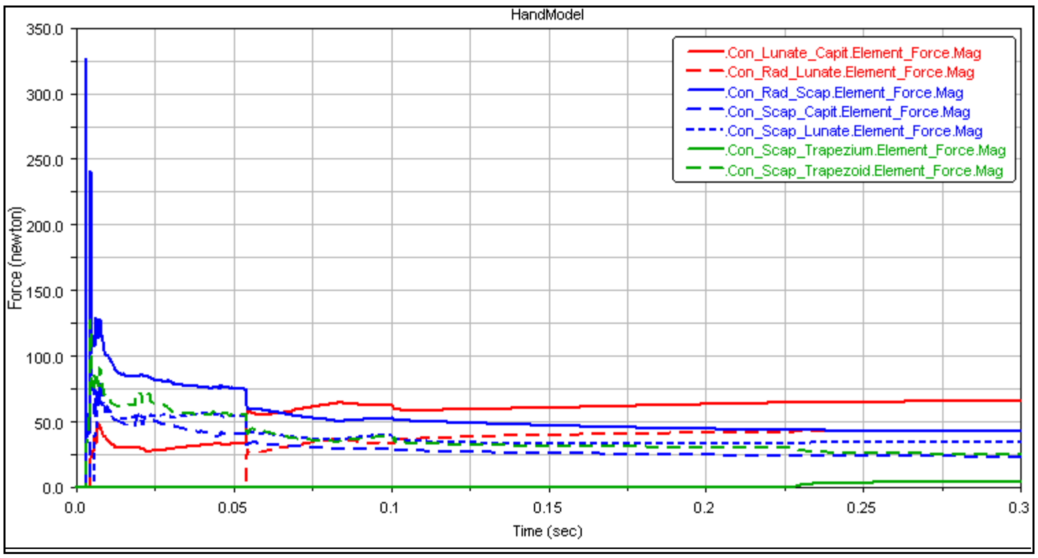

Figure 108 Contact force distribution between capitatum, scaphoid, lunatum and radius (healthy wrist).

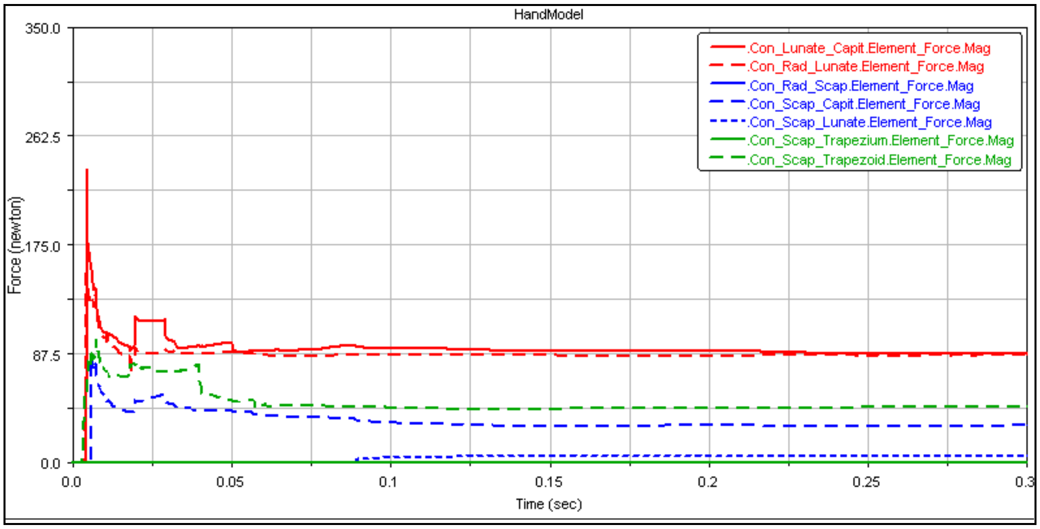

Figure 109 Contact force distribution between capitatum, scaphoid, lunatum and radius (wrist with scapholunate ligament tear).

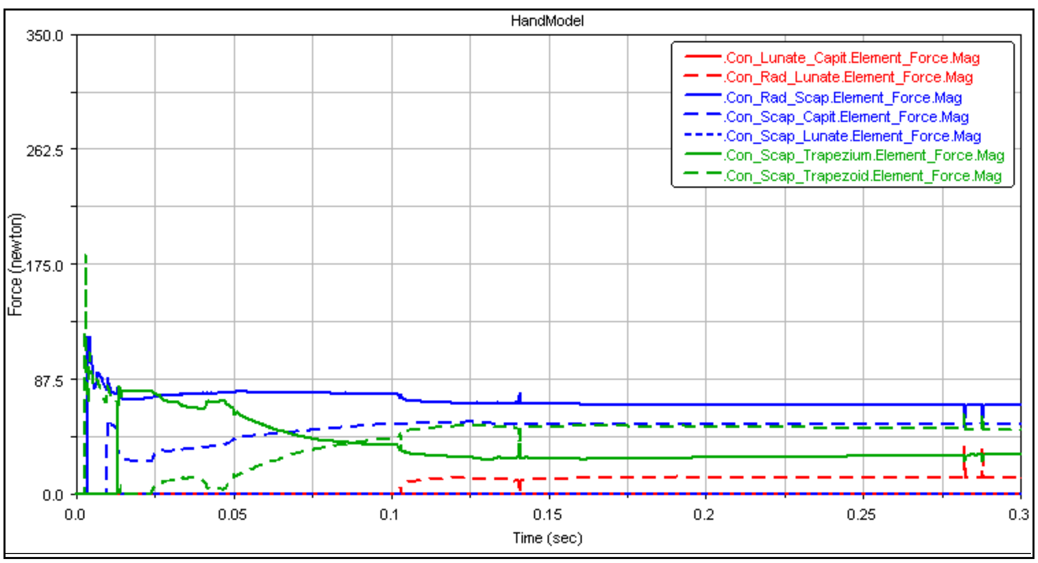

Figure 110 Contact force distribution between capitatum, scaphoid, lunatum and radius (wrist with scaphoid and lunatum fixed).

But, on the other side contact forces on lunatum bone were slightly decreased (Figure 110).

Rotation angle for radial deviation did not change for scapholunate ligament tear as shown in Figure 111. Both healthy and injured wrists made approximately 20 degrees of rotation. After fixation of scaphoid and lunatum bones ulnar deviation motion made approximately 20 degrees of rotation, too.

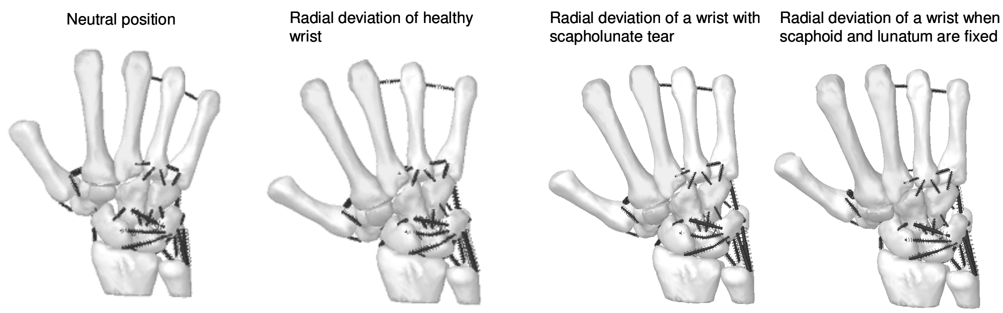

Figure 111 Angle of radial deviation for healthy, injured and treated wrists.

CHAPTER 5

DISCUSSION

In this study, a three-dimensional model of the hand was built to analyze healthy and injured wrists. Results of this study can be summarized as follows:

5.1. Analysis of healthy (uninjured) wrists

Healthy wrists were analyzed by using four motion types of the wrist: flexion, extension, radial and ulnar deviation motions. Additionally axial loading (tensile and compressive) of the wrist was studied, which was also required for comparison of injured wrists.

Flexion and extension motions were analyzed by applying forces as defined in sections 4.1.1. and 4.1.2. Beyazova [17] defines angle of rotation for flexion motion as around 80 degrees and for extension motion as around 70 degrees, but the results of analyzes gave different rotation values. In three-dimensional model, both for flexion and extension motions the wrist stopped at the angle of 90 degrees. Results of the analysis were checked by applying same external force on the author's wrist from which the model was constructed. For real wrist the rotation angle was 90 degrees for both flexion and extension motions. Thus, flexion and extension motions of the three-dimensional model made the same rotation angle with the real wrist. That was an important result to prove the biofidelity of the model for flexion and extension motions.

Another important point about flexion and extension motions was the load distributions between the ligaments. Most of the palmar ligaments were inactive during flexion motion where dorsal ligaments carried most of the load. On the other hand, dorsal ligaments were inactive during extension motion where palmar ligaments carried most of the load.

Scaphoid, lunatum and capitatum bones were the pivot points of flexion and extension motions. Most of the mid-carpal contact loads were shared between these three bones. While transferring mid-carpal contact loads to the forearm, lunatum carried a huge amount of load for flexion and scaphoid carried a huge amount of load for extension. Also, palmar/dorsal ligaments of scaphoid, lunatum and capitatum were active for supporting the wrist joint.

Radial and ulnar deviation motions were analyzed by applying forces as defined in section 4.1.3. Beyazova [17] indicates limits of rotation for ulnar deviation is around 30 degrees and for radial deviation is around 20 degrees. Results of the three-dimensional model analysis gave the same rotation angle values for ulnar and radial deviation motions.

Ulnar collateral ligament carried high tensile forces during radial deviation and radial collateral ligament carried higher tensile forces during ulnar deviation.

Like flexion/extension motions, scaphoid and lunatum bones were the main pivot points carrying significant amount of wrist loads. During radial deviation motion contact forces between scaphoid and trapezial region were very crucial. And during ulnar deviation motion contact forces between lunatum, triquetrum and hamatum were very crucial.

For radial deviation motion scaphoid bone did not make the required sliding motion. Instead scaphoid made a rotation motion, distal pole of the scaphoid rotated palmarly. That was the only point needed to be developed but the rotation angle of the wrist was close to the studies of Beyazova [17].

Compressive type axial loading caused a rotation of the wrist to the palmar side (flexion motion) which was the expected real life condition for such a loading. For compressive axial loading almost all of the axial force was transferred through bone contact regions; only a small amount of load was transferred through ligaments and joints. Figure 112 shows the resulting contact force distributions among carpal bones of the wrist. Results showed that approximately 60% of the axial load was transferred from lunatum to radius, where 40% of the load was transferred from scaphoid to radius.

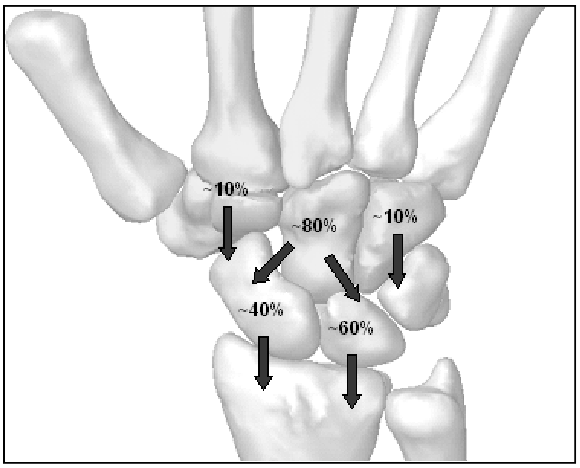

Figure 112 Load distributions among carpal bones under axial loading (compressive).

High amount of contact forces on lunatum bone was also analyzed for Kienböck's disease as a wrist injury.

For tensile type of axial loading, nearly all of the axial forces were carried by palmar and dorsal ligaments. Small amount of the load was carried by the joints.

5.2. Analysis of injured wrists

Kienböck's disease and scapholunate ligament injury were analyzed as pathological cases.

Kienböck's disease can be caused by different kinds of injuries. In this study extra loading on lunatum from capitatum bone was analyzed. The highest contact force in mid-carpal region was observed between lunatum and capitatum bones. As a treatment method a cup shaped part was removed (capitate shortening) from capitatum at the contact region with lunatum.

Analysis (especially for compressive type of axial loading) after capitate shortening proved that capitate shortening reduced contact force between capitatum and lunatum. However, reduction of the contact force on one region caused increases on other regions. Results revealed that contact forces between scaphoid and trapezial region was increased. Also, contact forces between lunatum, triquetrum and hamatum were increased. Such a treatment method prevented extra loading problem on lunatum bone but may cause some other kinds of diseases in future for the patients. Extra loading on trapezial region, hamatum or triquetrum bones should be considered before doing such a surgical operation.

Flexion motion analysis also figured out the change in motion range for Kienböck's disease. Wrist was to flex more after capitate shortening. Such changes were inevitable with modifications of wrist contact forces.

Scapholunate ligament tear was studied by being one of the most common ligament injuries of the wrist. For comparison healthy/injured wrists were analyzed and as a treatment method fixation of scaphoid and lunatum was observed.

Scapholunate ligament injury resulted in an increase for the distance between scaphoid and lunatum bones. Since ligaments hold the bones together, such an injury may cause changes in bone positions.

Another important effect of scapholunate ligament tear was the decrease in maximum rotation angles for flexion and extension motions. With ligament injury wrist flexed 20 degrees less than normal and extend 30 degrees less than normal (healthy wrist). Rotation angle of radial and ulnar deviation motions were not significantly changed with scapholunate injury.

Fixation of scaphoid and lunatum was modeled as the treatment method for scapholunate injury. Fixation of bones had serious effects on contact force. Especially contact forces on lunatum were increased in a considerable manner; resulting a decrease in contact forces of scaphoid.

Also, fixation of the bones caused wrist to flex 30 degrees less than normal and extend 25 degrees less than normal (healthy wrist).

Analysis for injured and healthy wrists gave acceptable results as compared to the real life examinations. Three dimensional model gave appropriate results for healthy wrists to make defined flexion, extension, ulnar and radial deviation motions. Also, the simulation of injured wrists for Kienböck's disease and scapholunate ligament injury gave approximate results to the real life surgical operations.

Therefore, three-dimensional model can be used to predict results of surgical operations without risking the patients' health. Also, without a surgical operation new treatment methods or surgery planning can be modeled on the wrist.

CHAPTER 6

SUMMARY & CONCLUSIONS

In this thesis a three-dimensional model of the human hand was built and real life activities of the human hand were analyzed. Namely flexion, extension, ulnar and radial deviation motions of the wrist were the main motions for the study. Additionally, axial loading was analyzed for examining contact forces.

Results of the three-dimensional model showed that the model was able to simulate real life movements of the wrist with an acceptable level of biofidelity. Flexion, extension, ulnar deviation motions and axial loading were successfully modeled. Only there was a problem with radial deviation motion, wrist made correct rotation angle but the sliding motion of the scaphoid could not be modeled. However, the complete radial deviation motion was simulated.

The success of three-dimensional model was not limited to analysis of healthy wrists but various mechanics of various pathology and treatment techniques (like scapholunate ligament injury and Kienböck's disease) were analyzed in the model. Effects of wrist injuries were simulated with the model and also results of surgical operations were studied.

Three-dimensional model of the wrist can be used to simulate wrist injuries with the observation of changes in loading of wrist components. Therefore, model would be useful for orthopaedics and hand surgeons to be used in analyzing and predicting results of surgical operations.

REFERENCES

[1] Dartmouth Medical School, Dartmouth College. Human anatomy. Available from World Wide Web: "http://www.dartmouth.edu/~anatomy/wristhand/radiograph/ radio1.html", Last accessed date: September 2006.

[2] K. Kuczynski, Articular Synovial Membrane, The Hand (by Raoul Tubiana), Ch. 18, Vol. 5, pp. 207-217, 1999.

[3] P. Robinson, (iii) MR imaging of the wrist, Mini-Symposium: The Wrist, Current Orthopaedics, Vol. 19, pp. 196-208, 2005.

[4] A. Özçelik, İ. Günal, N. Köse, S. Seber, H. Ömeroğlu, Wrist Ligaments: their significance in carpal instability, Turkish Journal of Trauma & Emergency Surgery, pp. 115-122, 2005.

[5] D. A. McGrouther, P. O. Higgins, Interactive Hand – Anatomy, Version 1.0.0, Primal Pictures Ltd., 1997.

[6] J. J. Crisco, S. Pike, D. L. Hulsizer-Galvin, E. Akelman, A. P. C. Weiss, S. W. Wolfe, Carpal Bone Postures and Motions in Both Wrists of Patients with Unilateral Scapholunate Interosseous Ligament Tears, The Journal of Hand Surgery, 28A, pp. 926-937, 2003.

[7] R. S. Reddy, J. Compson, Examination of the wrist – soft tissue, joints and special tests, Current Orthopaedics 19, pp 180-189, 2005.

[8] H. Moritomo, T. Murase, A. Goto, K. Oka, K. Sugamoto, H. Yoshikawa, Capitate-Based Kinematics of the Midcarpal Joint During Wrist Radioulnar Deviation: An In Vivo Three-Dimensional Motion Analysis, Midcarpal Kinematics, The Journal of Hand Surgery, pp. 668-675, 2004.

[9] J. D. Johnston, C. F. Small, M. L. Bouxsein, D. R. Pichora, Mechanical properties pf the scapholunate ligament correlate bone mineral density

measurements of the hand, The Journal of Orthopaedic Research, Vol 22, pp. 867-871, 2004.

[10] S.R. Moeini, W. Perry, J. R. Tamarapalli, J. E. Lemons, M. J. Wilkins, R.D. Meyer, BIOMECHANICS OF BONE-LIGAMENT-BONE UNITS FOR RECONSTRUCTION OF THE SCAPHO-LUNATE, Division of Orthopaedics, Department of Surgery University of Alabama at Birmingham, Birmingham, Alabama, pp. 98-100, 1995.

[11] J.K. Green, F. W. Werner, H. Wang, M. M. Weiner, J. M. Sacks, W. H. Short, Three-dimensional modeling and animation of two carpal bones: a technique, Journal of Biomechanics, Vol. 37, pp. 757-762, 2004.

[12] S. D. Carrigan, R. A. Whiteside, D. R. Pichora, C. F. Small, Development of a Three-Dimensional Finite Element Model for Carpal Load Transmission in a Static Neutral Posture, Annals of Biomedical Engineering, Vol. 31, pp. 718-725, 2003.

[13] Urban & Schwarzenberg, Sabotta Atlas der Anatomie des Menschen, München-Wien-Baltimore, Vol. 1, pp. 66-224, 1977.

[14] R. Tubiana, Architecture and Functions of the Hand, The Hand (by Raoul Tubiana), Ch. 4, Vol. 5, pp. 19-26, 1999.

[15] K-N. An, E.Y-S. Chao, Kinematic Analysis, Biomechanics of the Wrist Joint, Ch. 2, pp. 23-28, 1991.

[16] M. D. Nowak, S. E. Logan, ULTIMATE STRENGTH PARAMETERS OF 10 CLINICALLY SIGNIFICANT HUMAN WRIST LIGAMENTS, Biomaterials 1, IEEE Engineering in Medicine and Biology Society 10th Annual International Conference, Washington University, 1988.

[17] M. Beyazova, Y. G. Kutsal, Eklemlerin, Kasların, Motor ve Duyusal İşlevlerin Klinik Değerlendirilmesi, Fiziksel Tıp ve Rehabilitasyon, Cilt 1, Güneş Kitabevi, 2000.

[18] T.M. Moojen, J. G. Snel, M. J. P. F. Ritt, J. M. G. Kauer, H. W. Venema, K. E. Bos, Three-dimensional kinematics in vivo, Clinical Biomechanics, Vol 17, pp. 506-515, 2002.

[19] D. Nuttall, I. A. Trail, J. K. Stanley, MOVEMENT OF THE SCAPHOID IN THE NORMAL WRIST, Journal of Hand Surgery, British and European Volume 23B:6, pp. 762-764, 1998.

[20] M. Kobayashi, M. Garcia-Elias, L. Nagy, M. J. P. F. Ritt, K. An, W. P. Cooney, R. L. Linscheid, Axial Loading Induces Rotation of the Proximal Carpal Row Bones Around Unique Screw-Displacement Axes, Journal of Biomechanics, Vol. 30, pp. 1165-1167, 1997.

[21] A. Gupta, Change of carpal alignment under anaesthesia: role of physiological axial loading on carpus, Clinical Biomechanics, Vol 17, pp. 660-665, 2002.

[22] R.M. Patterson, H. Moritomo, S. Yamaguchi, H. Mitsuyasu, M. Shah, W. L. Buford, S. F. Viegas, SCAPHOID ANATOMY AND MECHANICS: UPDATE AND REVIEW, Operative Techniques in Orthopaedics, Vol 13, No 1, pp. 2-10, 2003.

[23] E. Güdemez, Lunatum Kemiği, Aktüel Tıp Dergisi, Vol. 6, No 4, pp. 52-55, 2001.

[24] R. E. Epsten, M. K. Dalinka, MAGNETIC RESONANCA IMAGING OF THE HAND AND WRIST, Operative Techniques in Sports Medicine, Vol. 5, No: 1 (January), pp. 37-49, 1997.

[25] C. Lamasa, A. Carrerab, I. Proubastaa, M. Llusàb, C. Majóa, X. Mirc, The anatomy and vascularity of the lunate: considerations applied to Kienböck' s disease, Chirurgie de la man, Vol. 26, pp. 13-20, 2007.

[26] M. Garcia-Elias, Carpal instabilities and dislocations. In: Green DP, Hotchkiss RN, Pederson WC (Eds) Operative hand surgery, New York, Churchill Livingstone, pp. 865–928, 1999.

[27] M. Garcia-Elias, A. M. Vidal, Kienböck' s disease, Current Orthopaedics, Vol. 11, pp. 28-35, 1997.

[28] G. Leblebicioğlu, M. N. Doral, Ö. A. Atay, O. Tetik, T. L. Whipple, Open Treatment of Stage III Kienböck's Disease With Lunate Revascularization Compared With Arthroscopic Treatment Without Revascularization, The Journal of Arthroscopic and Related Surgery, Vol. 19, No: 2, 99. 117-130, 2003.

[29] M. Schadel-Höpfner, G. Böhringer, L. Gotzen, I. Çelik, TRACTION RADIOGRAPHY FOR THE DIAGNOSIS OF SCAPHOLUNATE LIGAMENT TEARS, Journal of Hand Surgery (British and European Volume), Vol 30B, Chapter 5, pp. 464-467, 2005.

[30] M. Henry, ARTHROSCOPIC TREATMENT OF ACUTE SCAPHOLUNATE AND LUNOTRIQUETRAL LIGAMENT INJURIES, Operative techniques in orthopaedics, Vol. 13, No 1, pp. 48-55, 2003.

APPENDIX A: MECHANICAL PROPERTIES OF CONTACT ELEMENTS

Totally 20 contact elements were placed between the bones which are in contact. Stiffness and damping values of contact elements are presented in Table 1:

CONTACT ELEMENTS						
	1. bone	**2. bone**	**Stiffness k (N/mm)**	**Damping C (N.s/mm)**	**Max. penetration depth d (mm)**	**Impact force exponent e**
1	Radius	Scaphoid	2000	200	0,01	1,1
2	Radius	Lunatum	2000	200	0,01	1,1
3	Ulna	Lunatum	2000	200	0,01	1,1
4	Ulna	Triquetrum	2000	200	0,01	1,1
5	Scaphoid	Trapezoid	2000	200	0,01	1,1
6	Scaphoid	Trapezium	2000	200	0,01	1,1
7	Scaphoid	Capitatum	2000	200	0,01	1,1
8	Scaphoid	Lunatum	2000	200	0,01	1,1
9	Lunatum	Capitatum	2000	200	0,01	1,1
10	Lunatum	Hamatum	2000	200	0,01	1,1
11	Lunatum	Triquetrum	2000	200	0,01	1,1
12	Lunatum	Psiforme	2000	200	0,01	1,1
13	Triquetrum	Hamatum	2000	200	0,01	1,1
14	Triquetrum	Psiforme	2000	200	0,01	1,1
15	Capitatum	Metacarp. 4	2000	200	0,01	1,1
16	Hamatum	Metacarp. 4	2000	200	0,01	1,1
17	Hamatum	Metacarp. 5	2000	200	0,01	1,1
18	Hamatum	Psiforme	2000	200	0,01	1,1
19	Metacarp. 3	Metacarp. 4	2000	200	0,01	1,1
20	Metacarp. 4	Metacarp. 5	2000	200	0,01	1,1

Table 1 Stiffness and damping coefficients of contact elements.

APPENDIX B: MECHANICAL PROPERTIES OF BUSHING ELEMENTS

Totally 17 bushing elements were used in modeling the joints of the corresponding bones. Stiffness and damping values were taken as small as possible for both translational and rotational components. Stiffness and damping coefficient are presented in Table 2.

BUSHING ELEMENTS						
			Translational		**Rotational**	
	1. bone	**2. bone**	**Stiffness k (N/mm)**	**Damping C (N.s/mm)**	**Stiffness k (N/rad)**	**Damping C (N.s/rad)**
1	Radius	Scaphoid	0,02	0,02	0,02	0,02
2	Radius	Lunatum	0,02	0,02	0,02	0,02
3	Ulna	Lunatum	0,02	0,02	0,02	0,02
4	Ulna	Triquetrum	0,02	0,02	0,02	0,02
5	Scaphoid	Trapezoid	0,02	0,02	0,02	0,02
6	Scaphoid	Trapezium	0,02	0,02	0,02	0,02
7	Scaphoid	Capitatum	0,02	0,02	0,02	0,02
8	Scaphoid	Lunatum	0,02	0,02	0,02	0,02
9	Lunatum	Capitatum	0,02	0,02	0,02	0,02
10	Lunatum	Hamatum	0,02	0,02	0,02	0,02
11	Lunatum	Triquetrum	0,02	0,02	0,02	0,02
12	Triquetrum	Hamatum	0,02	0,02	0,02	0,02
13	Triquetrum	Psiforme	0,02	0,02	0,02	0,02
14	Hamatum	Metacarp. 4	0,02	0,02	0,02	0,02
15	Hamatum	Metacarp. 5	0,02	0,02	0,02	0,02
16	Metacarp. 3	Metacarp. 4	0,02	0,02	0,02	0,02
17	Metacarp. 4	Metacarp. 5	0,02	0,02	0,02	0,02

Table 2 Stiffness and damping coefficients of bushing elements.

APPENDIX C: MECHANICAL PROPERTIES OF LIGAMENTS

Totally 52 ligaments were used in the model given in Table 3 and Table 4 [16], [12]:

LIGAMENTS						
	Definition of Location	**1st Connection**	**2nd Connection**	**Stiffness (k, N/mm)**	**Damping (C, N.s/mm)**	**Preload (N)**
1	Palmar	Radius	Lunate	75	1,75	0.05
2	Palmar	Radius	Scaphoid	75	1,75	0.05
3	Palmar	Scaphoid	Lunate	230	1,75	0.05
4	Dorsal	Scaphoid	Lunate	230	1,75	0.05
5	Proximal	Scaphoid	Lunate	230	1,75	0.05
6	Palmar	Lunate	Triquetrum	350	1,75	0.05
7	Dorsal	Lunate	Triquetrum	350	1,75	0.05
8	Proximal	Lunate	Triquetrum	350	1,75	0.05
9	Dorsal intercarpal	Lunate	Capitatum	150	1,75	0.05
10	Dorsal intercarpal	Scaphoid	Capitatum	150	1,75	0.05
11	Dorsal intercarpal	Lunate	Hamatum	150	1,75	0.05
12	Dorsal intercarpal	Triquetrum	Hamatum	300	1,75	0.05
13	Palmar intercarpal-1	Scaphoid	Trapezium	150	1,75	0.05
14	Palmar intercarpal-2	Scaphoid	Trapezium	150	1,75	0.05
15	Palmar intercarpal-3	Scaphoid	Trapezium	150	1,75	0.05
16	Dorsal Carpometacarpal	Capitatum	Metacarpal 4	100	1,75	0.05
17	Dorsal Carpometacarpal	Hamatum	Metacarpal 4	100	1,75	0.05
18	Dorsal Carpometacarpal	Hamatum	Metacarpal 5	100	1,75	0.05
19	Palmar Midcarpal	Capitatum	Scaphoid	25	1,75	0.05
20	Palmar Midcarpal	Capitatum	Triquetrum	40	1,75	0.05
21	Palmar Carpometacarpal	Capitatum	Metacarpal 4	100	1,75	0.05
22	Palmar Carpometacarpal	Hamatum	Metacarpal 5	100	1,75	0.05
23	Dorsal	Radius	Lunate	50	1,75	0.05
24	Dorsal	Lunate	Triquetrum	50	1,75	0.05
25	Dorsal Midcarpal	Scaphoid	Lunate	50	1,75	0.05
26	Dorsal Midcarpal	Lunate	Triquetrum	50	1,75	0.05

Table 3 Mechanical properties of the ligaments.

LIGAMENTS						
	Definition of Location	**1st Connection**	**2nd Connection**	**Stiffness (k, N/mm)**	**Damping (C, N.s/mm)**	**Preload (N)**
1	Dorsal Midcarpal	Capitatum	Triquetrum	40	1,75	0.05
2	Dorsal	Ulna	Triquetrum	100	1,75	0.05
3	Palmar	Ulna	Psiforme	100	1,75	0.05
4	Dorsal Metacarpal	Metacarpal 3	Metacarpal 4	100	1,75	0.05
5	Dorsal Metacarpal	Metacarpal 4	Metacarpal 5	100	1,75	0.05
6	Palmar	Radius	Scaphoid	50	1,75	0.05
7	Palmar	Radius	Scaphoid	50	1,75	0.05
8	Palmar	Scaphoid	Capitatum	50	1,75	0.05
9	Palmar Radiocarpal	Radius	Lunate	50	1,75	0.05
10	Palmar Radiocarpal	Radius	Lunate	50	1,75	0.05
11	Palmar	Radius	Lunate	50	1,75	0.05
12	Palmar	Lunate	Triquetrum	50	1,75	0.05
13	Palmar	Ulna	Lunate	40	1,75	0.05
14	Palmar	Ulna	Triquetrum	40	1,75	0.05
15	Medial	Triquetrum	Psiforme	150	1,75	0.05
16	Palmar	Psiforme	Metacarpal 5	100	1,75	0.05
17	Palmar	Hamatum	Metacarpal 5	100	1,75	0.05
18	Palmar	Metacarpal 3	Metacarpal 4	100	1,75	0.05
19	Palmar	Metacarpal 4	Metacarpal 5	100	1,75	0.05
20	Palmar	Metacarpal 3	Metacarpal 4	100	1,75	0.05
21	Palmar	Metacarpal 4	Metacarpal 5	100	1,75	0.05
22	Palmar	Hamatum	Psiforme	100	1,75	0.05
23	Palmar	Trapezium	Metacarpal 1	100	1,75	0.05
24	Lateral	Trapezium	Metacarpal 1	100	1,75	0.05
25	Dorsal	Trapezium	Metacarpal 1	100	1,75	0.05
26	Dorsal	Trapezium	Metacarpal 1	100	1,75	0.05

Table 4 Mechanical properties of the ligaments.